Inaugural dissertation

for

obtaining the doctoral degree

of the

Combined Faculty of Mathematics, Engineering and Natural Sciences

of the

Ruprecht - Karls - University

Heidelberg

Presented by

M.Sc. Niharika Garg

born in: Jaipur, Rajasthan, India

Oral examination: 27-02-2023

Role of Non-Muscle Myosin II in the Morphogenesis of Nematocysts in *Hydra*

Referees: Prof. Dr. Suat Özbek

Prof. Dr. Thomas W. Holstein

Abstract

Nematocyst, the cnidarian stinging organelle, undergoes a sophisticated and complex morphogenesis, which begins as an unusual intracellular secretory process from the Golgi network. They consist of a capsule body attached to a long thread-like structure, the tubule, which is tightly coiled and invaginated inside the capsule matrix. The tubule is expelled to the outside in response to a mechanical or chemical stimulus during predation or defence. The firing action of nematocysts, driven by a high osmotic pressure of 150 bar, is the fastest reaction in nature and takes about 3 milliseconds. Although the structural assembly of nematocysts has been studied over the last few years, the molecular basis of tubule formation and invagination has so far been elusive. In this thesis work, it is shown that a non-muscle myosin II homolog (HyNMII) from the lower metazoan Hydra is an essential factor required to drive the morphogenesis of its stinging organelle. Non-muscle myosin II is commonly associated with stress fibres in the leading edge of migrating cells and cleavage furrow of cells in mitosis. More recently it has also been implicated to be associated dynamically with Golgi membranes where it regulates vesicle fission and trafficking. A specific antibody raised against the HyNMII head domain demonstrated an exclusive localization on nematocyst tubules from early to late morphogenesis stages. HyNMII condenses to a collar structure surrounding the apical constriction of the nematocyst vesicle in early nematocysts. HyNMII then facilitates tubule growth by providing a compressive force counteracting the increasing osmotic pressure as evidenced by blebbistatin treatment and genetic knockdown. HyNMII inhibition led to a depletion of early morphogenetic nematocyst stages by tubule disintegration. In addition, the glycoprotein NOWA was redefined in this thesis as a major component of the tubule. NOWA was shown to be essentially involved in the tubule invagination process as evidenced by genetic knockdown and live imaging using a transgenic NOWA::NOWA-GFP line. The data demonstrated in this thesis elucidates a novel function for actomyosin networks in the morphogenesis of the cnidarian nematocyst, one of the most sophisticated organelles in the animal kingdom.

Zusammenfassung

Die Nematozysten (Cniden) der Nesseltiere, durchlaufen eine komplexe Morphogenese, die mit einem ungewöhnlichen intrazellulären Sekretionsprozess aus dem Golgi-Netzwerk beginnt. Nematozysten bestehen aus einem Kapselkörper, von dem ein langes fadenförmiges Gebilde, der Schlauch, ausgeht, der sich eng aufgerollt in der Kapselmatrix befindet. Der Schlauch wird infolge eines mechanischen oder chemischen Reizes während des Beutefangs oder der Verteidigung nach außen geschleudert. Das Auslösen der Nematozysten, das durch einen hohen osmotischen Druck von 150 bar angetrieben wird, ist die schnellste Reaktion in der Natur und dauert etwa 3 Millisekunden. Obwohl der molekulare Aufbau von Nematozysten in den letzten Jahren eingehend erforscht wurde, ist die molekulare Grundlage für die Bildung des Schlauches und dessen Invagination bisher nicht bekannt gewesen. In dieser Arbeit wird gezeigt, dass ein nicht-muskuläres Myosin-II-Homologes (HyNMII) aus dem basalen Metazoen *Hydra* ein wesentlicher Faktor für die Morphogenese der Nematocysten ist. Myosin II wird häufig mit den Stressfasern an den „leading edges“ wandernder Zellen und den Spaltfurchen von Zellen während der Mitose in Verbindung gebracht. In jüngerer Zeit wurde auch eine dynamische Assoziation mit Golgi-Membranen nachgewiesen, wo es die Entstehung und den Transport von Vesikeln reguliert. Ein spezifischer Antikörper, der gegen die katalytische Domäne von HyNMII gebildet wurde, zeigte eine Lokalisierung in den Schläuchen von Nematozysten während der gesamten Morphogenese. In frühen Nematozysten kondensiert HyNMII zu einer Kragenstruktur, die die apikale Einschnürung des Nematozystenvesikels umgibt. HyNMII ermöglicht dann das Wachstum der Schläuche, indem es eine Kompression erzeugt, die dem zunehmenden osmotischen Innendruck entgegenwirkt, wie die Behandlung mit Blebbistatin und das genetische Knockdown zeigten. Die Hemmung von HyNMII führte zu einer Depletion früher morphogenetischer Nematocystentadien durch die Destabilisierung der Schlauchstrukturen. Darüber hinaus wurde in dieser Arbeit das Glykoprotein NOWA als Hauptbestandteil des Schlauches neu definiert. Es wurde gezeigt, dass NOWA wesentlich am Prozess der Schlauch-Invagination beteiligt ist, was durch genetischen Knockdown und Live-Imaging unter Verwendung einer transgenen

NOWA::NOWA-GFP-Linie belegt wurde.

Die in dieser Arbeit gezeigten Daten klären somit eine neuartige Funktion für Aktomyosin-Netzwerke in der Morphogenese der Cniden der Nesseltiere, einem der komplexesten Organellen im Tierreich.

Acknowledgements

This Ph.D. journey went smoothly because of the extensive support of certain people. First and foremost, I would like to thank my supervisor, Dr. Suat Özbek for not only his excellent supervision but also for his constant encouragement and valuable feedback. Thank you for giving me the opportunity to work on such an exciting project. I have learned a lot from you, and I cannot imagine navigating through the tough phases over the course of my Ph.D. without your support. Next, I would like to thank my TAC committee - Dr. Thomas Holstein and Dr. Rainer Pepperkok. I am truly grateful for your consistent scientific feedback which directed me to shape this project. I would also like to thank my examiners Dr. Steffen Lemke and Dr. Nicholas Foulkes for agreeing to participate and assess my final defense.

I would like to extend my gratitude to other members of Özbek lab. Gideon- Thank you for always making time for our little scientific (or sometimes goofy) conversations during work. It kept me going and made the workplace much more fun for me. Bérénice- Thank you for all your help and support, I always used to look forward to our coffee breaks and discussions, and I miss having you around. I am also grateful for all the students, whom I had the pleasure of supervising. It was a great experience to work with each one of you and really helped me to grow as a scientist.

Thank you to all the 6th-floor members- I was always excited to participate in social activities and fun events. It kept me motivated during my entire time here. I am fortunate also to find some great friends here. Marie- I cannot thank you enough for your endless support and encouragement. I was really glad to have you around and for the time we spent together brainstorming solutions to all my problems personally and professionally. I would also like to thank Tracy and Laasya for diligently reviewing my thesis and for their valuable feedback.

I am very thankful to my friends like my family- Sunidhi, Ritika and Alyona, you guys have made me feel at home even so far away from home. I am very thankful for your moral support. Abhinav- For your constant support and help during my work as well as writing. You are always there for me whenever I need a friend or a mentor, I am truly grateful to have you in my life.

Lastly, I would like to extend my gratitude to my family, Mummy, Papa, and Chunnu- Even though we are miles away, you always manage to encourage me and bring a smile to my face. Without your selfless sacrifices, prayers and unshakable belief in me, I cannot imagine achieving anything. Your love and support have been my foundation. I am truly grateful always and forever.

Contributions

The work presented in this thesis is my own, but I would like to mention some valuable contributions by the following people: The experimental work and image acquisition related to NOWA protein were partially done by Urška Knez Štibler. The Western blot analysis was done in cooperation with Maike Fath and Annika Ohl. Electron microscopy data was acquired by Michael W. Hess and his team (Karin Gutleben and Barbara). The mathematical modelling was performed by Moritz Mercker. The schematics were designed by Bruno Gideon Bergheim. Preliminary data such as WISH analysis and cytochalasin D-related data was partially acquired by Björn Eismann. Time-lapse imaging was performed in collaboration with Ulrike Engel (Nikon Imaging Center Heidelberg) and Annika Ohl. Yukio Nakamura and Patrizia Adamczyk helped with preparing the transgenic NOWA::NOWA-GFP. I have also indicated these contributions in the respective figure legends.

Publication of the thesis work

The work presented here is submitted for publication and is currently under revision under the Manuscript Number: ISCIENCE-D-22-03659

Contents

List of Figures

List of Tables

Chapter 1

Introduction

1.1 General introduction: Cell morphogenesis and cytoskeleton

In nature, the morphogenesis of an individual cell is an exquisitely organized process that depends on a series of biological operations such as cell division, specific oriented cell growth, cell shape changes and cell death [1]. Apart from these cellular mechanisms, for a cell to grow into a precisely defined shape or form, it needs building materials such as different types of proteins, to be transported from the cytoplasm to the cell surface and back. With the development of cell and molecular biology, several proteins have been characterized over time and can be distinguished based on their structure, functions, and composition. Some examples of protein functions are as follows –structural proteins such as keratin, elastin and collagen provide structure and support to the cell [2,3]; enzymes are the type of proteins that act as catalysts to drive the biological processes, for example, amylase, lipase and pepsin are digestive enzymes [4,5]; and motor proteins such as myosin, kinesin and dynein facilitate the cargo transport, cell movement and signalling [6].

This intracellular transport of the proteins is dependent on the cell's cytoskeleton [7–9] which is collectively formed by actin, microtubules, and intermediate filaments [10]. The name 'Cytoskeleton' originated due to its role in the maintenance as well as modification of the cell's shape during its movement. The cell movement and shape change are primarily driven by the forces generated by actin and microtubules which together make up the paths where cargos are anchored, delivered, and transported [11]. Cargo vesicles carry the building material of the cell such as proteins, enzymes and signalling molecules, which fuse to the cell membrane (figure 1.1). This not only provides the necessary structural support to the cell but also defines the cell's physiology [12,13]. The molecular motors function as an important part of the cytosolic machinery and help in the organization of cellular components and cell communication. For instance, microtubules act as tracks where their asso-

ciated binding motor proteins- kinesin and dynein act as cargo to transport proteins, organelles (for example, mitochondria), and also conduct internal transport within cells such as neurons (figure 1.1B). Microtubules also play a major role in mitosis (cell division) where they form centrioles. This in turn helps in the formation of the mitotic spindle by specialized interpolar and astral microtubules. It is also well established that the microtubule network along with its motor protein dynein maintains the structure of Golgi [14].

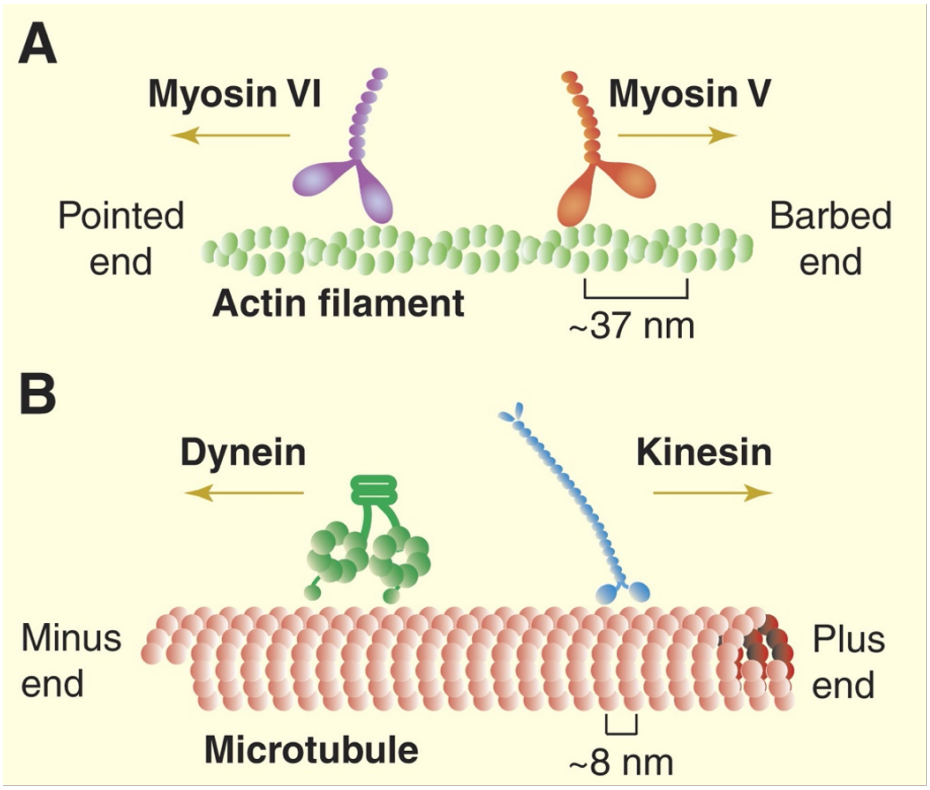

Figure 1.1 Cargo transport facilitated by cytoskeleton motors.
A) Two types of myosin motors slide along the actin bundles in a directional pattern during cargo transport. **B)** Kinesin and Dynein motors move along microtubules in a polarized manner. Figure adapted from [15].

1.1.1 Actin-Myosin cytoskeleton

Another cytosolic machinery is mediated by interactions of actin and myosin proteins. Myosins are a large superfamily of actin-dependent molecular motors [16]. Most of the myosins belong to class II which was also the first isolated form of myosin. The phylogenetic analysis of myosins has totally revealed 18 classes of distinguishable myosin types [17]. Myosins share a common domain architecture which includes subdomains as follows- first, the actin and ATP binding 'motor

domain' which are generally more conserved; second, light chain or calmodulin binding 'neck domain' which in turn binds to a helical sequence called as 'IQ motif' [18]and third, coiled-coil 'tail domain' which has the ability to dimerize and serve as an anchor during intracellular cargo transport and further orients the motor head. The domain organization of myosins can be seen in figure 1.2.

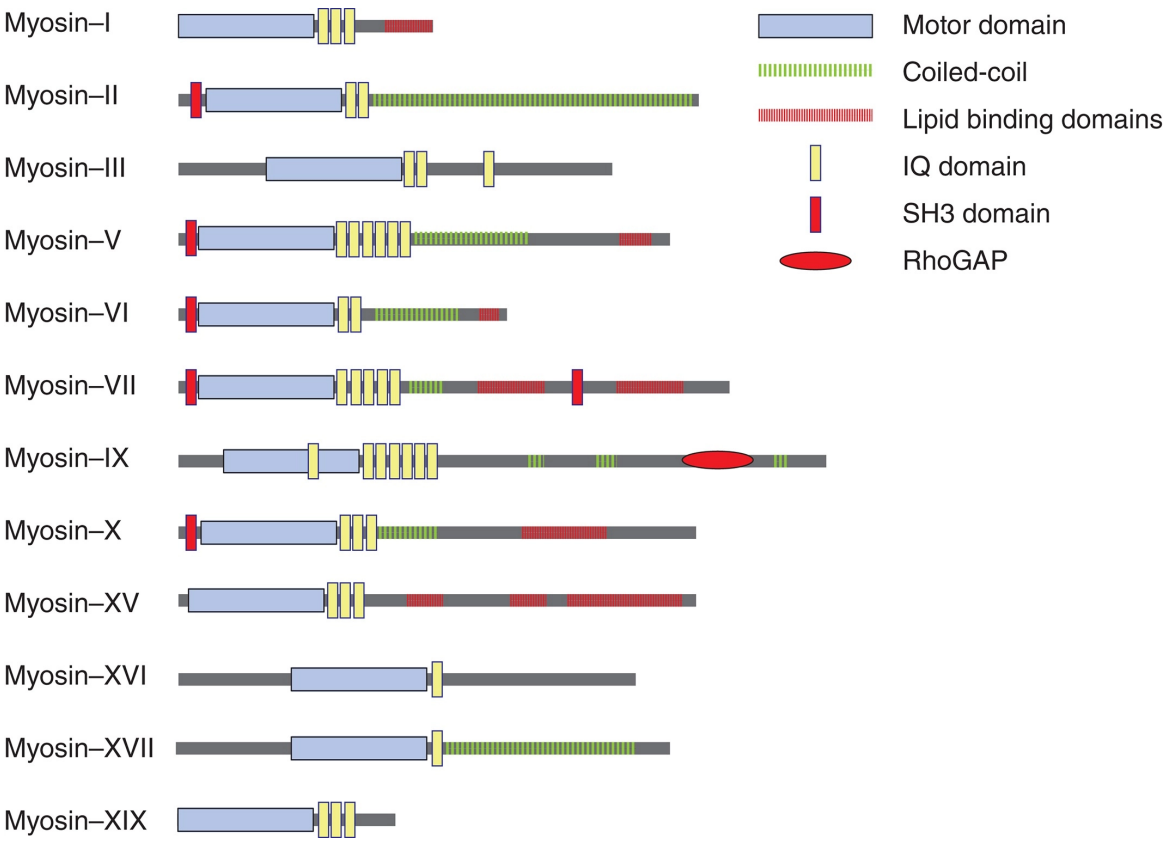

Figure 1.2 Domain organization of the members of the myosin family.
Basic domain architecture of members of the myosin family, representing their N terminus conserved globular motor domain, which is common to all myosins, C terminus coiled-coil tail domain, IQ domains and SH3 domains are not commonly present in all types of myosins. The motor domain consists of ATP binding site (not shown here). Figure adapted from [19].

Dynamic microfilaments made up of actin proteins serve as transport pathways for the motor protein myosin to act as a cargo for the transport of vesicles and ribonuclear proteins (figure 1.1A). Along with actin, they constitute the major contractile proteins in cardiac, skeletal, and smooth muscle. Smooth muscle expresses two isoforms of myosins- Smooth muscle (SM) myosin and non-muscle (NM) myosin. Based on the close relation of heavy chains (MHCs) and RLCs phylogenetically, Non-muscle myosin II is strikingly similar to smooth muscle myosin II [20–22]. The similarity is also due to the phosphorylation of the two myosins at the conserved

site on RLC by kinases [23]. Both SM RLC and NM RLC have been shown to participate in SM muscle contraction independently [24]. The muscle contraction is initiated by cross-bridge sliding of myosin II thick and actin-based thin filament. Interaction of myosin heads (cross-bridges) with thin filaments of actin generates a force which results in filament sliding. This is achieved by energy provided by hydrolysis of ATP molecules and alteration in the structure of cross-bridges attached to actin (figure 1.3). This leads to the conversion of chemical energy into mechanical energy, a mechanism called as 'power stroke'. Power stroke drives muscle contraction, which is vital for living processes such as breathing, blood circulation, lifting objects and pumping blood [25, 26].

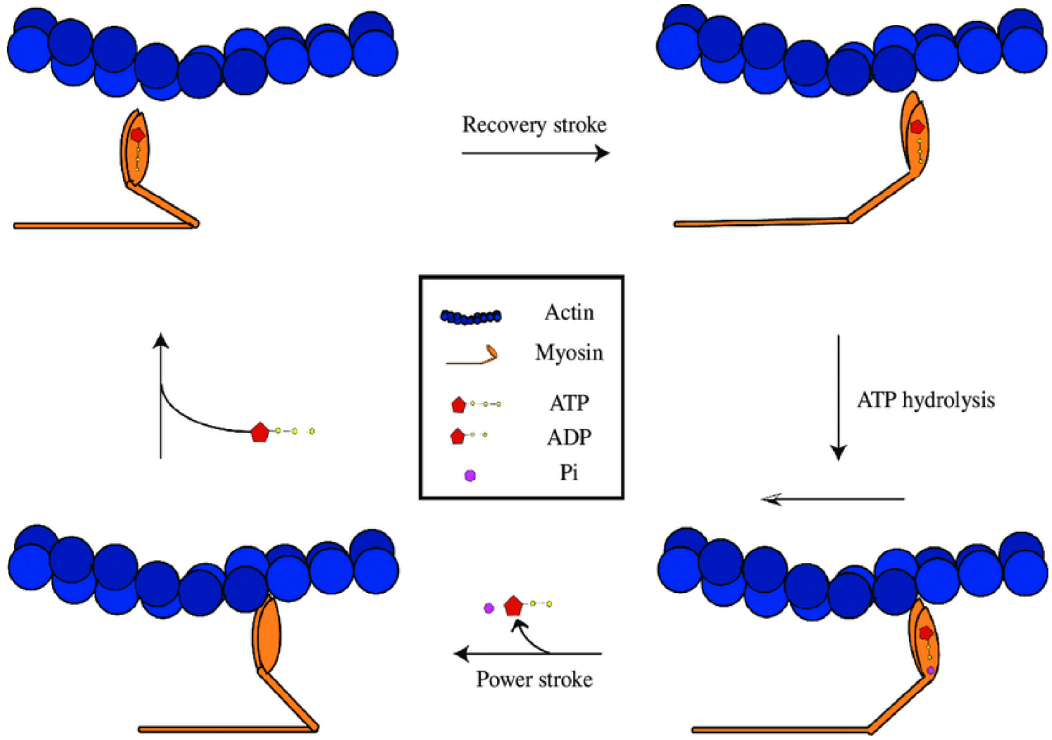

Figure 1.3 Cross bridge cycle during muscle contraction.
Myosin II binds to the actin cytoskeleton and slides on the actin fibre by hydrolysis of ATP, the mechanism is called 'power stroke', hence facilitating muscle contraction. Figure adapted from [27].

The distribution of classes of myosin is obviously not uniform in all living organisms. To investigate this, different model organisms have been used to study and furthermore probe the functions of these motor proteins. Budding yeast (*Saccharomyces cerevisiae*) was found to have only class I, II and V myosins [28, 29], while the genome analysis of *Caenorhabditis elegans* comprised of myosin from classes I, II, V, VI, VII, IX and XII. Myosin V and VI which move on opposite ends of bipolar

actin (figure 1.1) are known to be involved in the transport of cargo vesicles and protein complexes along the actin filaments [30]. Myosin I and VII are known to participate in cell-signalling pathways [31, 32]. A previous study stated that 'p200', a homologous protein to human non-muscular myosin II was detected on TGN-associated vesicles. Since it was shown to participate in the release of vesicular stomatitis virus G protein, [33] this study supported the role of myosin II in the assembly as well as the fission of transport vesicles. Previously, proteome analysis of *Hydra* nematocysts was carried out which revealed only one prominent motor protein of non-muscular myosin II type. In this work, the focus is on this specialized motor protein specific to *Hydra* nematocysts [34].

1.2 Cnidarians phylum

Cnidarians are a diverse clade of organisms, arising from early branching metazoans and a sister group to Bilateria. They are one of the most ancient existing phyla, originating approximately 700 million years ago [35–37]. They consist of about 9,000 species and are further subdivided into two categories anthozoans (e.g., Sea anemones and corals) and Cubozoa, Hydrozoa, and Scyphozoa collectively called medusozoas (e.g., Jellyfish and *Hydra*) (figure 1.4) [35, 38, 39]. One major difference between the two classes of cnidarians is that the anthozoans do not have a free-swimming stage in their life cycle as medusozoas. Due to their unique phylogenetic position, cnidarians serve as insightful model organisms in the field of evolutionary biology. They can not only regenerate their amputated body parts such as the head or foot but also from reaggregates when dissociated into single cells. Their remarkable regenerative capabilities are mediated from epithelial stem cells by a process called as morphallaxis in which the tissue patterning can take place without cell proliferation. Apart from the other common characteristics which cnidarians share, one of the most interesting common features of this phylum is a specialized 'stinging cell' called nematocyst or cnidocyst [40]. These loaded explosive cells constitute the taxonomically restricted feature of this phylum. Nematocysts are mainly used to capture food, while in some species within the phylum, these are also used for other activities such as predation, adhesion, locomotion, and defence [41, 42]. As after discharge, nematocysts must be constantly renewed, cnidarians invest a great deal of their energy in the maintenance of nematocysts.

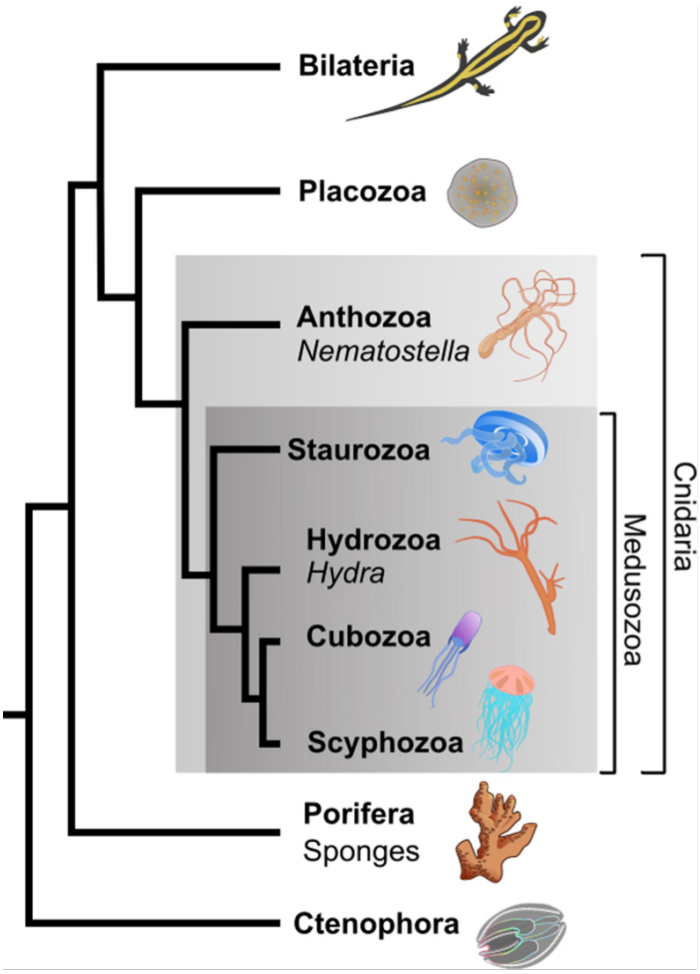

Figure 1.4 Cnidarian phylogeny.
Phylogenetic tree of the cnidarian phylum representing its position as a sister group to bilaterians. Cnidarians are subdivided into anthozoans and medusozoans. *Hydra* belongs to the medusozoans. Figure adapted from [43].

1.2.1 *Hydra* as a model organism

Hydra is a freshwater polyp which belongs to the medusozoan clade of cnidarians (figure 1.4) and has emerged as a very popular model organism amongst developmental biologists. It is known for its regenerative capability and was the first organism ever to be studied as a biological model in the field of developmental and evolutionary biology. It serves as an ideal research model due to its simple body plan described below. It takes about 2 to 3 days to regenerate the whole body. Its unique feature of rebuilding the entire body from dissociated cells makes it a fascinating species to address long-standing questions in developmental biology [44, 45]. Unlike other cnidarians, it has a reduced life cycle and exists only as

a polyp without any larval stage. It is radially symmetric like other cnidarians and diploblastic in nature and consists of only two germ layers- ectoderm(external) and endoderm(internal) [46]. The two layers are separated by a central extracellular matrix called Mesoglea (figure 1.5c). The other body parts can be divided as follows- the hypostome or the head region with a mouth opening which is surrounded by a ring of tentacles, the foot region at the base with a pedal disc and the hollow body column in between the head and foot consisting of the gastric cavity (figure 1.5b). The two germ layers comprise distinguishable cell types (figure 1.5c). There are three stem cell lineages which are responsible for self-renewal and at the same time populate the rest of the cells. The endodermal and ectodermal stem cells give rise to respective epithelial cells and interstitial stem cells give rise to neurons, gland cells, gametes and nematocytes [47–49].

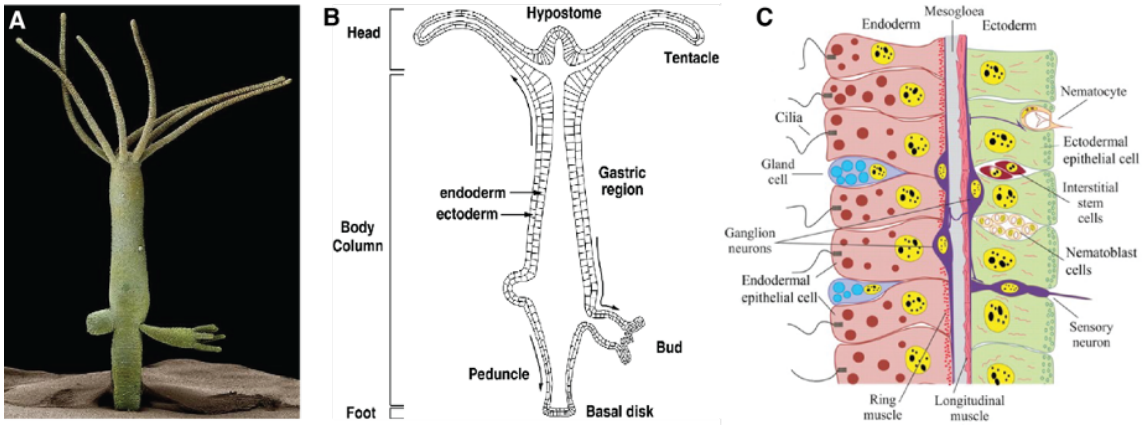

Figure 1.5 *Hydra* anatomy and germ layers.
A) Scanning electron microscopy image of *Hydra* demonstrating budding, **B)** Schematic representation of *Hydra*'s body plan **C)** The two germ layers ectoderm and endoderm along with the middle extracellular matrix-like layer. All the distinguishable cell types are marked which are distributed in the two layers. Adapted from A: [50], B: [51], C: [52].

Most of the studies in *Hydra* have been focused on tissue regeneration, symbiosis, innate immunity [53], and pattern formation but less is known about the molecular factors involved in the development of their phylum defining specialized stinging cells. The nematocysts after going through all their growth phases get docked into another cell called a battery cell [54]. The details of nematocyst synthesis and formation are explained in the following section. In this work, an attempt has been to visualize the development of nematocyst with the help of proteins already known to be specific to the nematocyst and further investigation of the developmental process of nematocyst from the perspective of the cytoskeleton.

1.3 Nematocysts structure and composition

The nematocysts, one of the most ancient cellular organelles act as venomous exocytotic weapons. They are the distinctive characteristic trait of the cnidarian phylum and play an integral role in predation, adhesion, and locomotive activities [40]. Nematocysts consist of four main structural parts, the capsule body (the outer cylindrical structure with a multi-layered wall), tubule (an inner thread-like structure which is released upon discharge and acts as the penetrant tool), operculum (head), and spines adorning the tubule [49]. The apical side is connected to the cnidocil which serves as a mechanosensory apparatus (figure 1.6c). However, spines might not be present in all types of nematocysts.

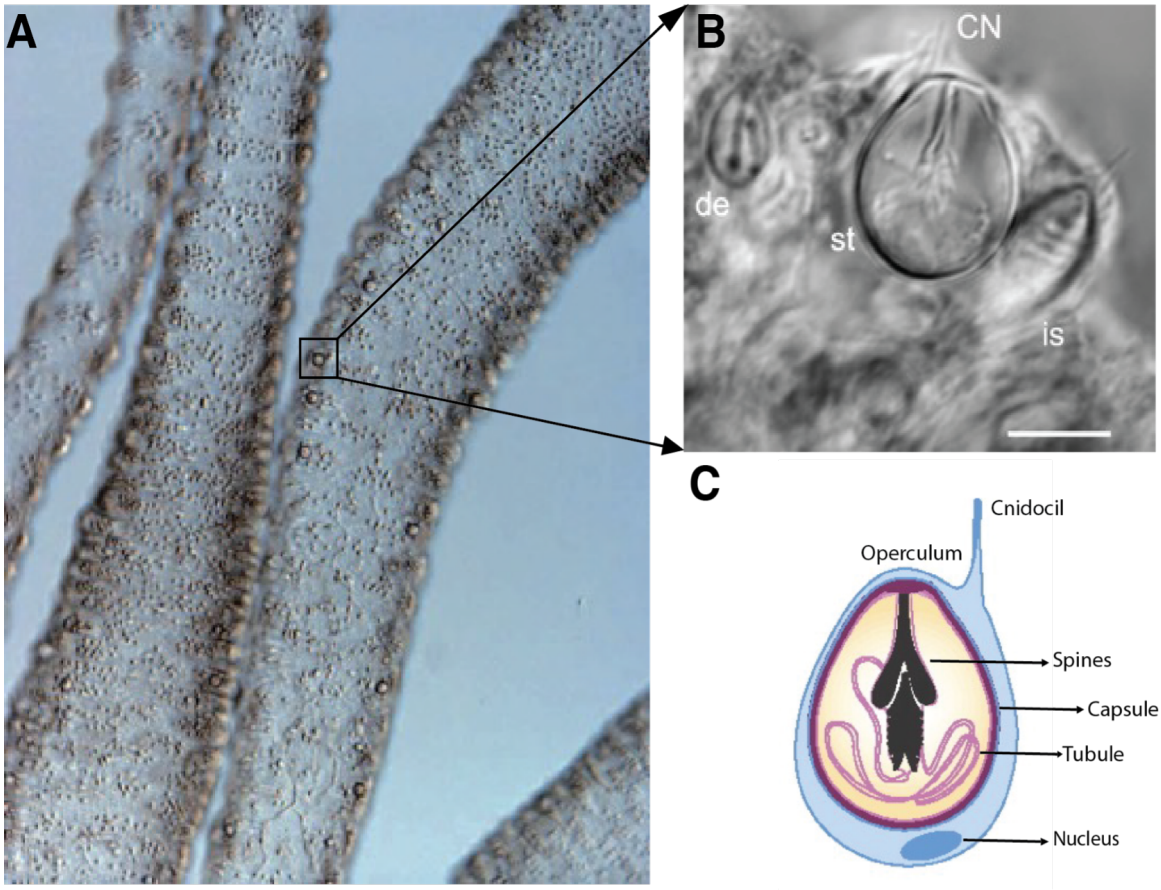

Figure 1.6 Nematocyst docked in the tentacles.
A) Mature nematocysts are exported to the tentacles where they are mounted in the epithelial cell layer, docked at the apical side of another cell called a Battery cell (st-stenotele, de-desmoneme, is-isorhizas, CN-cnidocil). **B)** Differential interference contrast (DIC) image of a battery cell with different types of nematocysts. **C)** Schematic of a nematocyst with labelled structural parts. Figure adapted from [55].

The structural morphology can vary from one nematocyst to the other and there are 25 -30 different types of nematocysts [41, 56, 57]. In *Hydra* there are four different types of nematocysts [58], and they are differentiated based on their size, shape, structure, and function [59, 60]. They are as follows: stenoteles, which represent the largest capsule type. They comprise large spines attached to the bottom of the tubule and act as the main penetrant capsule type; holotrichous isorhizas, act as glutinants but have also been implicated to have a stinging function; the atrichous isorhizas, are similar to holotrichous but differ slightly in size and lastly, the desmonemes, slightly pear-shaped, the smallest capsule type with a characteristic short, coiled tubule [60] (figure 1.6b).

It was shown previously, that gametes (sperm cell precursors) and somatic cell types such as neuronal cells and nematocytes arise from the same population of interstitial stem cells [61]. Thirty percent of the interstitial stem cells divide to proliferate into nematocyte progenitor cells in 2-4 days. This leads to nematocyte nests that further lead to the emergence of nematocysts of one type which grow within these nematocytes [62]. This development process takes place in the body column of the animal where all these nematocytes are interconnected to each other through cytoplasmic bridges and exist in the form of a syncytium [63]. The phase of capsule differentiation takes place for around 2.5-3.5 days. These nematocytes interconnected to each other in one nest undergo synchronized growth stages. The developed nematocysts, once fully matured, separate and migrate along the epithelial cells towards the tentacles to get incorporated into another cell called a battery cell [63]. A schematic elucidating these developmental stages of nematocyte formation, from the TGN to its maturation, is shown in figure 1.7.

1.3.1 Formation of the nematocyst

Nematocysts are the product of a giant post-Golgi vesicle which is synthesized in the cytoplasm of a specialized cell called a nematocyte. They undergo a series of developmental stages beginning with a vesicle primordium arising from the Golgi apparatus (figure 1.7a) [64, 65]. This is formed by the continuous incorporation of secretory vesicles harbouring secretory proteins that assemble in the growing nematocyst vesicle to form the matrix-like structure of the capsule wall (figure 1.7b) [58]. The capsule wall formation is followed by tubule morphogenesis which takes place at the apex of the capsule body. This is initiated by a membrane constriction which results in the onset of membrane tubulation, and the tubule then starts to elongate externally (figure 1.7c) [66]. After the elongation process is terminated, the tubule inverts and invaginates into the capsule (figure 1.7d). Here it coils

tightly, this is followed by hardening of the capsule wall (figure 1.7e) [67]. As the nematocyst structure matures, the capsule is filled with a very high osmotic pressure of 150 bar produced due to the synthesis of charged poly-gamma-glutamate polymers and the influx of associated cations [68, 69]. Mature nematocysts in the tentacles are in contact with sensory neurons and are coupled to mechanoreceptors called cnidocils which react to chemical and mechanical stimuli leading to the discharge of the stinging cell (figure 1.7f) [70]. The firing of nematocytes is known to be the fastest reaction in nature. The initial phase takes place in less than 700 ns at approximately 5 million x g acceleration [71]. The entire action of the release of the tubule and penetration into the dermis of the prey takes less than 3 milliseconds which is in the range of technical bullets. The discharge of nematocysts leads to a dramatic change in the volume of the capsule which gets reduced to 50% of its original size [71, 72].

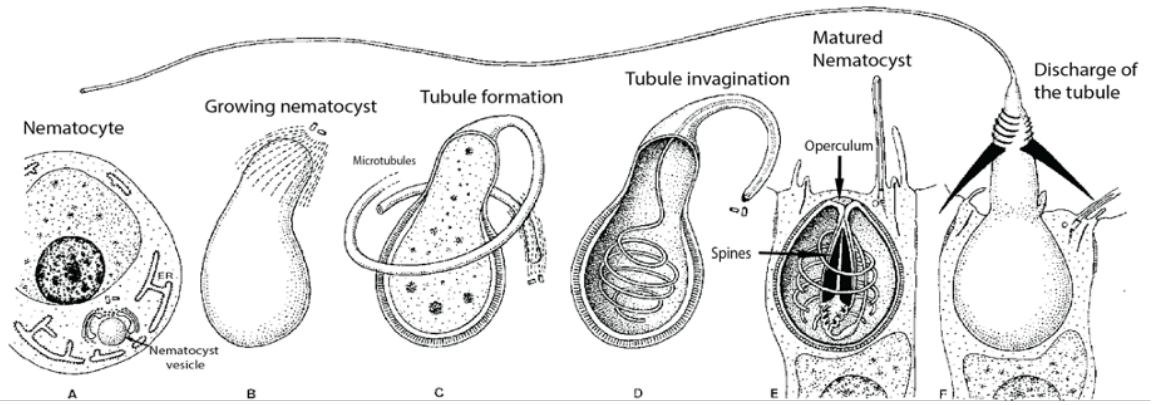

Figure 1.7 Nematocyst morphogenesis.
A) Beginning of nematocyst synthesis in a giant TGN primordium. **B)** Formation of the shaft region of a growing nematocyst with a pair of centrioles,[6] microtubules and TGN secretory vesicles at the apex of the growing vesicle. **C)** Formation and elongation of the external tubule are still accompanied by microtubules and TGN vesicles at the tip of the growing tubule. **D)** Tubule invagination process where the tubule is inverting into the capsule partially, the difference in the thickness of the external and partially invaginated tubule can be noticed clearly. **E)** The matured nematocyst with a tightly coiled tubule inside and is embedded in the battery cell. **F)** Discharge of the external tubule as a response to the external tubule. Figure adapted from [58].

1.3.2 Molecular composition in nematocyst morphogenesis

Nematocyst maturation is a complex intracellular process requiring a meticulous synchronization of several molecular factors to accurately reach its desired

outcome. Studying this process in detail can help shed light on the establishment of the roles of novel proteins and their interactions and provide more insights into the field of developmental and evolutionary biology. According to a recent study, the importance of studying these novel proteins was outlined in understanding the origins of new cell types [73]. Nematocytes are known to be neuronal cells arising from interstitial stem cells. A novel gene type has been shown to act as a molecular switch to decide the fate of nematocysts and simultaneously suppress the neuronal traits [74]. Hence, with the increasing acknowledgement of the importance of this highly specialized cell, extensive research has been conducted over the last few decades, to understand and unravel its sophisticated yet complex structure.

With the advances in research and technology, analytical tools such as mass spectrometry, Position-Specific Iterative Basic Local Alignment Search Tool, and microscopy techniques such as high-resolution imaging transmission electron microscopy, has made it possible to visualize this fascinating projectile organelle even on a molecular level. A previous report on the protein composition of *Hydra* nematocysts revealed that there are 410 proteins involved in its composition (figure 1.8). The proteins were categorized into three main classes: toxins, structural and novel proteins [34].

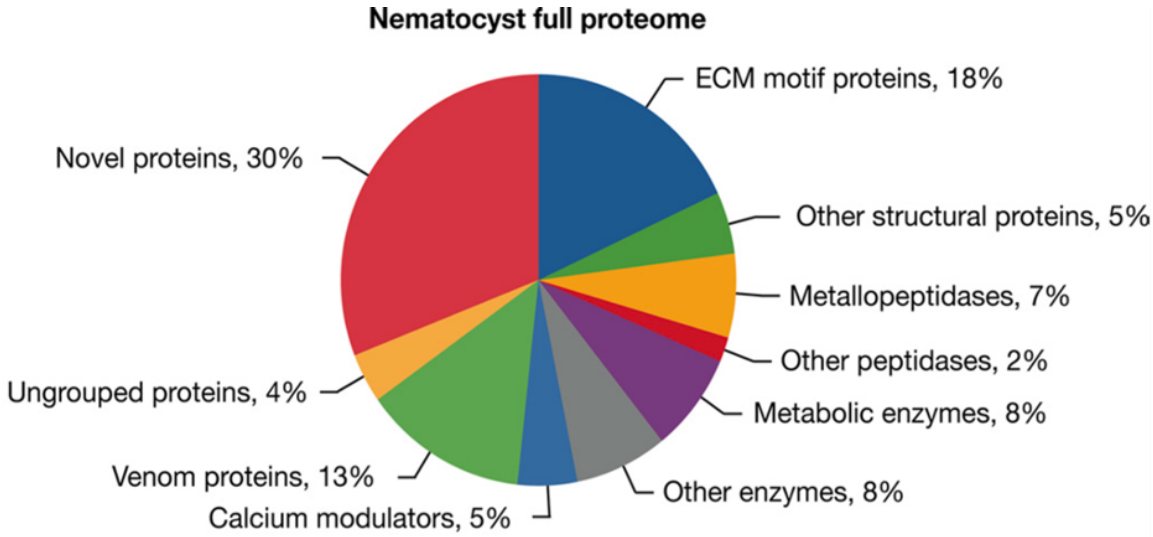

Figure 1.8 Proteome of *Hydra* nematocysts.
Distribution of proteins found in the isolated discharged capsules of different types of nematocysts. Proteins are categorised into groups based on their known functions. The domain structure of some of these proteins is shown in figure 1.9. Figure adapted from [34].

It was found that the largest group of annotated proteins were the structural proteins. These structural proteins had a domain characterization similar to ECM

motifs (figure 1.9). Amongst these, minicollagens constituted the largest family of proteins with 21 members. Minicollagens are a special group of short collagen proteins which are specific to the nematocyst which mediates the extremely high pressure and tensile strength of the inner wall of the matured capsule [75]. The domain structure of minicollagens consists of GLY-X-Y repeats in its centre flanked by a polyproline (PP) domain and cystine-rich domains (CRD) at the two ends (figure 1.9). The CRD domain was shown to participate in the formation of intermolecular networks which leads to wall compaction and capsule wall hardening [67]. A novel protein called Nematocyst outer wall antigen (NOWA) with homologous cysteine-rich domains at C-terminal as minicollagens was found to be involved in the formation of the more electron-dense outer layer of capsule wall [76] (figure 1.9).

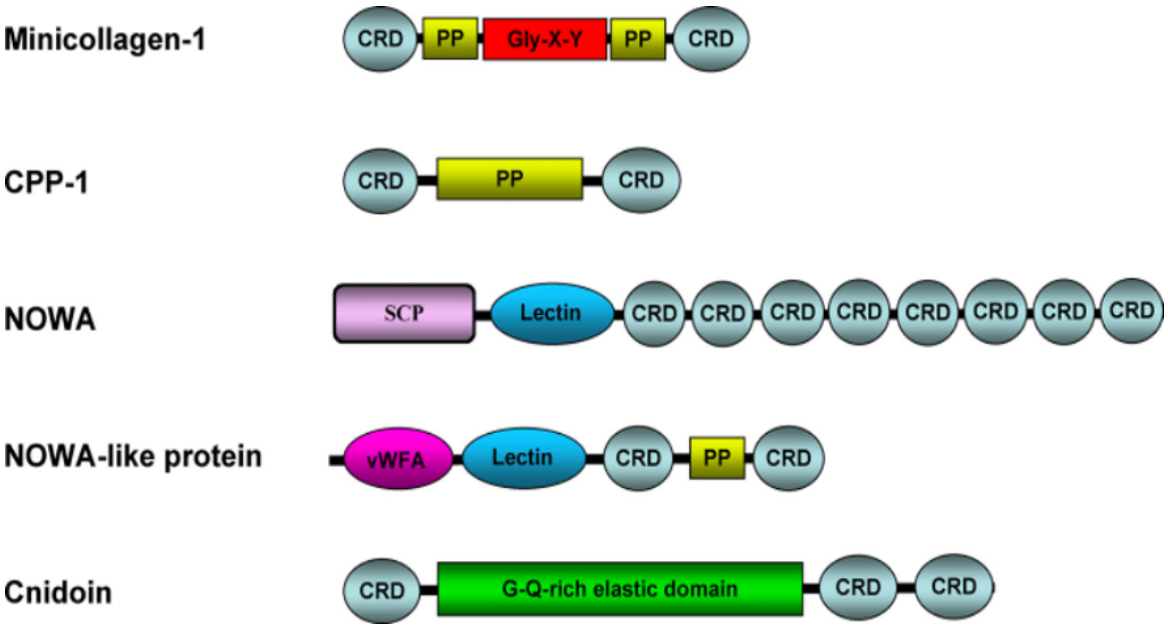

Figure 1.9 Domain structure of nematocyst ECM like proteins.
The domain architecture of annotated proteins found in the proteome participating in the structure of the nematocyst. The CRD domain is common to all the proteins and serves for cross-linking during maturation. Figure adapted from [34].

The localization and role of NOWA are reexamined and redefined in this project. Another novel protein, Cnidoin, with elastomeric functions was found to be co-localized with minicollagens. It is a non-collagenous structural protein and was found to be part of the inner wall of the nematocyst capsule. It is expressed exclusively in the developing nematocytes in the body column of *Hydra*. The molecular elasticity of Cnidoin gives insights towards the unusual biomechanical characteristic of nematocyst [77]. There are certain other proteins present that lack collagen se-

quences but are related to minicollagens, these are called Cnidarian polyproline-rich proteins (CPP). They have a signal peptide for secretion and possess nematocyst-specific propeptides. CPP-1, like minicollagens, has two CRD domains flanking a central polyproline domain [34](figure 1.9).

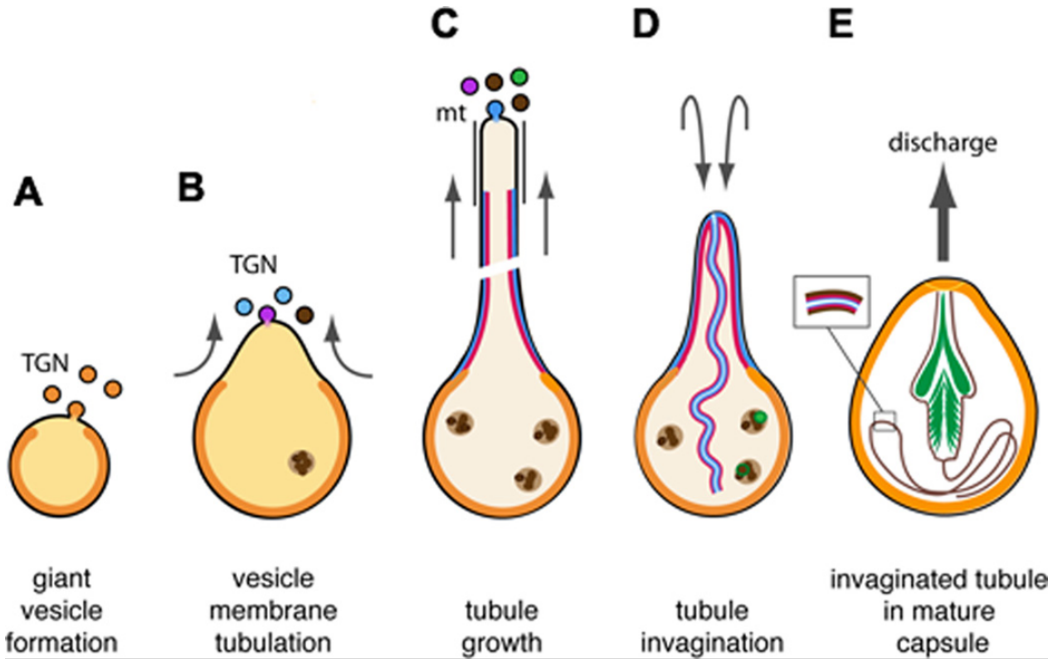

Figure 1.10 Schematic of the proteins involved during nematocyst morphogenesis. **A)** Minicollagen-1(NCol-1) (yellow) filled vesicles can be observed at the apex of the growing nematocyst vesicle at a very early stage, **B)** Chondroitin (blue) and Nematogalectin (Ngal) (red) and minicollagen-15 (NCol-15) (brown) along with NCol-1 fusing to form the capsule wall matrix at the apex. **C)** Elongation of the external tubule with Ngal forming the inner layer and chondroitin forming the outer layer, the process is still accompanied by a continuous fusing of TGN vesicles at the tip of the growing tubule. **D)** Invagination process with everted tubule inside the capsule with a highlighted layer of proteins localized at respective positions. **E)** Mature capsule with invaginated and coiled tubule with the formation of spines represented by localization of spinalin (green) protein. Figure adapted from [66].

There are a set of proteins that are identified exclusively to participate as molecular components of tubule morphogenesis. These are listed as follows- spinalin, minicollagen-15 (N-col-15) and nematogalectin. These proteins are incorporated in tubule morphogenesis at different time points; for example, Ncol-15 is added to the tubule only after invagination, while non-sulfated chondroitin was found to assist the tubule elongation or outgrowth and serves as a molecular scaffold for incorporation of minicollagens after the invagination process [66]. Nematogalectin is localized

on an inner layer facing the lumen in conjunction with chondroitin which forms an outer layer on the surface of the growing tubule [78]. Vesicles lined with chondroitin and nematogalectin have been observed right at the onset of membrane tubulation at the apex side of the capsule body (figure 1.10b, c). Spinalin is a glycine and histidine-rich protein exclusively associated with the spine structures which appear on the surface of the inverted tubule of certain types of nematocysts [79, 80]. The domain architectures of nematocyst-specific proteins are shown in 1.9.

It was also found that there was only one prominent motor protein as a part of the *Hydra* nematocyst proteome, and it was annotated to be a non-muscular myosin II type. Although the assembly of the stinging organelle is an integrated process of various molecular components, predominantly so far, structural proteins have been well-elucidated for their role in nematocyte morphogenesis, while there is data on the cytosolic machinery. Though microtubules were previously described to participate in the development process in the vicinity of growing capsule and tubule structures [76] [58], the role of other cytoskeleton proteins such as actin and myosin remains elusive. In this work, my focus is to address the role of nematocyst-specific non-muscular myosin II in the morphogenesis of the nematocyst.

1.4 Aims

During nematocyst development, the tubule morphogenesis process begins with a membrane constriction at the apical end of the capsule, followed by the tubule elongation and maturation phase with invagination and coiling. The molecular basis underlining these processes has so far been poorly understood. With this thesis work, I aimed to investigate the molecular aspects of tubule morphogenesis using nematocyst development in *Hydra* as the research model. The main research questions can be summarized as follows:

1. What molecular factors drive membrane constriction during tubule formation?

2. Which factors drive the tubule invagination process and is this an ATP-driven or a spontaneous process based on a molecular “zipper”?

The thesis is built upon the previous work of Prakash G. Balasubramanian, in which the *Hydra* nematocyst proteome analysis was performed. The proteome data revealed 410 proteins participating in nematocyst morphogenesis but contained only one prominent motor protein of non-muscular myosin II type. Nematocyst development involves continuous structural changes and modifications, and these mechanisms are normally driven by the cell cytoskeleton such as the actin cortex. Hence,

the drastic structural deformation events during nematocyst morphogenesis such as membrane constriction during the onset of tubulation might be due to actomyosin contractile movements. Moreover, given the previous findings about non-muscle myosin II during cellular events, it was hypothesized that HyNMII could be an ideal candidate to answer the above two questions. While there are some structural proteins which have already been established to play a role during the development of nematocysts, not much is known about the involvement of motor proteins such as myosin II. Thus, the overarching goal of my thesis was to investigate the role of HyNMII in the tubule morphogenesis process during the development of the stinging cell. To achieve this, firstly, I localized HyNMII during nematocyst morphogenesis using a polyclonal antibody specifically raised to bind its head domain. To investigate the function in an elaborate manner, firstly, I inhibited the HyNMII gene expression through genetic knockdown techniques and secondly, I studied the developmental process after using inhibitory drugs specific to the protein of interest such as actin or myosin II in this case.

As part of this thesis work, the role of NOWA protein was also redefined as a prominent tubule-specific protein, which was previously classified as a capsule wall-specific protein. NOWA was essentially used as a molecular marker to analyze the role of HyNMII during the tubule maturation process, but interestingly, it was found that NOWA is an essential molecular factor driving tubule invagination by a proposed molecular zipper process.

Chapter 2

Results

2.1 Identification of a non-muscle myosin in *Hydra* nematocyst proteome

Nematocyst formation is one of the most astonishing processes in nature, involving the orchestration of a series of molecular factors. Therefore, determining which proteins are involved in nematocyst formation is fundamental to understanding this fascinating process. Using mass spectrometry and one- and two-dimensional electrophoresis, the proteome analysis of *Hydra* nematocysts was carried out on different types of isolated undischarged capsules (stenoteles, desmonemes, atrichous and holotrichous isorhizas). This proteome analysis, performed by a former Ph.D. student from our lab, led to the identification of 410 unique proteins participating in nematocyst morphogenesis [34]. These proteins were categorised based on their Gene Ontology (GO) classification, such as structural, enzymatic, venomous, and others. Amongst these, only one prominent motor protein was recognised, which was found to be of myosin II type (T2MG36), hence named *Hydra* nematocyst specific Non-Muscle Myosin Type II (HyNMII).

With the help of protein search and alignment tools such as Position Specific Interactive Basic Local Alignment Search Tool (PSI-BLAST) [81], InterProScan [82], ExPASy-Protpram and Conserved Domains Database, the analysis of HyNMII was used to predict its structure, function, and homology. The in silico amino acid sequence analysis predicted a primary structure of 1945 amino acids with a molecular weight of 224.62 kDa ([34])(figure 2.1a). Moreover, the respective gene sequence was also recently identified as a member of non-muscle myosins(XM_047288384.1, *T2MG36*) [83].

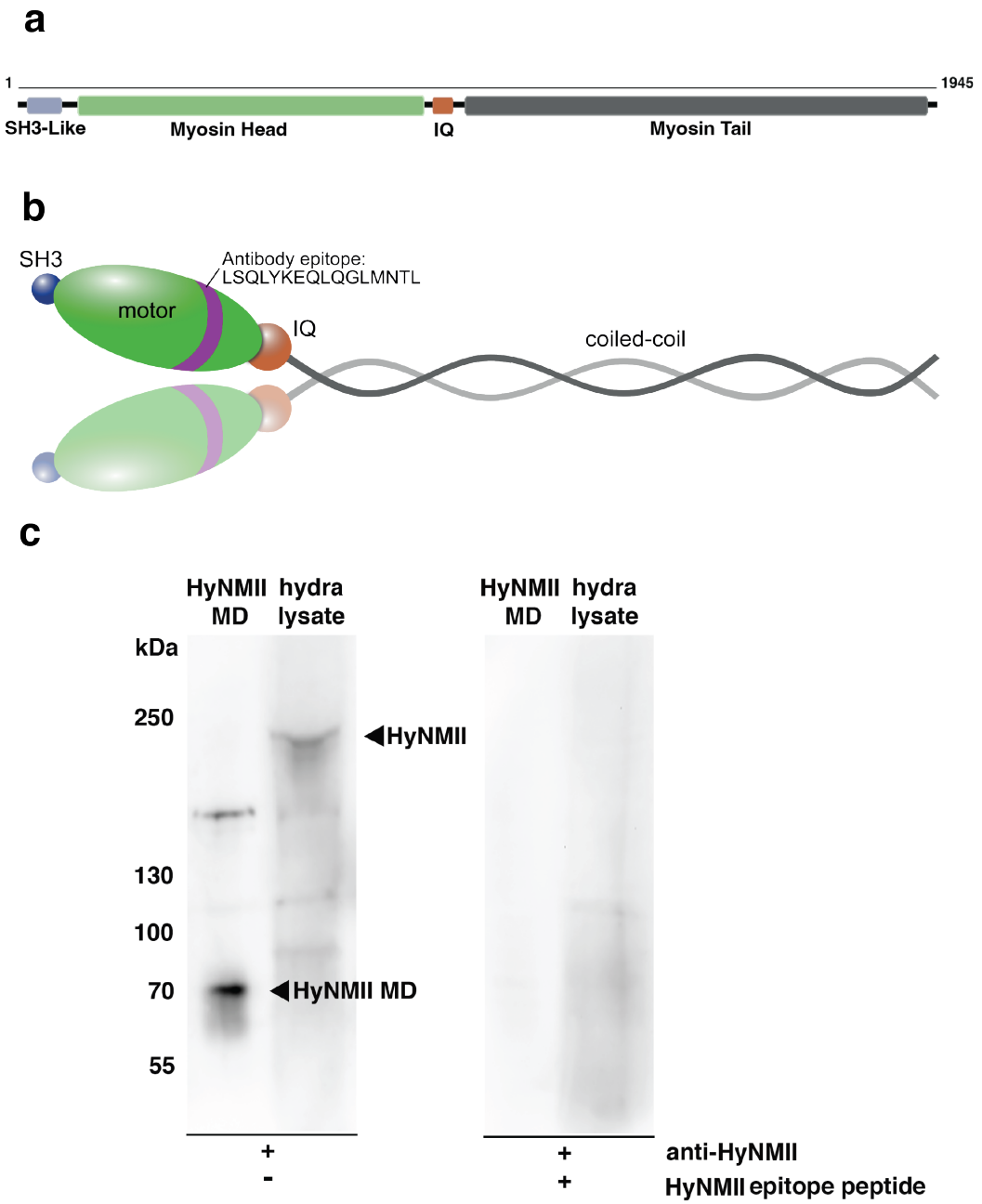

Figure 2.1 Domain organization and Western blot detection of HyNMII.

a) Domain characterization of (HyNMII) consisting of an SH3-like domain, a myosin motor head domain, an IQ motif and an alpha-helical coiled-coil tail. **b)** Representation of a typical NMII structure forming a homo-dimer. The antibody(ab) epitope region in the head domain is highlighted (the binding site of the polyclonal antibody raised against HyNMII). **c)** Western blot with HyNMII antibody showing a band at approximately 230 kDa for whole *Hydra* lysate (left) and 70 kDa for recombinant motor domain protein (left panel). These signals were effectively removed by antigenic peptide competition (right panel). Western blot analysis is done in cooperation with Maike Fath.

The domain architecture of HyNMII is similar to a typical non-muscular myosin II, comprising the domain organisation represented in figure 2.1a and b. At the N-terminus, a regulatory element is found, the src homology 3 (SH3) domain (six-stranded, antiparallel, β-barrel) which is present in almost all myosin type II proteins and participates in the assembly of protein complexes [84]. This is followed by a highly conserved globular head domain with an actin-binding site where ATP is hydrolysed, converting chemical into mechanical energy which in turn enables the power stroke [85, 86]. A short central IQ motif is located between the head and tail region, comprising Ca2+ and Calmodulin-like light chain binding sites [18]. At the C-terminus, an alpha-helical coiled-coil tail enables homo-dimerization and may also affect cell localization [87] (figure 2.1a,b).

To investigate the function of HyNMII, a polyclonal antibody was raised to bind a unique epitope in the head domain (figure 2.1b). Antibody specificity was analysed by Western blot using whole *Hydra* lysate and recombinantly expressed motor domain protein as shown in figure 2.1c. A band at approx. 230 kDa was detected in the *Hydra* lysate and at 72 kDa for the recombinant motor domain. Both bands correspond to the predicted molecular weight of the respective proteins. The Western blot signals were effectively removed by peptide competition using the antigenic peptide confirming the specificity of the antibody.

2.2 Expression pattern of *HyNMII* as detected by *in situ* hybridisation

To determine the mRNA(Messenger RNA) expression of HyNMII in *Hydra* polyps, the whole mount in situ hybridisation (WISH) was conducted. The mRNA encoding HyNMII was expressed in endodermal cells of the tentacles (figure 2.2a) as well as in early buds (figure 2.2a'). HyNMII expression in the tentacle region was strong at the base and faded towards the tips (figure 2.2a). These results are in line with the previously published gene expression patterns for HyNMII which was mainly detected in endodermal cells of the tentacle base region and the bud detachment site.

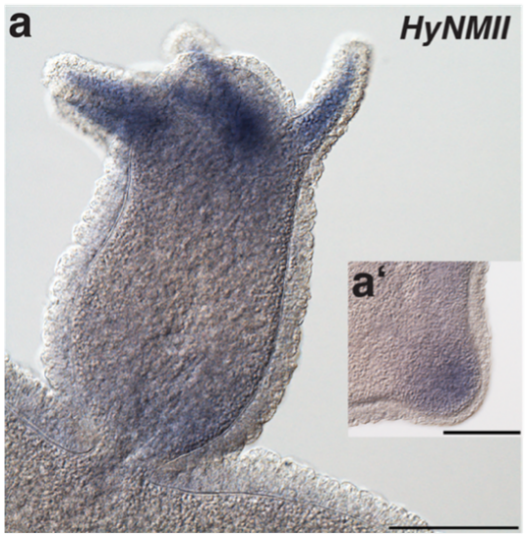

Figure 2.2 WISH showing the HyNMII expression pattern in *Hydra* polyps.
a) HyNMII is expressed in endodermal cells of the tentacles in steady-state polyps and in early buds **a')** as determined by ISH. Scale bars = 200 µm. WISH conducted by Björn Eisman.

2.3 Single cell expression of *HyNMII* in published cell clusters

The gene expression analysis for *HyNMII* at the single cell level was possible with the help of the published cell clusters by [88]. First, a BLAST search was performed to find the gene of interest using the 'Juliano aep' transcriptome database. This search revealed two genes of interest: *T2MHH5* (t10222aep), which was shown to be related to vertebrate striated muscle myosins and *T2MG36* (t8308aep), a non-muscle myosin according to recent phylogenetic studies [83]. The expression of these genes could be visualized using the transcriptome database along the trajectories of all cell lineages. Below, the t-distributed stochastic neighbour embedding (t-SNE) data distribution plots for cell clusters in ectodermal, endodermal, and interstitial cell lineages are shown (figure 2.3b, c, d), where it can be noted that an expression of *HyNMII* could be seen prominently in nematocytes in interstitial stem cells cluster (figure 2.3b). The comparative analysis of *HyNMII* and the *Hydra* muscle myosin homolog revealed that *HyNMII* was expressed both in epithelial cell lineages and throughout the whole developmental trajectory of nematocytes (figure 2.3a), compared to the muscle myosin, which appears to be expressed more strongly in ectodermal and endodermal cell lineages. Here, the size of the dot is directly proportional to the percentage of cells expressed and colour signifies scaled mean expression ranging from 0 (blue) to 1 (red).

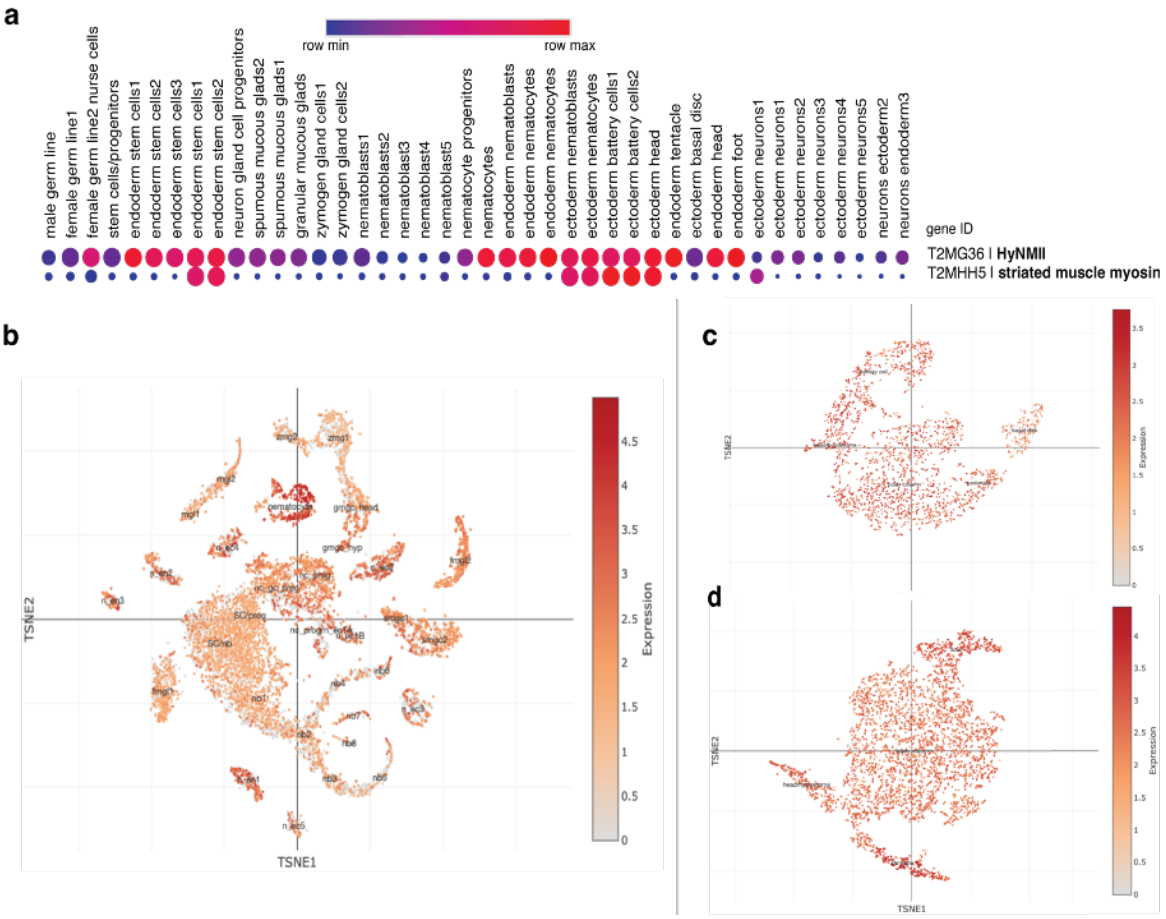

Figure 2.3 Single cell expression data of *HyNMII*.

a) Comparative expression analysis of *Hydra* muscle myosin (T2MHH5, t10222aep) and HyNMII (T2MG36, t8308aep) of the whole transcriptome clustering. Dot size and colour represent the counts of mapped transcripts in the respective cell cluster. **b)** t-SNE plot of interstitial stem cells cluster in HyNMII (t8308aep). **c)** t-SNE plot of ectodermal cluster in t8308aep. **d)** t-SNE plot of endodermal cluster in t8308aep. This single-cell expression data is obtained from the published cell clusters identified according to the presence and absence of marker genes by [88].

2.4 Localisation of HyNMII during the development of nematocysts

2.4.1 HyNMII localized during tubule morphogenesis shown by immunofluorescence

Nematocysts undergo a series of developmental stages beginning with a vesicle primordium arising from the Golgi apparatus [55]. A schematic elucidating these developmental stages of nematocyte formation, from the TGN to its maturation, is shown in figure 2.4a. The vesicle development has been described in detail

in the previous section (section 1.4) and results in the formation of a functioning mechanosensitive nematocyst structure. There are methods with which it is now possible to capture these developmental stages and visualise them with fluorescent tags associated with a target protein or specific antibodies [89].

Employing immunohistochemistry, I wanted to elucidate the stages of nematocyst morphogenesis in which HyNMII is involved and gain insights into its localisation in the nematocyte structure. Using the primary antibody raised to bind the head domain of the HyNMII protein, HyNMII was detected in *Hydra* whole mounts. This allowed the localization of HyNMII during different stages of development as shown below in figure 2.4b-i. HyNMII could be visualised mainly at nematocyst tubules in different types of nematocyte nests as shown in figure 2.4b. To understand the organisation of HyNMII and get a more defined and distinguishable localisation on the nematocyte structure at various stages of development, a co-immunostaining along with the capsule wall marker, cnidarian poly-proline protein (CPP1) [34, 90] was performed. It was found that HyNMII is strongly associated with tubule morphogenesis at different stages of development as shown below in closeups for two different types of nematocyte- stenoteles (figure 2.4d-f) and isorhizas (figure 2.4g, h and i). HyNMII starts to bind to the tubule at an early stage, from the onset of membrane tubulation (figure 2.4d,g; stage I in figure 2.4a). Here, it forms a collar structure around the neck of the outgrowing tubule. In the following developmental stages, it is located along the full length of the external tubule for the entire duration of the elongation process (figure 2.4e and h). This is followed by tubule invagination and coiling inside the capsule body (figure 2.4f and i). These three stages were most prominently visible in different types of nematocyte nests in the body column of *Hydra*. For clarity, these developmental stages are represented as a schematic assorted chronologically from top to bottom in figure 2.4j. Using immunofluorescence, antibody specificity was verified by peptide pre-absorption as shown previously in section 2.1 for Western blotting (figure 2.1c). The immunofluorescence signal was markedly reduced when using the antigenic peptide in combination with the primary antibody as shown below in figure 2.4b'.

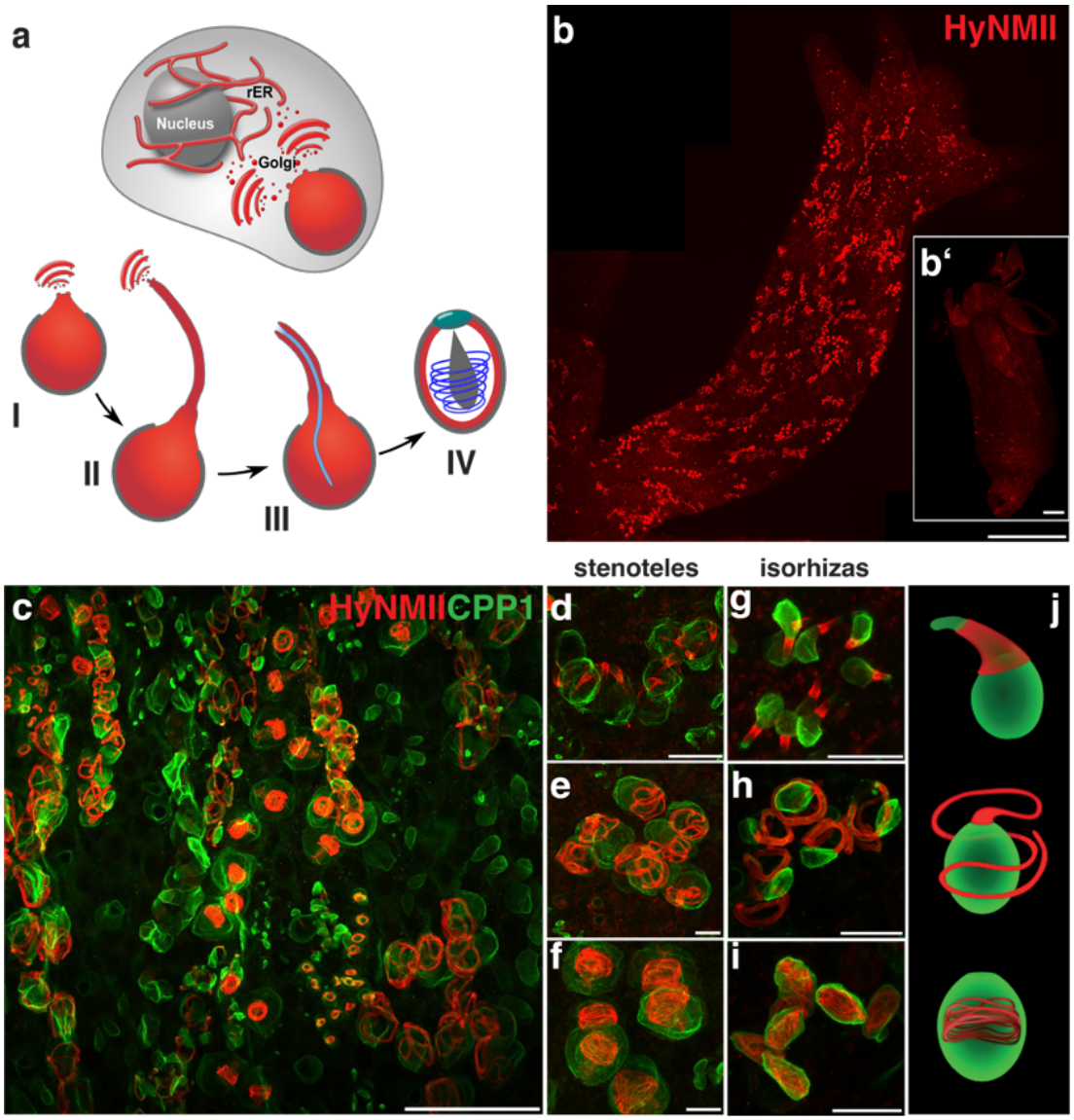

Figure 2.4 Localization of HyNMII during nematocyte morphogenesis.

a) Schematic of a nematocyte undergoing morphogenesis, I, tubule protrusion with TGN vesicles. II, external tubule elongation. III, tubule invagination. IV, nematocyst maturation with coiled internal tubule. **b)** Whole mount immunostaining with anti-HyNMII (red). Insert **b')** demonstrates peptide blocking by antigenic peptide at 1mg/ml. **c-i)** Double immunostaining with anti-HyNMII (red) and anti-CPP1 (green). **c)** Overview of different types of nematocytes in their syncytial nests in the body column at different stages of development. **d-i)** Capsule and tubule morphogenesis is represented chronologically in one nest in 2 types of nematocytes at higher magnification - stenoteles and isorhizas, as indicated. HyNMII (red) accumulates at the apical side of the early nematocyst forming a neck-like structure around the growing tubule (d and g), followed by assembly of HyNMII on the elongating tubule **(e** and **f**) and finally at the coiled and invaginated tubule (f and i). Scale bars (b) = 200 µm, b' = 100 µm , c= 20 µm and d-i = 10 µm. j) Schematic representation of HyNMII localization in different developmental stages from early (top) to late stages (bottom) illustrating the stages in d-f and g-I, respectively. a and j created by Gideon Bergheim.

2.4.2 Immuno-electron microscopy detection of HyNMII during developmental stages of tubule

Immuno-Electron microscopy(immuno-EM) serves as another efficient method for visualisation of the protein of interest at an ultrastructural level [91]. Using immuno-NANOGOLD™ silver particles, the localisation of HyNMII was visualised at the ultrastructural level through electron microscopy. The imaging revealed three developmental stages I, II and IV (figure 2.4a) of morphogenesis of the nematocysts most prominently, which were also found using immunofluorescence as reported in section 2.4.1. The silver particles were seen at the cytoplasmic membrane face as indicated by the yellow arrows in longitudinal and cross-sectional slices in figure 2.5. Figure 2.5a shows the intricately detailed structure of neck formation at the early stage of tubule formation. Figure 2.5b shows a cross-section of an elongated external tubule with immuno-NANOGOLD™-silver particles at the cytoplasmic membrane face. Figure 2.5c shows cross-sections of a completely invaginated tubule in the capsule matrix with labels lining the tubule wall structures. These results support patterns for HyNMII previously observed by immunofluorescence results (figure 2.4c-i).

2.5 Myosin inhibition leads to impaired tubule morphogenesis in nematocysts by Blebbistatin treatment

Blebbistatin (BBS) is well known for its inhibitory action of ATPase-mediated myosin II activity [92]. It is known that a developed functional mechanosensitive nematocyte, once fully matured, is incorporated as a part of the battery cell. The turnover time for nematocytes is 7-9 days [93]. Since the development and translocation of nematocytes to the tentacles takes approximately 7 days and it is hypothesized that myosin is implicated in nematocyte maturation, a continuous treatment with BBS over 7 days should affect this developmental process and lead to a depletion of nematocysts. Hence, to test this hypothesis, BBS treatment was used to inhibit the action of HyNMII and immunohistochemistry was employed to read out the resulting phenotypes.

The animals were co-stained with HyNMII and CPP-1. The morphological changes were then tracked each day for 7 days. The BBS treatment time series revealed that there was an overall depletion in nematocyte nests which was directly proportional to the duration of the treatment as shown in figure 2.6a-e. The depletion was quantified by counting the number of HyNMII-marked stenotele nests during BBS treatment (figure 2.6f) for three animals per day of treatment. It was

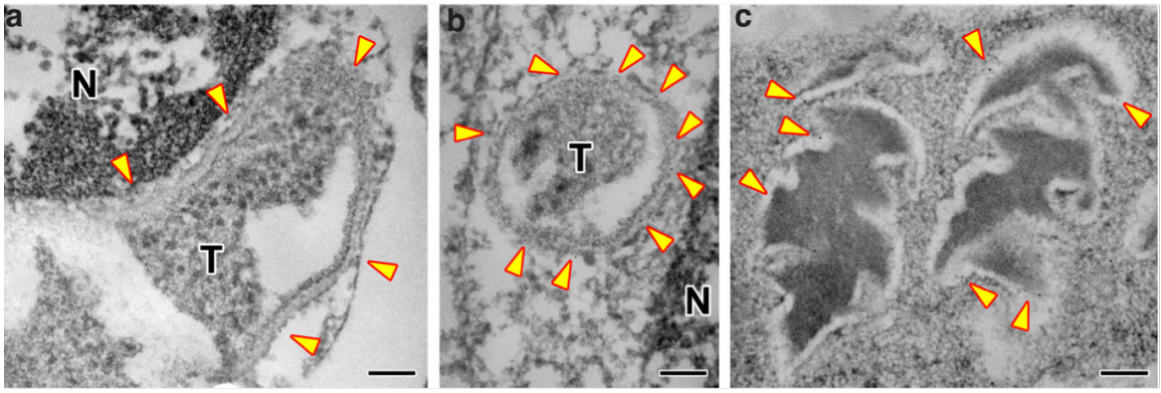

Figure 2.5 Localization of HyNMII at the ultrastructural level visualized through immuno-EM.

Three prominent developmental stages of nematocysts visualized by electron microscopy were in line with the phenotypes from immunofluorescence data (figure2.4). **a)** Longitudinal section showing the initial neck formation representing the onset of tubule formation at the apex. Arrows mark the labels at the cytoplasmic face of the protruding tubule. **b)** Cross-section of the external tubule. Arrows mark the labels at the cytoplasmic face of the tubule. **c)** Cross-sections of a tubule inside the capsule matrix. Arrows mark the labels at the tubule wall structure. Animals were fixed with MeOH + DMSO and visualized by immuno-NANOGOLD™-silver particles at the cytoplasmic membrane face. N = nucleus, T = tubule. Scale bar = 200 nm. Immuno-EM performed in collaboration with Dr. Michael Hess.

observed that the depletion was significant over the days of treatment compared to the control (Day 0). Interestingly, when the stages of development were quantified individually, it was noticed that the late stages such as IV showed a different trend compared to early morphogenesis stages I-III. While stage IV increased from 19% to 43% at day 7 of treatment but the stage I was almost completely missing (figure 5.3) (also see 2.4a). Apart from the overall depletion, granule-like structures (‘puncta’) appeared during the treatment starting from day 3, which became striking at day 5 (figure 2.6c’ and d’ marked by arrows). These puncta were observed in the vicinity of external tubule structures, indicating dissociation from the growing tubule (figure 2.6b’-d’). Using high magnification images, these puncta were quantified and had an average diameter of 2.7 µm, ranging from 1 to 4.5 µm (figure 2.6g).

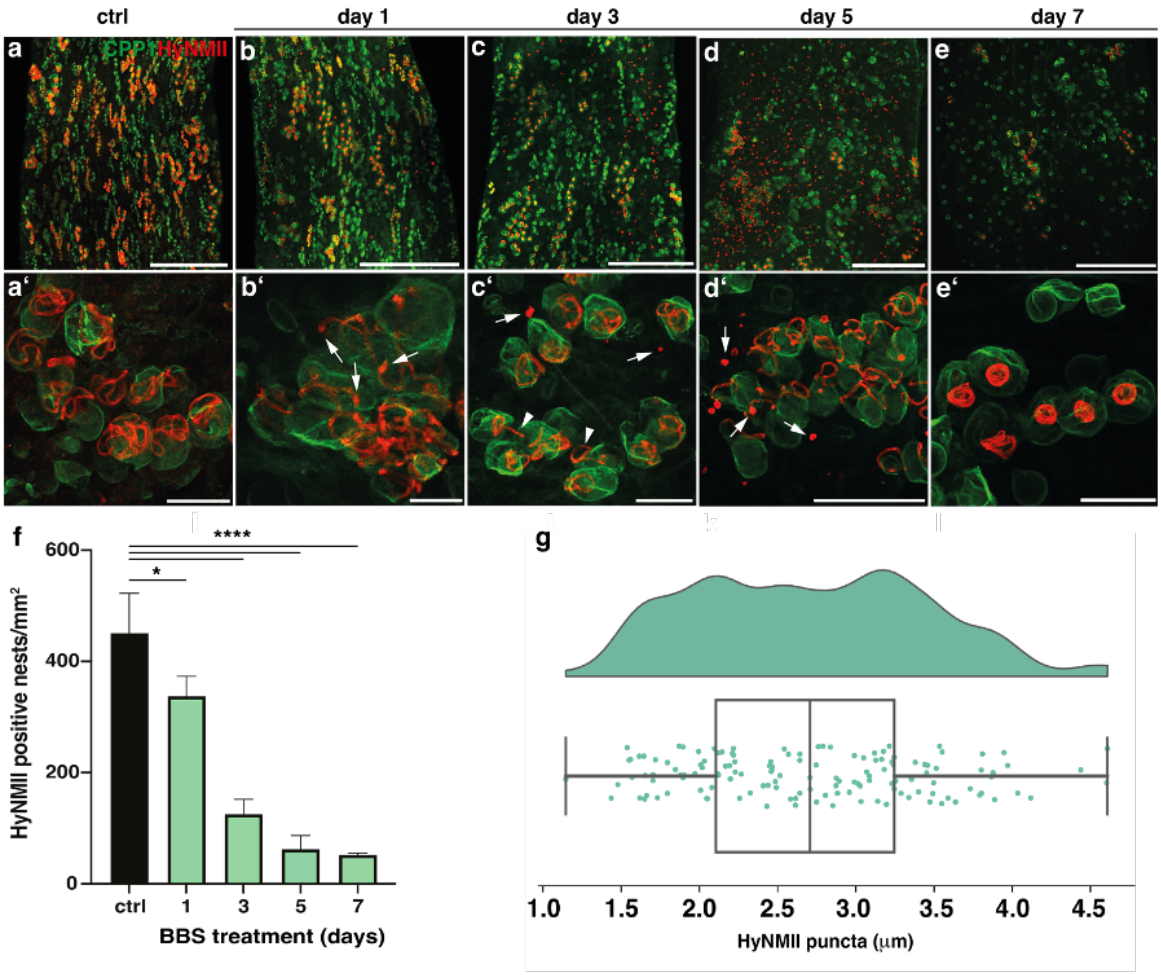

Figure 2.6 Myosin inhibition by BBS affects tubule development.

Blebbistatin treatment led to the overall depletion of nematocyte nests in the gastric region of polyps over time. Animals were stained with HyNMII (red) and CPP1 (green) antibodies. **(a-e)** The gastric region of a representative polyp from day 0 (ctrl) to day 7 from left to right. **(a'-e')** Higher magnification images of stenotele nests from day 0 (ctrl) to day 7 as indicated. Day 1 is already accompanied by bulges at external tubule structures, while the nests on day 3 and day 5 show large puncta near external tubules. **f)** Quantitative analysis of HyNMII-positive nests in the body column of polyps during BBS treatment shows a significant decrease from day 1 on and a dramatic reduction at day 7. **g)** Rain cloud plot quantifying the size of puncta at day 5 by considering the longest diameter. Scale bars = a-e: 100 µm; a'-e': 25 µm. Data represent mean +/− S.D. from three animals compared to control polyps. ****P value < 0.0001, *P value < 0.05. The data was analysed using a one-way Analysis of variance (ANOVA) test.

When observed closely at day 5, the tubule structures appeared to be shorter than in untreated control conditions as shown in figure 2.7c. Another interesting observation was that the puncta were also found in the tentacle region and were incorporated in the battery cells as shown in figure 2.7a and b. This means that myosin II inhibition results in abnormal morphogenesis of nematocysts by hampering tubule synthesis but does not interfere with the regular tissue flow in *Hydra* [63].

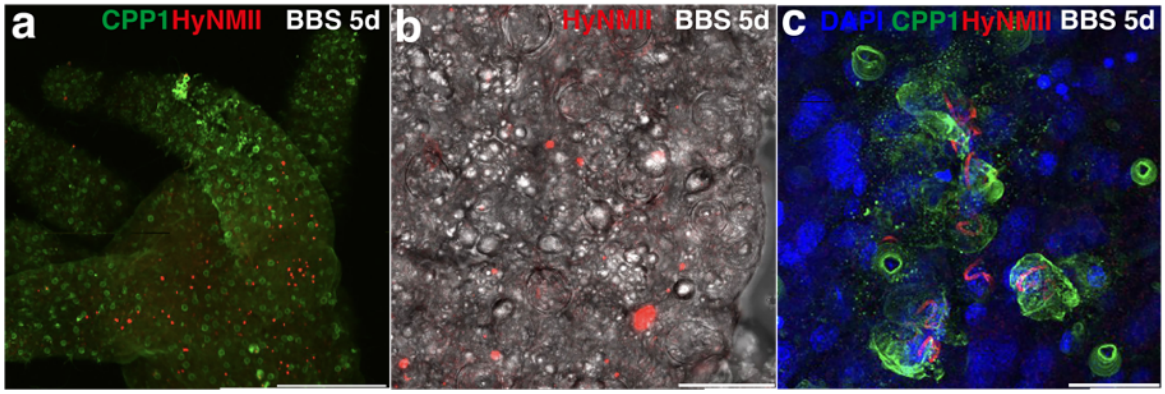

Figure 2.7 BBS treatment revealed displacement of HyNMII puncta in battery cells and disintegrated structures of nematocysts.
Animals were double stained with CPP1 (green) and HyNMII (red) antibodies. **a)** The head region of the animal in which HyNMII-positive aggregates are seen entering the tentacles. **b)** Differential interference contrast (DIC) image of battery cells with HyNMII-positive dots shows that even though nematocyst development is impaired, they are still able to move towards the head region. **c)** Higher magnification of a stenotele nest representing disintegrated structures of capsule bodies, as well as shortened external tubules. Scale bars = a: 200 µm, b: 20 µm, c: 25 µm.

It is known that BBS has a global effect on cellular functions that depend upon myosin II. Additionally, nematocytes are a product of mitotic divisions from multipotent interstitial stem cells (i-cells). Hence, it was essential to make sure that the depletion in nematocytes for the duration of treatment was not due to a global effect of BBS on i-cell proliferation. In order to address this, a transgenic line was used expressing GFP under the control of the *Hydra* nanos promotor (Cnnos::GFP) [94]. Here, undifferentiated i-cells express GFP and therefore could be used to monitor the i-cell population density during BBS treatment. As demonstrated in figure 2.8(a-e), i-cell numbers were unaffected within the 7 days of BBS treatment when compared to the drastic depletion in the nematocyte population. This shows that the i-cells are much less sensitive to Myosin II inhibition compared to nematocytes, where much more prominent effects could be seen on day 7. BBS treatment was further prolonged until day 14 to assess if there were any long-term effects of Myosin

II inhibition by BBS. Towards the end of day 14, the body column appeared to be completely deprived of the i-cells as shown in figure 2.8g, indicating an effect on cell proliferation by myosin II inhibition.

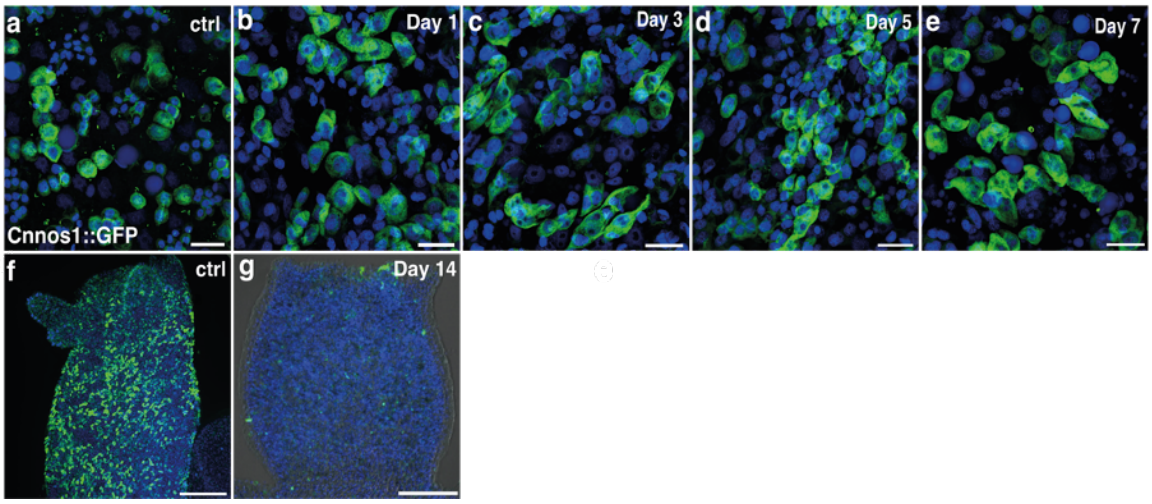

Figure 2.8 i-cells are less sensitive to BBS treatment compared to nematocytes. Gastric region of transgenic polyps (Cnnos::GFP) showing that the i-cell population is unaffected until day 7. **(a-e)** GFP expressing i-cells in the body column from Day 0 (ctrl) to day 7 (left to right). **f)** Day 0 image of polyp densely populated with i-cells. **g)** Polyp at day 14 showed the body column almost completely depleted of i-cells. Scale bars - (a-e): 20 µm f and g: 20 µm. Images acquired by Björn Eismann.

2.6 HyNMII knockdown confirms the role of Myosin in normal growth and morphogenesis of nematocysts

To directly test whether HyNMII is implicated in nematocyst morphogenesis, I used RNA interference. I designed siRNAs which bind to specific sequences of the HyNMII mRNA and thus block the expression of the target protein. siRNA knockdown (KD) was achieved by electroporation of siRNAs (siHyNMII, siNOWA, and siGFP) into transgenic animals expressing GFP in the ectoderm and RFP in the endoderm (Act::Endo-RFP/Ecto-GFP) (5.4), which were then fixed for imaging. Gene silencing was verified using immunofluorescence with confocal microscopy to read out the phenotypes. siGFP in combination with siHyNMII served as an identifier to sort out which animals were electroporated as siGFP resulted in the loss of GFP in the portion of the ectoderm layer that was hit by the electric pulse.

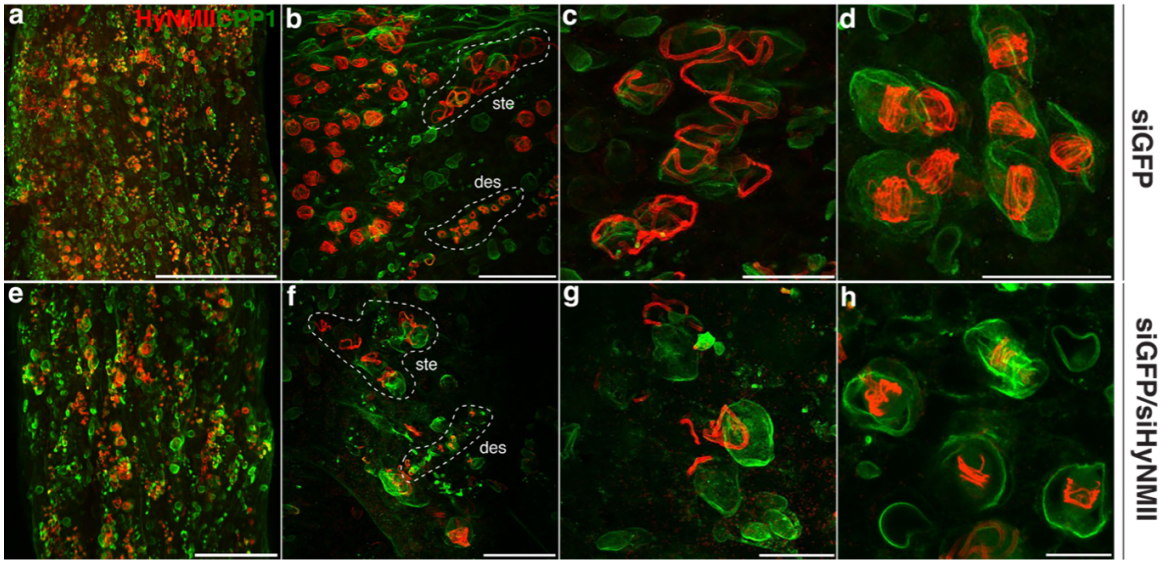

Figure 2.9 HyNMII knockdown affected the tubule morphogenesis.
(a-h) Double staining with HyNMII (red) and CPP1 (green) antibodies. **a)** Overview of nematocyst nests in the body column of a control animal **e)** siHyNMII condition where HyNMII-positive nests are reduced compared to control. **(b, f)** Nests with external tubules marked by a dotted line, in two different types of nematocyte nests as indicated. Compared to control **(b)**, the knockdown conditions show disordered tubule structures **(f)** and partially disintegrated capsule bodies. **(c, g)** Higher magnification image of a stenotele nest; in the knockdown condition shows a prominent malformation of tubule structures and missing capsules. (**d, h)** The late stages show invaginated and coiled tubules. In the knockdown, condition tubules are markedly shorter compared to controls. Scale Bars = a-h: 50 µm.

2.6.1 siHyNMII affected nematocyst tubule development at different stages

Two siRNAs directed against different binding sites of the HyNMII mRNA were used and the phenotypes of nematocytes were investigated. In knockdown (KD) conditions, it was observed that there was a general lack or partial loss of HyNMII-stained structures in nematocyst nests within the body column (figure 2.9e). Apart from this reduction in HyNMII protein, the phenotypes of developing nest revealed regions of external tubules that were missing or disintegrated, and sometimes included syncytia with missing nematocysts (figure 2.9f and g). In the late stages, it was seen that invaginated tubules were distorted and structurally disintegrated (figure 2.9h) compared to the control (figure 2.9d). The effect on tubule morphogenesis observed here is in line with the results after the BBS treatment, when stained with the same protein markers. However, it should also be noted that siRNA KD comes with some limitations. siRNA KD is done through electroporation, a process that is unidirectional and hits only one side of the animal, which may result in only partial KD

of the protein. Therefore, based on these observations, one cannot comment conclusively on the effect of *HyNMII* KD on the phenotypes observed here. However, these results together with the BBS treatment provide a more comprehensive and concrete outlook towards the importance of HyNMII in the development of tubules during nematocyst development.

2.7 Formation of nematocysts is assisted by TGN vesicles and microtubules

It was previously shown that during nematocyst development, the tubule is surrounded by a cluster of trans-Golgi network (TGN) vesicles, which continuously fuse with the tubule membrane to support the development of the nematocyst structure [58]. These TGN vesicles are arranged and organised with the help of microtubules surrounding the apical pole of the growing tubule. I was able to visualise this structure using an anti-beta tubulin antibody through immunofluorescence as shown in figure 2.10f. To visualise the TGN vesicles and localise their position respective to the growing structure of the nematocyst, a molecular marker designated as Minicollagen-1-Propeptide (Ncol-1pp) was used. Minicollagens were previously described to contain a pro-peptide, which is cleaved shortly before the TGN vesicle fuses with the nematocyte membrane [95]. The antibody directed towards this propeptide (anti-Ncol-1pp) makes it possible to visualize the TGN vesicles around the growing nematocytes [66].

In general, anti-Ncol-1pp-positive TGN vesicles are found in various kinds of syncytial nests in the gastric region of polyps as shown in figure 2.10a. These TGN vesicles form crown-like structures at the apex of the capsule body (figure 2.10b-d). To better localise the TGN vesicles, double staining was done with a capsule wall marker ‘cnidoin’ (CN), which has been previously described to localise to the capsule wall (citation) in the nests of developing nematocytes. This co-localization of cnidoin-lined capsule walls and Ncol-1pp-positive TGN vesicles reveals that the TGN vesicles fuse specifically to the apex of the growing nematocytes. These markers are used later as a read-out to define and understand how the nematocyte structures are affected in different conditions.

According to previously defined literature, microtubules run in a spiral-like course to the external tubule, and the tip region of the tubule is surrounded by a circle of microtubules [58, 67]. A co-staining was carried out using a beta-tubulin (tub) antibody along with HyNMII as shown in figure 2.10f, to visualise the microtubule localisation in association with the developing tubule during the nematocyte mor-

phogenesis. Tubulin was seen to be localized at the tip of the elongating tubule (marked by arrows in figure 2.10f), as demonstrated before by electron microscopy and immunohistochemistry, confirming their role in supporting the morphogenesis of tubule most probably by facilitating TGN vesicle transport. The schematic shown in figure 2.10e describes the association of microtubule and TGN vesicles directed towards the apex or around the tip of the growing tubule.

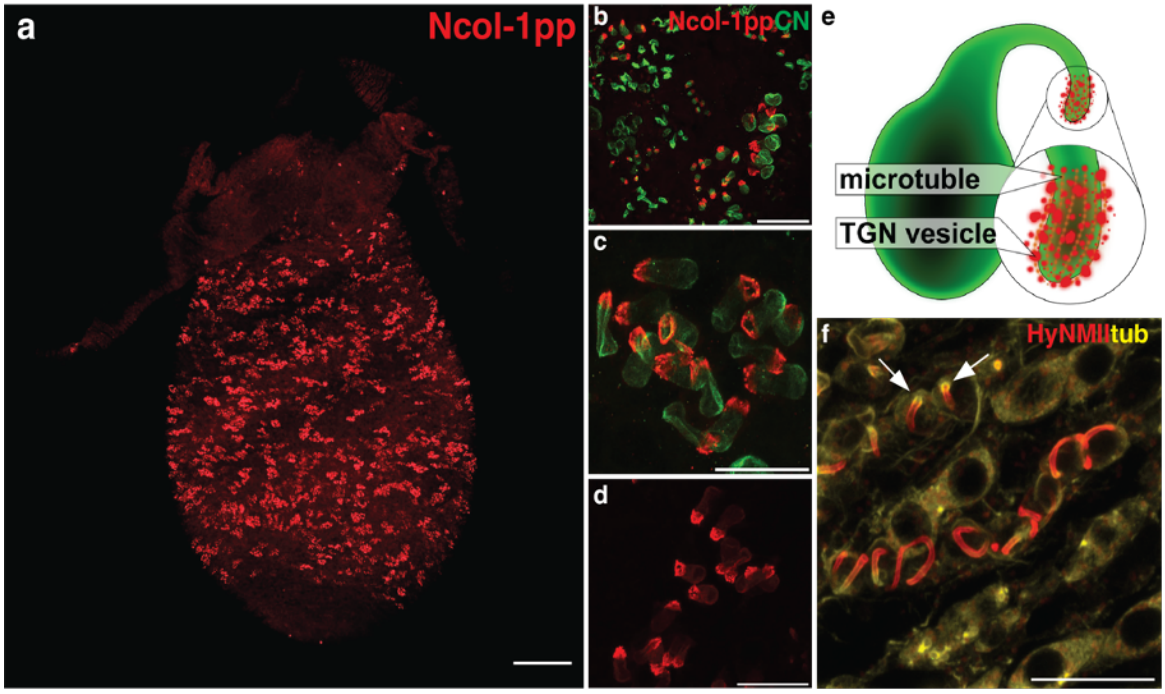

Figure 2.10 TGN vesicles and microtubules during developmental stages of nematocytes.

Whole-mount *Hydra* double immunostaining with anti-Ncol-1pp (red) and anti-Cnidoin (green) and anti-Beta-tubulin (yellow). **a)** Expression of Ncol-1pp throughout the body column of PFA fixed *Hydra* in various types of nematocyte nests. **b)** Higher magnification image of CN and Ncol-1pp double staining in nematocyte nests. **c)** Close-up of a stenotele nest in which the capsule body is marked by CN and TGN vesicles forming a crown-like structure at the apex by Ncol-1pp. **d)** Single staining with Ncol-1pp showing the tip of the nematocyte with assembled TGN vesicles. **e)** Diagram of a growing NC structure with an external elongating tubule where microtubule and TGN vesicle positions are marked to show their assembly respectively. **f)** Double staining of microtubules marked with Beta-tubulin (yellow) around the growing tubule (red, marked with HyNMII). Scare bars = a: 200 µm; b: 50 µm; c, d 20 µm and f:20 µm. (Schematic 'e' by Gideon Bergheim).

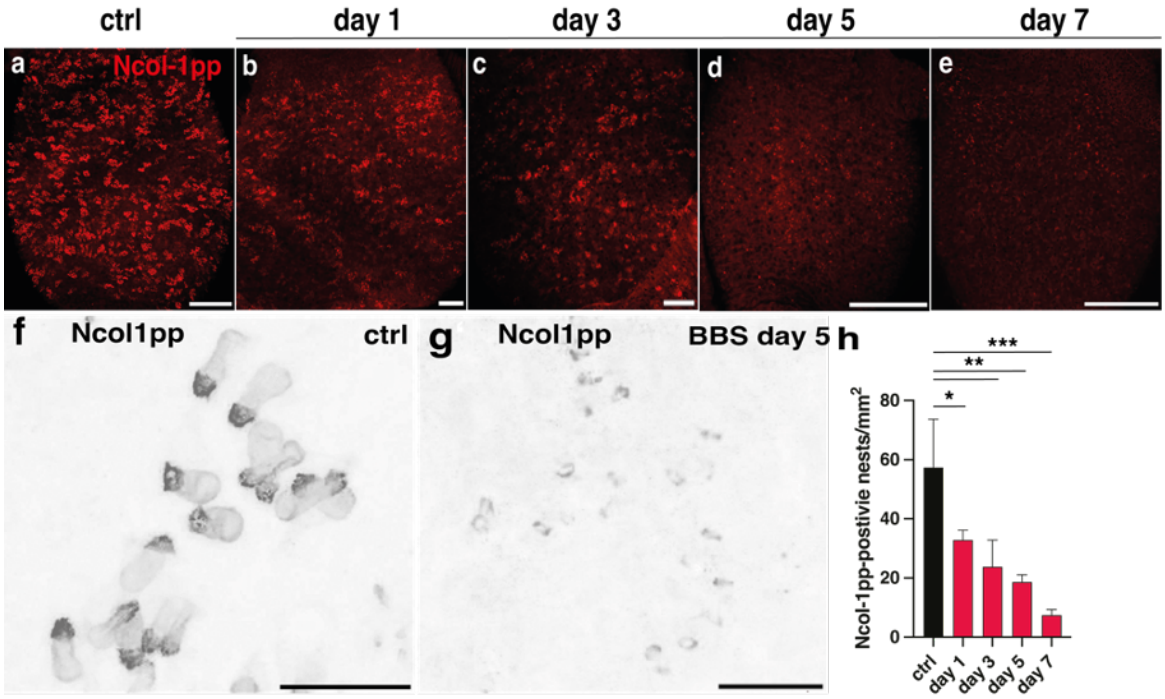

Figure 2.11 ABlebbistatin treatment affected the population of TGN vesicles at growing nematocyst.

a-e) The body region of polyps treated with BBS shows a prominent depletion of Ncol-1pp-positive (red) nematocyst nests. **f, g)** High magnification images of a stenotele nest from a and d portraying the scarcity of Ncol-1pp-positive vesicles at the tip of nematocytes. For clarity, the image in which the TGN vesicles are marked with the Ncol-1pp protein marker (red) is converted to grayscale and shown in inverted contrast. **h)** Statistical representation showing the depletion of Ncol-1pp-positive nematocyst nests directly proportional to the days of treatment. Scale bars- a, b, c, e: 200 µm; d: 100 µm; f and g: 20 µm. Data represent mean +/− S.D. from 3 animals compared to control polyps. ***P value < 0.0005, **P value < 0.005. *P value < 0.05. The data were analysed using a one-way ANOVA test.

2.7.1 Myosin inhibition affects the formation of TGN vesicles targeting nematocytes

It has been shown that nematocytes derive from a giant post-Golgi primordium. As continuous treatment with BBS led to an almost complete depletion of nematocytes including the early stages before tubule synthesis, I speculated that HyNMII is already participating in the initial budding process of TGN vesicles targeted at the nematocyst. To test this hypothesis, the protein marker Ncol-1pp was used (described above). Animals were treated with BBS continuously for 7 days and Ncol-1pp was detected using immunofluorescence. As seen in figure 2.10b-d, Ncol-1pp formed a crown-like shape at the apex of early-growing nematocysts. In figure 2.11a, the body column is filled with these Ncol-1pp-positive nematocyst nests,

which started to decrease in correlation with the days of BBS treatment. At day 7, Ncol-1pp-positive nematocysts were almost completely depleted in the body column (figure 2.11e). This depletion was quantified by counting the number of Ncol-1pp-positive stenotele nests in the body column in three animals per day of treatment. As shown in figure 2.11h, there was a significant reduction in the number of nests over the days of treatment, which was already prominent at day 1 when compared to the day 0 control (without BBS treatment). Not only just the overall population of nematocytes over time but also the early vesicles per nests involved in forming the capsule wall matrix was depreciated as shown in figure 2.11f and figure 2.11g.

2.8 Nematocyst outer wall antigen (NOWA) is involved in tubule invagination

Nematocyst outer wall antigen (NOWA) has been previously described to participate in the capsule maturation process and as a major component of the capsule wall [96]. It is an 85 kDa C-type lectin protein with multiple minicollagen cysteine-rich domains at its C-terminus. It was originally identified by Edman analysis of a spot excised from a 2D gel detected by the monoclonal antibody (H22 mab) which was raised against isolated mature capsules. It stained developing nests as well as the outer wall of the capsule body in the tentacles. A polyclonal antibody directed against the recombinantly expressed C-type lectin domain of NOWA, named NOWA-CTLD was used to confirm the localization of NOWA. Western blot analysis of this antibody recognized a band at 88 kDa as shown in figure 2.12g, which is the same as the molecular weight of the antigen detected by the H22 antibody, hence the antigen detected by H22 and CTLD antibodies were believed to be identical. Immunofluorescent stainings using the NOWA-CTLD antibody revealed that the protein is localised in large aggregates in the capsule matrix at early developmental stages (figure 2.12a. I and II) where the tubule protrusion and elongation process begins. Apart from this, it stained the fully invaginated stages of the tubule structure (figure 2.12a. III and IV). The phenotypes were similar to the localisation of NCol-15 and Spinalin [97] with dense globular-like particles filling the capsule body at the onset of tubule morphogenesis. These spots disappear as the nematocyst proceeds towards maturation. In tentacles, the tubules of discharged nematocytes were NOWA-CTLD-positive (figure 2.12f), while the mature, undischarged capsules did not stain due to impenetrable wall compaction (figure 2.12c).

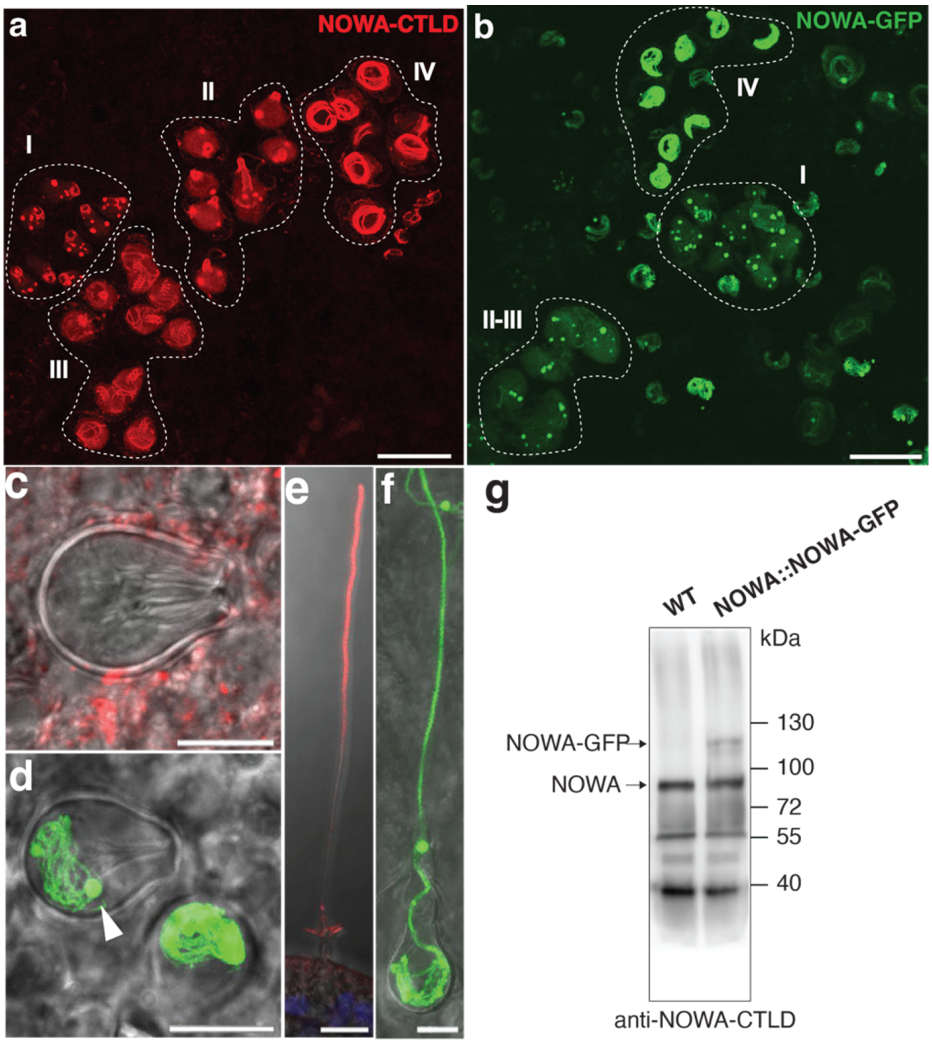

Figure 2.12 Detection of NOWA by NOWA-CTLD ab and in the NOWA::NOWA-GFP strain during nematocyst morphogenesis.

a) Stages of nematocyst development detected by NOWA-CTLD antibody (red), where 'I' is an early stage with the assembly of protein globules before tubule protrusion, 'II' is the onset of membrane tubulation, 'III' is tubule invagination showing loosely coiled tubules in the capsule matrix with the shaft forming a triple helix structure and 'IV' the maturation stage when the tubule is invaginated and tightly coiled inside the capsule. **b)** Same as 'a', stages of development in the transgenic strain NOWA::NOWA-GFP where the NOWA-GFP fusion protein is localized in aggregates in the capsule lumen and at the tubule after invagination. **c)** Matured nematocyst, with unstained tubule **d)** Matured capsule in transgenic strain with invaginated GFP-positive tubules. The arrowhead marks the protein aggregate. **e)** A discharged nematocyst with tubule stained by NOWA-CTLD antibody. **f)** NOWA-GFP positive discharged tubule. **g)** A Western blot analysis with NOWA-CTLD antibody using isolated capsules from wild-type animals (left) revealed the expected molecular weight of 88 kDa, the same was also seen in capsules of the NOWA::NOWA-GFP transgenic line (right) which in addition showed a weaker band of 115 kDa corresponding to the NOWA-GFP fusion protein. Scale bars-a-b: 25 µm; c-f: 5 µm. Data was partially acquired by Urška Knez Štibler and Western blot analysis was done by Annika Ohl.

To resolve the conflicting results obtained by immunofluorescence staining with the H22 and NOWA-CTLD antibodies, a transgenic strain was created expressing NOWA-GFP fusion protein under the control of the NOWA promoter (figures 2.12b, d and f). The GFP patterns observed in the developing nematocysts of the transgenic strain confirmed the staining pattern obtained by NOWA-CTLD ab, with the exception that in mature, discharged and undischarged capsules tubule structures were GFP-positive as well (figure 2.12d and f). Another observation worth noting was that the protein aggregates were only partially dissolved in mature capsules of the transgenic line, which was not the case using the NOWA-CTLD antibody. So, it is likely that the fusing of N-terminal GFP hampers the process of dissolution of these aggregates. In parallel with the immunofluorescence methods, a Western blot analysis was performed for detection of NOWA using isolated nematocysts from both, the wild-type (WT) and the transgenic strain. According to the results, it was seen that the NOWA-CTLD antibody recognized a band matching the predicted molecular weight in both conditions. In the sample from the transgenic strain, an additional band at 115 kDa was detected, accounting for the NOWA-GFP fusion protein.

2.8.1 Tubule integrity in developing nematocytes is affected by BBS treatment detected by NOWA-CTLD

As previously discussed, NOWA is mainly localised on tubules during late nematocyst development, hence it serves as an ideal protein marker to observe tubule morphogenesis during its maturation stage. The Blebbistatin treatment was performed for up to 5 days on wild-type as well as transgenic animals expressing NOWA-GFP fusion protein. NOWA-CTLD and CPP1 were used as protein markers in wild-type animals to image both the capsule and tubule morphogenesis simultaneously. Apart from an expected decrease in the overall nematocyst population in correlation to the days of the treatment, there were also some prominent anomalies which were observed in the BBS treated animals when compared to control animals. Early nests, characterized by globular NOWA aggregates inside the developing capsule (figure 2.13a), showed asynchronous development of nematocysts within one nest (figure 2.13d). Additionally, in the ensuing stage, where tubules are in the invagination process and show a triple helix structure at their shaft region (figure 2.13b and stage II in figure 2.12a), was altered upon treatment with BBS. Specifically, the nests were incomplete and tubule shaft regions were distorted (figure2.13e). At later stages, a clear tubule structure indicative of NOWA's association with the invaginated tubule was not evident in the capsule body (figure

2.13f) when compared to the late control stages, which are characterised by the presence of coiled tubules (figure 2.13c and figure 2.12a.IV). Interestingly, NOWA persisted in BBS-treated animals in an amorphous state dispersed in the capsule lumen (figure 2.13f). The BBS treatment performed in the NOWA::NOWA-GFP transgenic line confirmed this phenotype, where instead of coiled, invaginated tubules (figure 2.13g), nematocyst ”ghosts” seemingly lacking tubules could be detected in figure 2.13h). Taken together, myosin inhibition interferes with nematocyst development by disrupting normal tubule growth and invagination/maturation processes as revealed by NOWA detection.

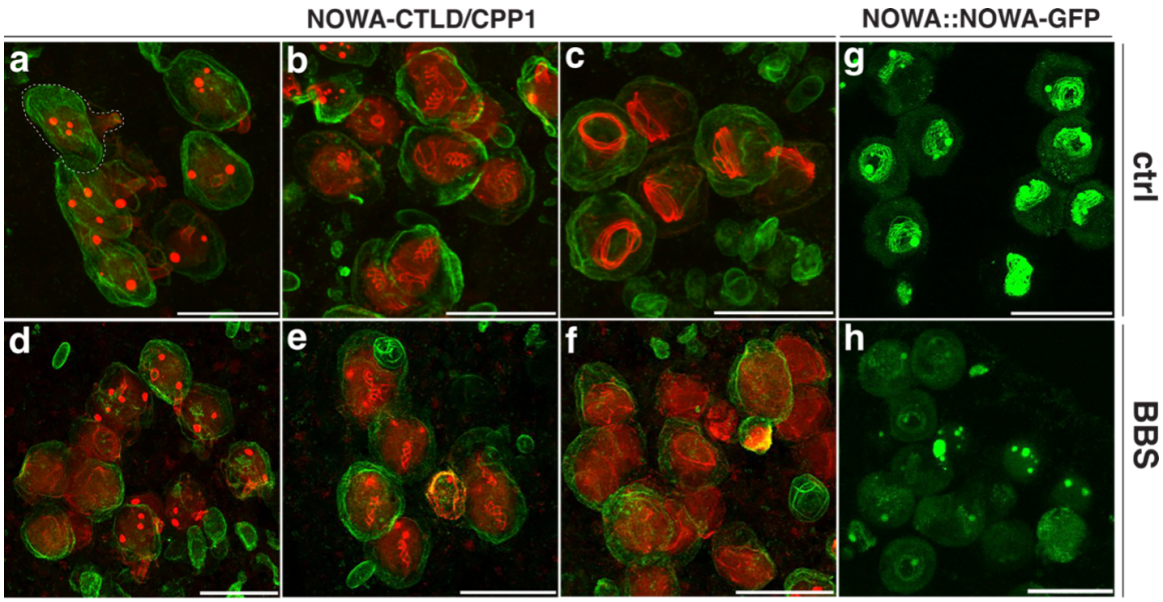

Figure 2.13 Inhibition of myosin II leads to compromised nematocyst tubule maturation.

The morphogenesis of nematocysts was visualised using NOWA-CTLD (red) and CPP1 (green) antibodies in both control and BBS-treated animals for 4 days (a-f). **(a, d)** The early stages, characterised by the onset of tubulation, in BBS treated animals (d), the large NOWA-positive protein spots portray an asynchronous development within the same nest. **(b, e)** This stage is characterised by the formation of a triple helical fold and loosely coiled tubule structure inside the capsule body. In the BBS condition, the triple helical structures were distorted and NOWA protein aggregates which normally are dispersed at this stage were in part still aggregated. **(c, f)** In the late stage when the tubule completely invaginates and coils, internal tubule structures were missing in the BBS condition and NOWA protein persisted in an amorphous state. **(g, i)** Mature Nematocysts in the transgenic NOWA::NOWA-GFP strain show similar phenotypes of missing internal tubules as in f in the BBS condition (5 days) as compared to controls. Scale Bars = 25 µm.

2.8.2 *HyNMII*knock-down affects tubule morphogenesis detected by NOWA-CTLD

Tubule morphogenesis is radically obstructed when HyNMII is inhibited, which was demonstrated with both chemical inhibition through BBS and siRNA KD. To further visualise this effect, the newly established NOWA-CTLD tubule marker (localization previously described, section 2.8) was used after the animals were subjected to siHyNMII. To visualise the effects on morphogenesis of both capsules and tubules during development from early to late stages after KD (figure 2.14), immunofluorescence was performed using NOWA-CTLD and CPP1 antibodies.

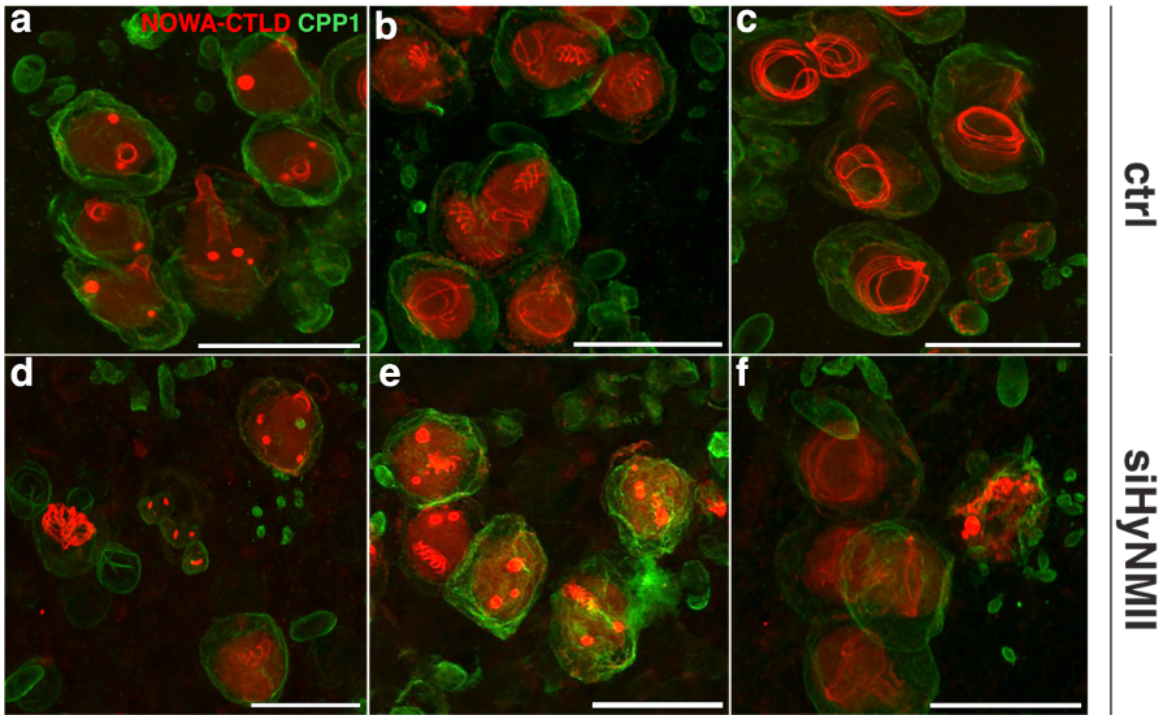

Figure 2.14 The knock-down (KD) of *HyNMII* leads to impaired tubule development evidenced by anti-NOWA-CTLD staining.
(a-f) Higher magnification of nematocytes visualised by double staining for Cpp-1 (green) and NOWA-CTLD (red). **(a, d)** The early stage, where tubule protrusion takes place at the apex of the capsule body, in KD conditions, showed asynchronous development of nematocyte structures within the same nest. **(b, e)** The intermediate stage where the tubule is loosely coiled and the formation of a triple helical fold at the shaft is visible is replaced by capsules with distorted tubule shafts and undissolved NOWA protein aggregates. **(c, f)** The late stage where the tubule is coiled and invaginated inside the capsule, in KD conditions is replaced by partially lacking tubules and disintegrated capsule bodies (f). Scale bars- (a-f): 25 µm.

The phenotypes observed here are comparable to those observed after BBS

treatment, which includes (1) impaired synchronicity during development within the same nests (figure 2.14d), (2) distorted shaft regions and persistent NOWA conglomerates (figure 2.14e), and (3) distorted or lacking invaginated tubule structures and partly disintegrated capsules (figure 2.14f). These observed phenotypes, together with similar results obtained after BBS treatment, demonstrate the impaired development of tubules in the absence of HyNMII. The missing tubule structures detected by NOWA-CTLD staining in the late stage indicate that the protein is not able to bind to its target and hence is still dispersed in the capsule matrix.

2.9 NOWA facilitates tubule invagination

To investigate the possible role of NOWA during nematocyst morphogenesis, NOWA specific siRNAs were designed for knockdown experiments. HyNMII antibody was used to visualise the tubule and CPP1 for the capsule to read out the results in the KD conditions.

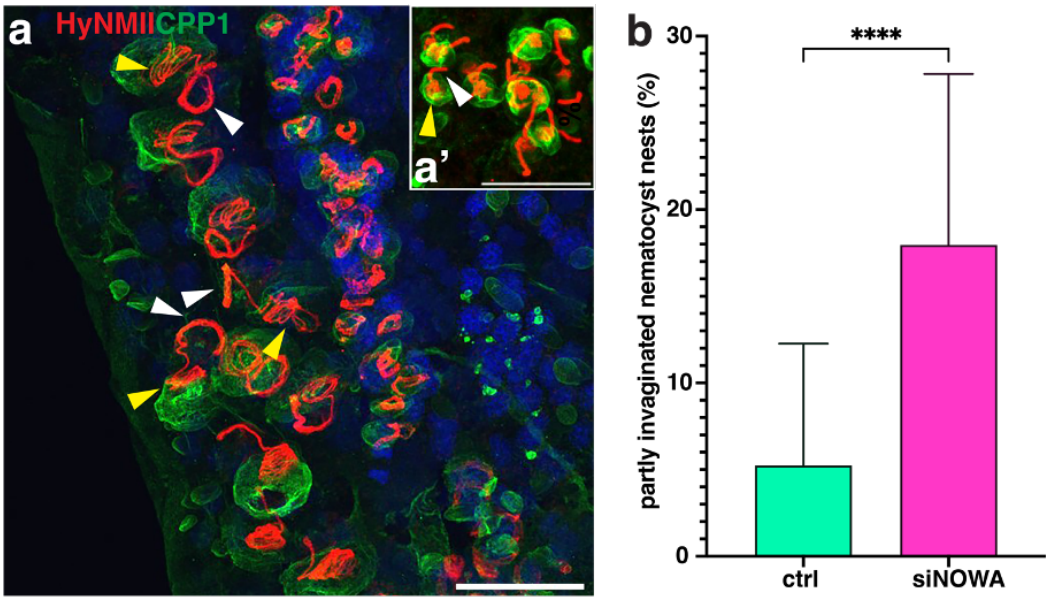

Figure 2.15 Deprivation of NOWA affects tubule invagination.
a and a') HyNMII (red) marked tubules and CPP1 (green) marked capsules in nests of developing nematocysts in the stage of tubule invagination with partly invaginated and coiled tubules (yellow arrowheads) and thickened double-layered outer tubules (white arrowheads). **b)** Quantification of nematocyte nests at invagination stage in control (green) vs siNOWA (pink) conditions. Data represent mean +/− S.D. from 21 (ctrl) or 34 (siNOWA) random areas of 85434.286 µm² in the gastric regions of 3 animals in each treatment group. ****P value < 0.0001. The data were analysed using an unpaired t-test. Scale bars- a and a':25 µm. The experiment is done in collaboration with Urška Knez Štibler.

It was observed that there was an enrichment of tubule invagination stages in KD conditions. This represents a rarely captured stage due to its highly transient nature (figure 2.15a). These stages are characterised by a thickened double layer of the external tubule connected to a more delicate thread of the invaginating distal tubule which is partly coiled inside the capsule lumen. This is marked by white and yellow arrowheads, respectively, in two different types of nematocyst nests shown in figure 2.15a and a'. A quantification of nematocyst nests captured in this state of early invagination showed an increase to an average of 18% in animals electroporated with NOWA siRNAs compared to 5.2% in control animals (figure 2.15b). The significant increase in this transient stage shows that NOWA is assisting in the completion of the tubule invagination process.

2.10 HyNMII is cytosolically associated with the nematocyst membrane

It was previously shown that nematocytes are a product of a giant post-Golgi vesicle and several proteins are involved in the assembly process of the structure. It would be interesting to find out how the protein of interest, HyNMII, is recruited and localised topologically during this process of formation. According to previous studies, Myosin II is known to be transiently associated with the Golgi membrane [98], hence, to also confirm this for the nematocyte-specific Myosin II, HyNMII, Brefeldin (BFA) treatment was used. BFA is a fungal metabolite and acts as a chemical inhibitor, which is known to inhibit the membrane binding of proteins which are peripherally attached to the Golgi.

When animals were exposed to BFA for defined time points, irregular phenotypes were observed during the developmental process (figure 2.16b and c). Double staining with HyNMII and CPP1 was used to observe the tubule and capsule wall structures simultaneously. At 2 hours of treatment, external tubules showed dissociation of the HyNMII protein indicated by weaker and more diffuse staining (figure 2.16b), while the capsule bodies were intact. Longer treatment induced a structural disintegration of the nematocyst vesicle (figure 2.16c), which is in line with the observation in cell culture experiments that prolonged BFA treatment leads to Golgi disassembly. I could conclude from this that HyNMII is peripherally attached to the cytoplasmic face of the nematocyst membrane.

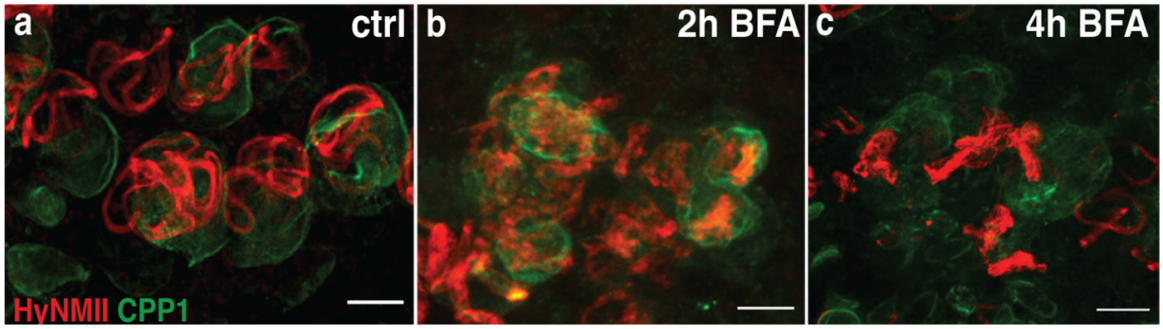

Figure 2.16 HyNMII transiently binds to the nematocyst membrane.
a-c) Double staining of Nematocysts with HyNMII (red) and CPP-1 (green) antibodies, showing a higher magnification of single nests at various time points of BFA treatment. **a)** The close-up of a nematocyst nest in a control animal showing normally shaped external tubules. **b)** A nest at a similar stage as in 'a' but after 2 hours of BFA treatment showing dissociation of HyNMII from the tubule surface. **c)** Same stage as in a and b after 4 hours of BFA treatment showing complete nematocyst disintegration. Scale bars- (a-c): 5 µm.

2.11 An Actin-Myosin interaction is important for the morphogenesis of the nematocyst tubule

The formation of nematocytes is a complex intracellular process which requires more than 400 proteins for the successful assembly of the nematocyte structure. Moreover, some tubule-specific proteins have already been defined, such as 'non-sulphated chondroitin' which forms the outer layer of the molecular scaffold while supporting membrane tubulation during the initial stages of development. This scaffold helps to incorporate 'minicollagen'. Another protein, nematogalectin, on the other hand, forms the inner layer facing the lumen. Altogether these proteins support the structural integrity of the tubule. Apart from these nematocyst-specific proteins, the cell cytoskeleton plays a fundamental role in the development of nematocysts, as well as supporting other mechanisms, such as protein and vesicle transport from the TGN. As previously described in section 2.7, at the distal end of the tubule there is an array of microtubules which supports the growth of the external tubule. This was also shown through fluorescent images (figure 2.10f). Microtubules are also known to form a basket-like structure around the capsule body, supporting the outer nematocyst structure [58, 99]. But, so far, the role of the actin cytoskeleton has not been implicated for the formation of nematocysts.

Since, in this thesis, HyNMII was extensively studied and determined to drive critical steps during the morphogenesis of both tubules and capsules, it is likely that the actin cytoskeleton is vital for this process. Cortical Actin network known to facilitate the movement of cells across surfaces and membrane shaping through

self-organisation [100]. Additionally, the cooperative action of actin and myosin is known to play an important role for the 'power stroke' mechanism, which is essential for muscle movement as it generates the force required for the functioning of myosin motor proteins. Hence, I decided to explore the role of actin during the process of nematocyst morphogenesis. For this, firstly, immunofluorescence was used to colocalise actin and HyNMII in growing nematocytes using Phalloidin and the HyNMII antibody. Unfortunately, this was not successful even after many iterations of staining and fixation protocols.

Another method, immuno-EM, was employed to gain insights on the localisation of actin during nematocyst development. This was performed in collaboration with Dr. Michael Hess in Innsbruck. Immuno-EM images did not give a concrete outlook towards the exact localisation, but the two different complementary protocols used to perform electron microscopy yielded consistent results described as follows. NANOGOLD™-silver nanoparticles were used to improve actin antibody detection and enrichment of these nanoparticles categorizes the ultrastructure of the phenotypes observed during development. Actin was found throughout the cytoplasm of the nematocytes (figure 2.17a). Sometimes (as seen in cryosections) actin was also visualised in loose clouds or locally associated with organelles, such as the Golgi. There was a prominent assembly of nanoparticles around the external and elongating tubule (figure 2.17a and b), but this was not directly attached to the membrane which surrounded the tubule. The actin label was seen to co-localise with the fine filamentous elements which are perpendicular to the growing tubule (figure 2.17c) which might be an indication that it supports tubule elongation from a distance and had a diameter of 7 nm, on average, during nematocyte morphogenesis.

The above two immuno-EM methods, however, did have some limitations - enhancement in intensity could be achieved by pre-embedding labelling but led to moderate ultrastructure preservation due to strong detergent extraction, while the post-embedding labelling led to good ultrastructural preservation but immunodetection was compromised. Other approaches such as rapid cryofixation or optimized chemical fixation for sample preparation resulted in the visualisation of a loose meshwork or single microfilaments ranging between a diameter of 6-7 nm during the entire nematocyst morphogenesis (figure 5.7).

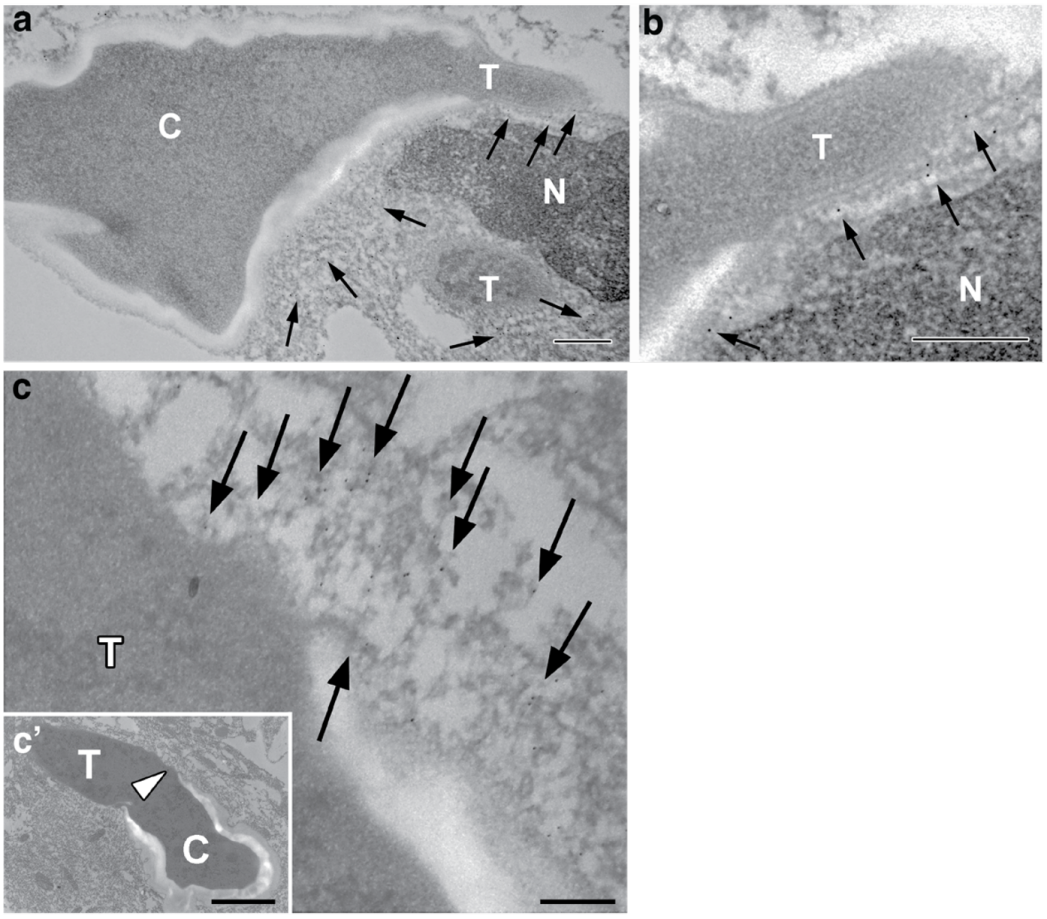

Figure 2.17 Immuno-EM representation of actin at the vicinity of developing Nematocysts.

Overviews of nematocysts in formaldehyde + Triton X-100 fixed *Hydra*, **a)** Actin is visualised by immuno-NANOGOLDTM silver particles shown by arrowheads in an elongating tubule (T) at the apex of the capsule (C), N=Nucleus, **b)** A detailed representation of figure 2.16a, highlighting the labels more prominently in the vicinity of the elongating tubule. **c)** Immuno-EM detection of actin very close to the right side of an elongating tubule marked by arrows, showing the orientation of fine filaments which is decorated by anti-actin immuno-NANOGOLD silver particles. **c')** Low magnification image of the stenotele is shown in detail in figure 2.17c. Arrowhead shows the side of the nematocyst which is shown in detail in figure 2.17c. Scale Bars - a, b :500 nm; c, c': 200 nm. Immuno-EM was done in collaboration with Dr. Michael Hess.

2.11.1 Actin depolymerization led to affected tubule initiation

Next, to get more insights about the role of actin during the morphogenesis of nematocysts, an actin depolymerising drug 'Cytochalasin D' (CytD) was used [101]. Animals were subjected to Cytochalasin D treatment. CytD was first diluted in DMSO and then in *Hydra* medium (HM). After 3 hours of treatment with CytD/HM, a dramatic effect on the polyps was observed. Two types of stainings were used: A double stain with CPP1 and HyNMII antibodies and single staining with Cnidoin to read out of the fluorescent images (figure 2.18).

In animals that had received a more homogenous CytD treatment the shape of developing nematocysts was markedly altered compared to controls. Using the capsule wall marker Cnidoin, I found that the capsule body appeared shrunken and the tubule diameters were expanded. In control-treated animals, the capsule body was larger and the tubule shaft was narrowing towards its distal end (figure 2.18a, a', b and b'). Another notable observation made here with CPP1/HyNMII double stain was that early nematocysts showed a larger diameter of the HyNMII collar that is usually narrow at the onset of tubulation (figure 2.18c and c'). These disordered structures in CytD-treated conditions were also associated with HYNMII-positive puncta. This is in line with the results obtained after BBS treatment, when the nematocyte structure, especially tubule formation, was hampered upon myosin inhibition and disintegrated tubule structures were found scattered around the nests of developing nematocysts. The same observation after inhibition of actin polymerisation indicates the importance of the collaborative function of actin and myosin during the developmental process.

Actin depolymerization by cytochalasin D treatment seems to relax the external tubule compression which perhaps results in a disbalance of the forces required to keep the outgrowing tubule contained or compressed and hence the expansion of the tubule diameter can be explained by this pressure compensation between capsule body and tubule. This theory has been represented in a schematic in figures 2.18e and f. Hence, it appears that the actin cytoskeleton at the vicinity of the tubule structures (shown in immuno-EM images in figure 2.17) supports the tabulation process as well as capsule body formation. These observations, together with the BBS treatment results, point towards the role of functioning Actin-Myosin machinery for the normal growth and development of the nematocysts.

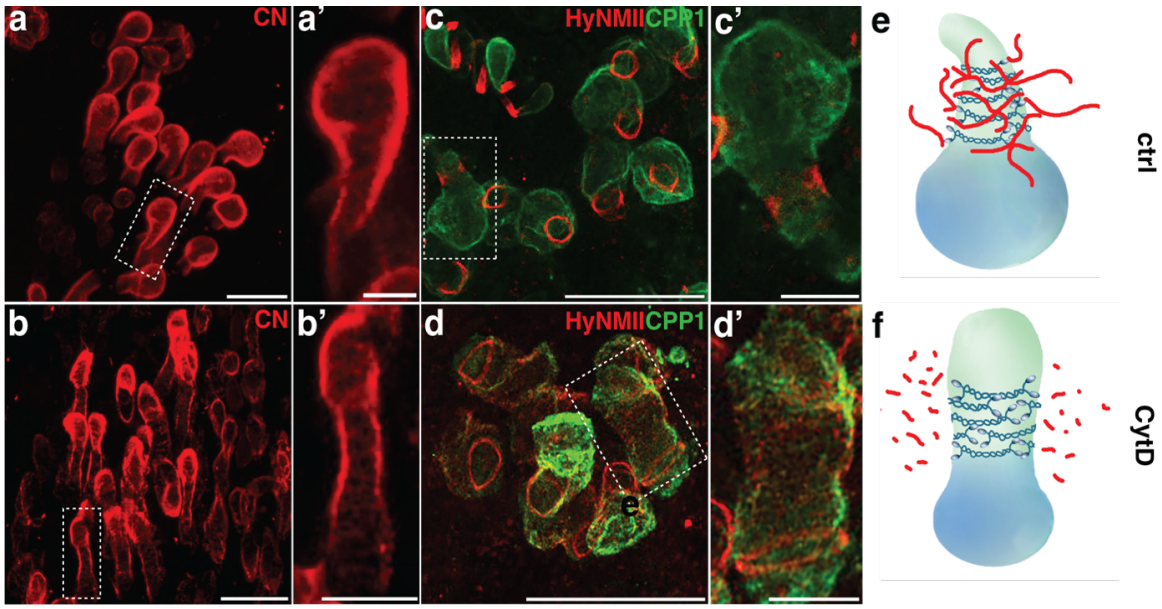

Figure 2.18 CytD treatment affects the morphogenesis of the growing tubule at initial stages.

(a) Cnidoin (CN)-marked stenotele nest in an early developmental stage in control conditions, **a')** A single nematocyte marked with a dotted line in figure 2.18a, portraying a clear morphology of the stenotele in control conditions exhibiting a roundish capsule body and a constriction of the tubule towards the distal end. **b)** A similar stage as in figure 2.18a, but after CytD treatment causing a reduced volume of the capsule body and a dilated tubule lumen as exemplified in b'. **c)** Nest of nematocytes double stained with HyNMII/CPP-1 in control conditions at the tubule protrusion stage where the tubulation is characterised by a broad and narrow collar marked by HyNMII (red) at the apex of CPP1- stained capsule (green). **c')** Higher magnification of the nematocyte marked by a dotted line in figure 2.18c, showing the characteristic morphology of this stage. **d)** A similar stage as in figure 2.18c after the CytD treatment showed an abnormally large diameter of the collar and a loss of the drop-like capsule shape when compared to the control conditions. This can be seen more clearly in d', the higher magnification image of the single nematocyte marked in (d-f) A scheme of the hypothesized role of HyNMII (blue) and Actin (red) stabilizing the early stage nematocyte by providing compressing forces to define the characteristic narrowing of the outgrowing tubule in control and the loss of longitudinal compression in CytD conditions, respectively. Scale bars - a, b, c, d: 20 µm; a', b', c', d': 5 µm. Figures a, a',b and b' acquired by Björn Eismann; e and f schematics by Gideon Bergheim.

Chapter 3

Discussion

3.1 HyNMII, a non-muscle myosin 2 type

A proteome study focused specifically on *Hydra* nematocysts revealed that 410 proteins are implicated in the structural assembly of the nematocyst [34]. Amongst these proteins, only a very small fraction has been investigated. Previously the structural proteins which provide the much-required tensile component of the nematocyst structure have been discussed. These structural proteins share common characteristics with the extracellular matrix (ECM). They consist of a well-categorized family of minicollagens, which, along with other structural proteins, underline the highly dense di-sulfide-linked collagenous wall of the capsule body. While these minicollagens provide the high tensile strength to the capsule wall to withstand the pressure as high as 150 bars [67, 102, 103], the elasticity nature of the capsule wall is accounted by elastomeric proteins such as Cnidoin. Cnidoin is a spider silk-like novel protein which colocalizes with minicollagens in the nematocyst wall and has been shown to contribute to the mechanistic property of fast kinetics happening during nematocyst discharge [104]. Although the sophisticated intracellular structure of the nematocyst also involves the coordination of other molecular factors as well to reach its final functional state, only one prominent motor protein has been found in the proteome. When this motor protein was further investigated through PSI-BLAST, it was found to be of non-muscular myosin II (NMII) type and designated as HyNMII. The primary sequence of the protein lacked an N-terminal signal peptide motif, which implies that it should be cytosolic.

Since an elaborate analysis of the assembly of the nematocyst structure remains to be elucidated, it is essential to analyze novel molecular factors and define their role in the synthesis of nematocysts. some structural proteins that contribute to provide structural integrity to the capsule wall have been investigated [34]. However, based on previously described nematocyst morphogenesis stages [58, 64] [47, 105]

several biochemical and biomechanical pathways, such as vesicle trafficking, budding, and protein complex assembly must also be involved for the ultimate synthesis of the functional nematocyst structure. The cell's cytoskeleton: actin, myosin, and microtubules are known to participate in and drive essential cellular mechanisms such as mitosis, cell cytokinesis, and vesicle transport [106–108]. Indeed, microtubules have already been shown to play an important role during the formation of nematocysts [58] but the role of actin-myosin networks has not been yet clearly stated in nematocyst morphogensis process. The identification of HyNMII in the *Hydra* nematocyst proteome drove my interest in understanding the role of this nematocyst-specific motor protein during the morphogenesis of the cnidarian stinging organelle.

As a first step to characterize this motor protein, I was able to confirm the presence of HyNMII in *Hydra* lysates by Western blot with specifically raised antibody (figure 2.1). In the following sections, I will discuss an elaborate study on the localization and the role of HyNMII in *Hydra* using different protein markers at different conditions.

3.2 *HyNMII* expression in *Hydra* supports its specificity towards nematocysts

HyNMII transcripts were detected through the whole mount *in situ* hybridization (WISH) in the endodermal epithelial cells at the site of bud formation as shown in figure 2.2a'. This reflects upon the possible role of HyNMII in bud detachment, which is also in line with a previous study where myosin II was shown to be involved in the control of cell shape changes [109]. Moreover, the *HyNMII* mRNA was expressed at the base of the tentacle region and faded towards the tip of the tentacles 2.2a, which might be an indicator of the presence of matured activated nematocyst. Mature nematocysts are transported to the tentacles from the body column and merged with the battery cell. Hence, the *HyNMII* mRNA expression in the endodermal cells might point out the possibility that HyNMII is involved in assisting the cell's orientation while they migrate to the tentacles. Fortunately, there are also other methods such as immunofluorescence and transmission electron microscopy, which provided much clearer and more elaborate insights towards the visualization of the protein of interest, discussed in the following sections.

The expression signatures of the genes of interest in *Hydra* could also be visualized in the published *Hydra* single-cell transcriptome database [88, 110]. Single-cell expression analysis data for *HyNMII* showed that it was expressed both in epithelial

cell lineages as well as during the entire life cycle of nematocytes. This indicated that HyNMII could play a role in nematocyst morphogenesis and, at the organismal level, could be involved in morphallactic tissue evagination processes at buds and tentacles that have been described to be induced by curvature and reorientation of the endodermal cell layer [111]. Also, *HyNMII* expression in the epithelial cell lineage can be explained by the fact that non-muscle myosin II is known to regulate and maintain cell size and shape [112–114].

3.3 Localization of HyNMII during growth stages of nematocyst morphogenesis

A very effective and straightforward method to visualize the protein of interest is through immunofluorescence (IF) [115], where proteins can be detected by an antibody specifically raised to bind the target or epitope. These epitopes are short amino acid sequences to which the complementary antibody binds and trigger a direct immune response [116]. The primary antibody was raised to bind against the epitope on the head domain of HyNMII and selected after it showed low sequence similarity to other myosins in *Hydra* genome. This primary antibody is further tagged with a fluorescent protein (direct IF) or identified by a fluorescently labelled secondary antibody (indirect IF), which results in the detection of the protein of interest through fluorescence microscopy. Using indirect IF of whole-mount *Hydra*, HyNMII was visualized throughout the gastric region of the animals in different types of developing nematocytes (Figure 2.4b results). The double staining with CPP-1, a capsule wall marker, revealed a clearer and segregated overview of the localization of HyNMII while the nematocytes go through different developmental stages chronologically (figure 2.4c-i). Using higher magnification, HyNMII was localized in developing nematocysts and could be visualized in specific structural parts of the nematocyst. Firstly, HyNMII was assembled at the neck of the nematocyst or base of the tubule right at the onset of vesicle membrane tubulation (figure 2.4d,g). This might indicate that the modifications in the membrane shape, which take place at the beginning of the formation of a tubule, might be a myosin-assisted process. Accumulation of HyNMII at this position hence might mean that it contributes to the force required for membrane constriction and tubule formation. This can be supported by the already known role of myosin II accumulation along with actin at cleavage furrow which is a precursor to membrane constriction event taking place during cytokinesis [117, 118].

Next, HyNMII was localized on the entire growing and elongating external tubule

(figure 2.4e and h). So, it might be the case that HyNMII binds to the cytosolic face of the tubule membrane and is also involved in tubule morphogenesis-specific processes such as the recruitment of proteins and stabilization or maintenance of the tubule during the structural modifications. This is in line with non-muscle myosin II being a characteristically cytosolic membrane protein, supported by a previous report [119]. It has been shown that a protein called 'p200' was characterized as an actin-based non-muscle myosin II motor and peripheral membrane protein, associated dynamically with Golgi membranes moreover, it has also been shown that it is part of the coat proteins involved in TGN vesicle trafficking [33, 98]. These findings support the fact that HyNMII is localized at the cytosolic face of the membrane and also possibly involved in the formation of shaft region by the fusion of HyNMII-coated vesicles from the TGN with the nematocyst vesicle membrane at its apical side through vesicle transport and budding.

Lastly, HyNMII was also detected when the tubule is completely invaginated and coiled inside the capsule body (figure 2.4f and g), which leads to an interesting observation about its localization. This indicates that HyNMII might be relocalised from the cytoplasmic face and into the capsule lumen as tubule invagination is accompanied by a complete inversion of the tubule. The morphogenesis of the tubule could involve a retraction of the membrane by a parallel exocytosis process into the nematocyst matrix. This assumption is supported by a similar mechanism that occurs during endocytosis-mediated cell migration where membrane retraction takes place [120].

Apart from this, there were some transient stages in which HyNMII could be visualized: during the intermediate stages where the tubule is partially invaginated and the remaining part is outside the capsule body (figure 5.1). It should be noted, however, that these phenotypes were rarely captured compared to the three stages mentioned above, which were visualized more prominently.

The localization of HyNMII in the three developmental stages determined by IFs were also confirmed by immuno-EM (figure 2.5a-c). The combined results from these two different localization methods indicate that HyNMII might participate in the assembly and stabilization of the tubule structure - from the onset of tubule formation, at the apex of the capsule, until it is invaginated and coiled inside the capsule body.

This specific association of non-muscle myosin II protein with Golgi membranes has also been shown earlier [121] and it is also known to be associated peripherally with the Golgi membrane. Hence, confirmation of recruitment of HyNMII was tested using Brefeldin A (BFA). BFA inhibits the interaction of coat proteins with the Golgi

membrane and these peripheral proteins are sensitive to BFA [122]. When animals were treated with BFA/HM, a prominent dissociation of HyNMII from the vesicle membrane was seen already after a few hours of treatment (figure 2.16b). Longer treatments led to more dramatic effects on nematocyst integrity and led to disruption of the CPP-1 lined capsule wall as well (figure 2.16c). This observation is the same effect seen after BFA exposure to cell culture which leads to the disassembly of the Golgi apparatus. The dissociation of HyNMII during the tubule formation upon exposure to BFA indicates that HyNMII is peripherally associated with the membrane. Additionally, according to the immuno-EM analysis (figure 2.5b), the immunogold label was found at the cytoplasmic face of the outgrowing tubule membrane. Taken together, these results confirm the peripheral attachment of HyNMII.

3.4 HyNMII - driving force for tubule morphogenesis in nematocysts

Myosin II is already known to play a role in cellular events such as membrane constriction, cytokinesis, vesicle transport, and Golgi vesicle fission and fusion. Because nematocyst morphogenesis involves such events, it is interpreted that the formation of the stinging organelle is a HyNMII-mediated process. After localizing HyNMII during nematocyst morphogenesis, the next step was to investigate or confirm the predicted role of HyNMII during the development of the nematocyst. Inhibiting or depleting the protein of interest and observing how the biological system is affected in its absence is a well-known method to understand the role of that protein. To perturb the function of a protein there are different techniques that can be employed. I used genetic knockdown and protein-specific inhibitors discussed as follows.

3.4.1 HyNMII inhibition through blebbistatin

As previously mentioned, one method to inhibit the function of the protein of interest is through chemical inhibitors. I used blebbistatin (BBS), a well-known myosin II inhibitor [123] and used a combination of various protein markers to visualize the effects of HyNMII inhibition on nematocyte development. It was hence hypothesized that continuous inhibition of HyNMII with BBS over a 7-day period would lead to a reduction in the population of nematocytes due to the turnover time of nematocyst in battery cells being 7-9 days [47]. Indeed, when visualized by a CPP-1/HyNMII double stain, continuous BBS treatment resulted in a dramatic reduction in the nematocyte population which was directly proportional to the days of treatment. The quantification of this reduction was statistically significant, according to

which the population was reduced up to 89% at day 7 of treatment when compared to day 0 (without BBS) (figure 2.7) . At the growing stage of the tubule, normally myosin seems to form a sheath around the tubule to provide structural support by a mechanical counterforce. The closeups at this stage post-BBS treatment were characterized by HyNMII-positive particles or puncta in the vicinity of nests with disintegrated external tubules which must be a cause of destabilization of tubule structure due to inhibition of HyNMII.

Another interesting observation was that these HyNMII-positive particles which apparently constitute fractions of the tubule, although failing to participate in nematocyst morphogenesis, were still able to move to the tentacle region and be incorporated into the battery cells. This indicates that even when nematocyst formation fails, the stinging cells can still follow the normal tissue flow, suggesting that these processes are independent of each other (figure 2.7 a, b) [63]. The diameter of the disintegrated vesicles was measured using higher magnification pictures and they were found to range from 1-4.5 µm. The diameter of these vesicles is quite close to phagosomes which are known to compartmentalize the unwanted cellular material through endocytosis and fuse with the lysosomes for the purpose of breaking down and recycling degraded proteins. Hence, it could be hypothesized that these disintegrated structures might be phagosomal vesicles that are involved in the recycling of these disintegrated particles which dissociated from tubule structures.

Since it is known that BBS as a myosin II inhibitor has a global effect on cellular processes like cytokinesis, I asked whether the observed nematocyst depletion might be caused by the inhibition of i-cell proliferation [48, 124]. To elucidate the specificity of the BBS effect on nematocysts, a transgenic strain expressing GFP under the control of the nanos promotor and thus marks undifferentiated i-cells was used (Cnnos::GFP), (figure 2.8) [94]. During the continuous 14-day BBS treatment (figure 2.8a-g), there was almost no effect on the population of interstitial stem cells (I cells) until 7 days post-treatment, while the nematocyte population showed a drastic depreciation by the end of 7 days of treatment. The overall i-cells only seem to be affected after 7 days and showed a reduction in their population only towards the end of 14 days (figure 2.8g), indicating the global cell morphology could be only an indirect secondary effect. This result, taken together with the previous findings, shows that HyNMII and in turn nematocytes synthesis are the primary target of BBS. Hence, this led to the conclusion that HyNMII plays a specific role in nematocyst morphogenesis.

The same continuous treatment with BBS was evaluated by staining with NOWA-CTLD and CPP-1 antibodies, which visualized late morphogenetic stages. Apart

from an overall reduction in the population of nematocytes, as expected, there were additional anomalies in the phenotypes observed. Early-stage nematocysts showed a non-synchronized development within one nest (figure 2.13d). Moreover, later developmental stages were characterized by distorted shaft structures along with incomplete nests due to disassembled nematocytes (figure 2.13e), and dispersed NOWA protein with unidentifiable tubule structures inside the capsule body instead of coiled tubules (figure 2.13f). This indicates that the assembly of NOWA at the invaginating tubule was affected due to missing tubule structures. This was also confirmed by the transgenic line in which NOWA-GFP fusion protein which normally detects mature tubules. Here, late-stage capsules showed missing tubule structures in the capsule matrix, and instead filled with dispersed NOWA protein (figure 2.13h). Taken together, these phenotypes underscore the essential role of HyNMII for tubule formation and nematocyst development in general.

3.4.2 Genetic knockdown of HyNMII through siRNA electroporation

The loss of function studies in *Hydra* has been achieved through the RNA interference method done by injecting the siRNA through electroporating the polyps [125, 126]. I used the siRNAs specific to HyNMII and analyzed the effects of the siRNA knockdown by using a combination of different protein markers for the readout. A double staining with CPP-1 (capsule wall marker) and HyNMII revealed interesting anomalies in the phenotypes of the KD condition (siHyNMII) compared to the control. The nematocysts in the siHyNMII treated animals showed HyNMII/CPP-1 lined irregular structural pattern on the tubule and rarely, sometimes even on capsule , as well as a loss of HyNMII in nests (figure 2.9e and f). This is likely a direct result of the knockdown of HyNMII. HyNMII KD during the early stages, when the tubule is undergoing external elongation, caused the tubule structures to disintegrate, parts of syncytium to be absent in the developing nests, and also sometimes capsule structures were seen distorted (figure 2.9f and g) when compared to the control (figure 2.9b and c). In later stages, when the tubule is invaginated and coiled inside the capsule body (figure 2.9d), HyNMII KD resulted in coiled tubules to disintegrate, which could be caused by the lack of HyNMII protein function or a result of the inability of the antibody to identify its target. The overall effect on the capsule and tubule morphology observed through the abnormal phenotypes after HyNMII KD indicates that the lack of HyNMII resulted in impaired and disordered nematocyst assembly and development, which mostly affected tubule morphogenesis.

Since HyNMII binds specifically to tubules during nematocyst development, I

also used another tubule marker, NOWA-CTLD (discussed in detail in section 3.9) to analyze the KD phenotypes. This offered to visualize the tubule morphology with a HyNMII-independent marker to rule out that the observed phenotypes are a consequence of diminished HyNMII detection. Hence, a different pair of protein markers were used, NOWA-CTLD (tubule marker) and CPP-1, to stain the animals under KD conditions. The nematocyte nests marked with these markers revealed asynchronous development of nematocysts within the same nest (figure 2.14a and d). Secondly, at the intermediate stage, the triple helical structure inside the capsule was distorted and blurry and, in rare cases, the entire capsule wall was also disrupted (figure 2.14b and e). This indicates that the knockdown of HyNMII led to malformed tubule structures probably by blocked tubule synthesis. The fact that the capsule body was also affected further suggests that, generally, the transport of structural proteins to the nematocyst was impaired, ultimately resulting in these anomalies. Lastly, the stage, which is characterized by invaginated and coiled tubules, was replaced by nematocysts with markedly reduced tubule lengths again indicating impaired tubule synthesis (figure 2.14c and f). In summary, these knockdown results, visualized by a combination of different markers, portray collaboratively that the structure of nematocysts, in particular tubule formation, is obstructed during its development in the absence of HyNMII.

The inhibition of HyNMII by either of the methods resulted in direct effects on the growth stages of nematocysts. The BBS treatment led to the disintegration of the tubule and dramatic effects on the population of nematocysts, while the HyNMII knockdown inhibits the tubule synthesis. This confirms that HyNMII drives the nematocyst tubulation process.

3.5 Role of HyNMII in vesicle assembly and fission

Nematocyst morphogenesis seems to be driven by HyNMII as discussed previously (section 3.4) although there was no information about when HyNMII began to exert its effects on the process. The synthesis of nematocysts is highly dependent on the incorporation of secretory proteins from the TGN, and these proteins must be transported to the nematocyst membrane from TGN. A previous study showed that Myosin II binds to the isolated Golgi membranes and shares similar characteristics as COP1(a coat protein on Golgi-derived vesicle), hence, it was characterized as a molecular motor that regulates the assembly and fission of transport vesicles from the TGN [119]. Another study claimed that Myosin II was part of novel coat proteins associated with Golgi-derived vesicles and was implicated to participate in vesicular transport [121].

Based on these previous findings, I was interested to verify if HyNMII also participates in the vesicle transport and fusion/fission secretary proteins involved to form the post-Golgi vesicle primordium, one of the earliest steps in nematocyst morphogenesis. The protein marker Ncol-1pp was used which marks transport vesicles of the TGN which fuse with the nematocyst membrane at the apex of the capsule. The fission/budding required for the generation of nematocyst-specific secretary vesicles was affected in absence of HyNMII. This could be observed evidently by the reduction in Ncol-1pp vesicles (figure 2.11a-e) post-BBS treatment. The decline of the overall population of Ncol-1pp-positive nests on Myosin II inhibition points towards the active participation of HyNMII in de novo nematocyst formation. This must be due to the inhibition of Golgi vesicle assembly/fission which must have resulted in the reduction of structural proteins required for nematocyst matrix formation. Hence, it could be hypothesized that HyNMII is necessary for the fission of TGN secretory vesicles which fuse with the nematocyst membrane to release structural proteins for capsule wall and tubule synthesis. However, it should also be noted here that the other effect of BBS on nematocysts during tubule formation/elongation where the tubule structure is mechanically destabilized is due to a lack of myosin function, not by depletion of additional vesicles from the Golgi.

3.6 Microtubule assisted nematocyst development

Microtubules are known for their role in cellular functions such as cell division, migration, and vesicle trafficking [11, 127] and these processes seem to be vital for stinging organelle formation (as discussed in previous sections). Given that nematocyst morphogenesis is dependent on HyMNII, I wanted to also study if other cytoskeletal structures such as microtubules also act in tandem to facilitate nematocyst formation. It has been shown previously that microtubules are abundant in the tentacles and organized in the form of a basket around matured nematocysts [99]. They have also been observed to be involved in the tubule invagination process in nematocysts in *Hydra* and also other cnidarians [128]. They are situated at a distance of 12 nm and are arranged as a spiral around the tip of the outgrowing tubule. Additionally, the number of microtubules accompanying the external tubule also varied depending on the type of nematocyst and specific regions of the tubule. Based on this, it was also hypothesized earlier that the external tubule thickness might be dependent on the ring of the microtubule present around it [58]. Thus, I checked for the presence of microtubules and confirmed through immunofluorescence the presence of β-tubulin at the tip of the growing tubule (shown by arrows in figure 2.10f). Hence, given the previous findings and the localization of the microtubules

in close vicinity of the growing capsule and tubule, tubulin seems to determine the diameter and also the type of nematocyst.

3.7 Interaction of HyNMII and Actin during membrane constriction initiating tubulation

The actin cytoskeleton is known to lay out a pathway for the myosin motor protein. Since the actin filament is polar [129], the movement of myosin is normally towards the 'plus' end of the filament. The actin-myosin interaction generates a pull and push force (contractile movements) which might be necessary for the formation of the tubule structure during nematocyte morphogenesis. Moreover, the self-organization of the actin cortex along with myosin II motors is known to be involved in pattern formation [100]. Tubule formation requires extensive structural modification from the onset of membrane tubulation at the apex of the capsule until invagination and coiling. The constriction that takes place during the beginning of tubule formation, or the initial neck formation, is shown to be marked by HyNMII (figure 2.4d and g). Thus, I asked whether the constriction in these early stages might be a result of contractile forces that are generated due to actin-myosin interactions. The actin cytoskeleton is known to be associated with plasma membranes and along with acting binding proteins it forms the cell cortex which in turn has been shown to be the principal determinant monitor of cell shapes. So, it can be assumed here that actin detection through electron microscopy at the vicinity of the growing tubule has to do with supporting the structure of the tubule during its growth phase [130].

Moreover, it was seen that treating the animals with the actin-depolymerizing drug, cytochalasin D led to abnormal nematocyte development, especially at the onset of membrane tubulation. The neck region at the beginning of tubule formation was much wider in the actin-inhibitory conditions compared to the control. Similarly, anti-Cnidoin immunofluorescence directed towards the capsule wall revealed an unusually expanded neck with shrunken capsule bodies (figure 2.18b, b') upon cytochalasin D treatment. This points towards the possible role of actin-myosin contractile forces playing an important role in maintaining tubule thickness and inducing membrane constriction (figure 2.18c-d').

It was shown earlier that the binding of Myosin II might be dependent on the membrane curvature and is biased towards a high curvature [131, 132]. Membrane protrusion during tubule initiation at the apical pole is characterized by a constriction, and the accumulation of HyNMII at the neck on the onset of tubule formation

could still be visualized even in actin-inhibitory conditions. This points towards the hypothesis that the primary force which drives membrane protrusion for tubulation might be made possible by HyNMII solely. A recent report stressed that Myosin VI, a molecular motor protein, is involved in remodelling the membrane and that myosin favours saddle-shaped membrane geometries. This study supports the hypothesis that a motor protein alone can drive the essential steps for membrane sculpting and modification. A mathematical simulation was also carried out to understand the interaction of HyNMII with the membrane (see section 3.8), which also supports the premise that HyNMII might be the sole force to drive essential morphogenesis steps described as follows.

3.8 Mathematical Model portraying the role of HyNMII

Nematocyst morphogenesis was further investigated using a mathematical simulation. The accumulation of HyNMII at the emergence of tubules was explained by a simulation approach in this mathematical model. The mathematical model is based on the mechanism called “bud-neck” scaffolding, which was shown in 2015 for an endosomal sorting complex required for transport (ESCRT) molecules [133]. The model explains how the shape of ESCRT molecules is sufficient to create membrane buds from a flat surface without the involvement of any other shaping components. This, in turn, results in the accumulation of similar shaped proteins leading to a protein ring. In this model, the simulation approach is based on a passive, or energy-minimizing, process, where shape patterning is purely dependent on membrane-mediated protein sorting and serves as an attractive force for proteins, which leads to bud formation. In this approach, the membrane is considered a 2D surface in a 3D system. Using a similar principle, this mathematical simulation was applied to investigate the binding of HyNMII during tubule formation in the nematocyst. In the simulation, it was demonstrated that the saddle-shaped HyNMII binding at the apex of the capsule (figure 3.1f right) is sufficient to trigger ‘neck’ formation, which initiates the formation of the external tubule. The shape of protrusion seen in the model can be reflected by the shape observed in the early stages of nematocysts morphogenesis (figure 3.1a-c). According to the mathematical model, HyNMII shows an affinity for a negative Gaussian curvature and forms a protein ring or belt-like structure around the growing tubule, which might be the prime force that drives the shape modification during tubule emergence without any assistance of contractile forces by actin.

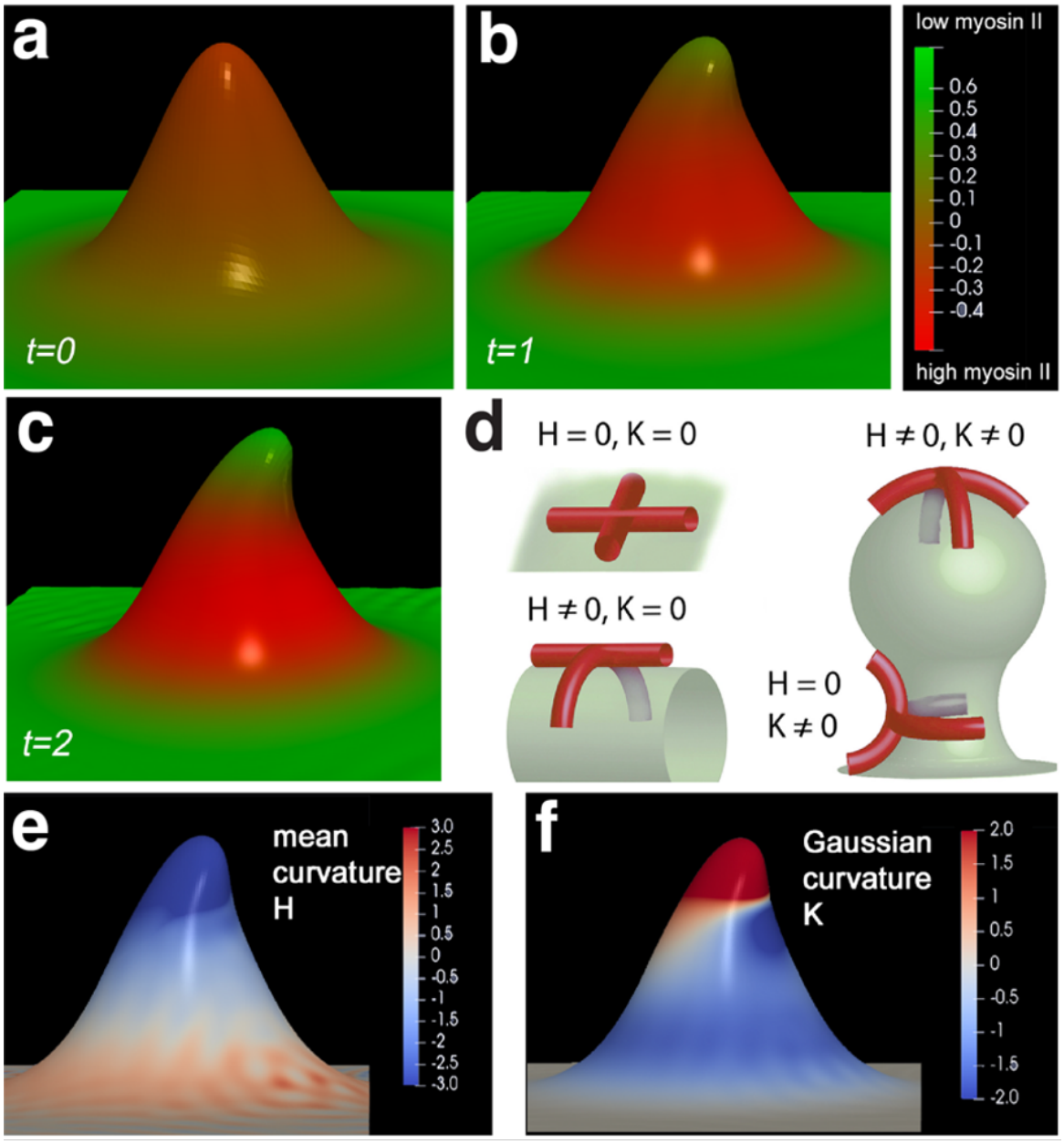

Figure 3.1 Mathematical model demonstrating that the accumulation of HyNMII leads to tubule formation. (a-c) Membrane geometry modifications are shown via mathematical simulations at three different increasing time intervals. The high density of HyNMII is represented by red and low by green colour respectively. d) Protein shapes and their association with the membrane of different mean curvature (H) and Gaussian curvature (K) including a membrane shapes tube, flat and budded-vesicle. (e and f) Mean curvature and Gaussian curvature for a membrane geometry where positive values are presented by red and negative values by blue. Mathematical model by Dr. Moritz Mercker.

3.9 NOWA assists the tubule invagination process in nematocysts

HyNMII seems to be an essential driving factor for the membrane constriction taking place at the onset of tubulation, as well as a support during the entire elongation process. Similarly, the remarkable phase of invagination accompanied by the formation of spines, during nematocyst morphogenesis must also require a driving force. As part of this project, I investigated and redefined the localization and function of NOWA as a major contributor to the tubule invagination process.

NOWA was already characterized as one of the major components of the nematocyst wall [96] previously but there were some doubts concerning the exact localization of the protein. With a polyclonal antibody raised against its CTLD domain, it was localized in the overall morphogenesis of nematocysts from early to late stages (figure 2.4d-i). It was seen as large protein granules inside the capsule matrix which undergo a phase conversion and disappear when tubule invagination begins, becoming fully integrated into the tubule during invagination. This is likely due to the binding of the lectin domain of NOWA to the chondroitin matrix [66], which acts as an outward scaffold on the outgrowing tubule. The transmission- EM images showed the local presence of NOWA spots inside the capsule matrix in form of a transient, lattice-like structure figure 5.5. It was also shown previously that under oxidizing conditions, NOWA forms disulphide-linked oligomers due to its CRD repeats at the C-terminus of the protein. Hence, a shift in the redox potential in the capsule matrix might be a responsible factor for the observed NOWA aggregates accompanying the tubule invagination. Spinalin, the spine proteins also accumulate as large granules in the capsule matrix during the early nematocyst morphogenesis. To reach their prospective destination on the outer surface of the tubule, they must pass through the tubule wall. Hence, it seems that NOWA also takes the same route from the capsule lumen during the onset of the invagination process that is when the tubule is bent inwards. This ensures that there must be a continuous feeding of NOWA proteins into the incoming tubule lumen to facilitate the invagination process.

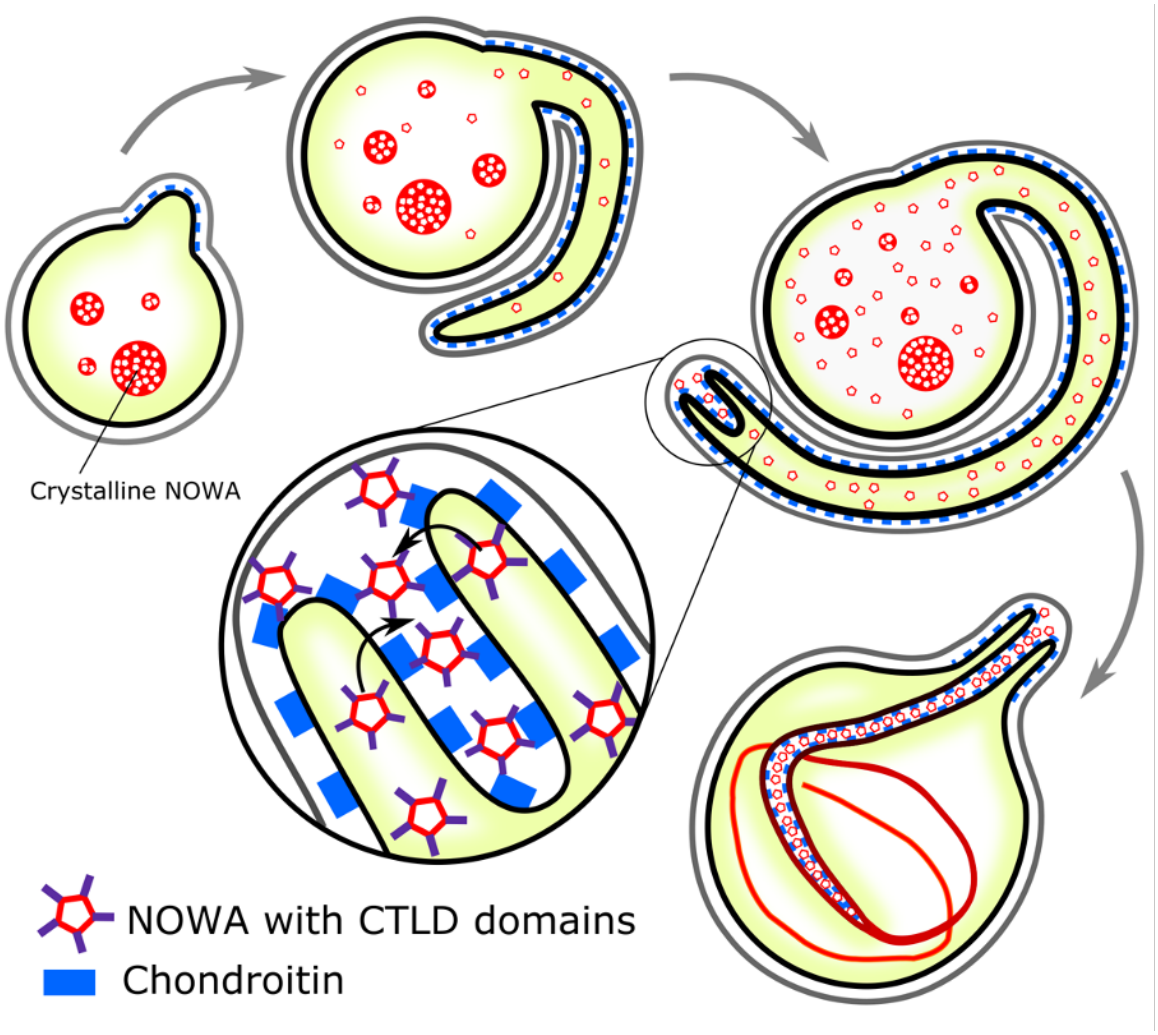

Figure 3.2 A Schematic showing the 'zipper' mechanism facilitated by NOWA to enable tubule invagination. Early to late stage of nematocyst morphogenesis with focus on the visualization of NOWA as the driving force specifically for tubule invagination by binding to Chondroitin and thereby creating a pulling mechanism to drive the tubule invagination like a 'zipper'. Schematic designed by Gideon Bergheim.

NOWA's domain architecture and its localization during nematocyst morphogenesis made it an ideal candidate to follow the invagination process. Hence, the transgenic NOWA::NOWA-GFP strain described earlier (section 2.8) was used for live imaging to track the trajectory of nematocyst morphogenesis (figure 5.6). This live imaging of nematocyst morphogenesis demonstrated that tubule invagination is closely correlated with both the dispersal of NOWA aggregates as well as the gradual condensation of NOWA at the coiled tubule structure within the capsule. This process takes about 6-7 hours. When the animals were electroporated with siRNA specific to NOWA, the tubule invagination process was hampered and the partially invaginated tubule stages were highly enriched. Due to the transient nature

of this stage, it is rarely detected in control animals. Hence, this leads to an interesting hypothesis that NOWA could induce an ATP- free, zipper-like mechanism, by a multivalent protein-carbohydrate interaction for the continuous, stable invagination of the inverted tubule. A schematic model portraying the localization and role of NOWA protein during the tubule invagination process is shown below in figure 3.2.

3.10 Conclusions

Using *Hydra* as the model organism, it is demonstrated that a non-muscle myosin II (HyNMII) drives critical steps in the formation of the tubule by forming a shaft-like structure by assembling to a collar that acts as a stabilization factor during tubule morphogenesis. The localisation of HyNMII during the development of nematocyst is visualised and confirmed by confocal and electron microscopy. The relation of HyNMII in the generation of nematocysts can be directly seen by depreciation in the nematocyst population upon blebbistatin treatment. HyNMII was also seen to be involved in the generation of TGN cargo vesicles which fuse to form the early nematocyst vesicle. The mathematical modelling pointed out HyNMII as a primary crucial factor driving the development steps such as membrane constriction. The role of HyNMII during tubule development was further confirmed by genetic knockdown which inhibited the tubule morphogenesis process. The Cytochalasin D treatment led to expansion in the diameter of the tubule shaft region in actomyosin dysfunctional conditions. Based on these findings, we suggest the hypothesis that the myosin sheath formed around the tubule exerts comprehensive forces on the tubule while contacting the actin filaments present at close vicinity of the external tubule. In addition to HyNMII's role in tubule morphogenesis, revision of the function of NOWA has been also addressed in this work. NOWA which was previously established as a protein specific to the capsule wall of nematocyst has been demonstrated as a major tubule component using the novel antibody along with the NOWA-GFP transgenic line. The live imaging and electron microscopy revealed that NOWA undergoes a phase transition from protein aggregates to dispersed solutions in the capsule lumen. siRNA knockdown results confirmed that NOWA is playing an essential role in tubule invagination by acting like a driving force in form of a zipper-like action by lectin-carbohydrate binding. This thesis work addresses the molecular basis of the sophisticated intracellular assembly of nematocyst, a hallmark organelle of cnidarians. Hence, the work can be extrapolated and might help to address the fundamental questions in the field of evolutionary biology such as tubule development and invagination in other members of the cnidarian phylum. Figure 3.3 shows a schematic summarizing the role of HyNMII and NOWA

during nematocyst morphogenesis.

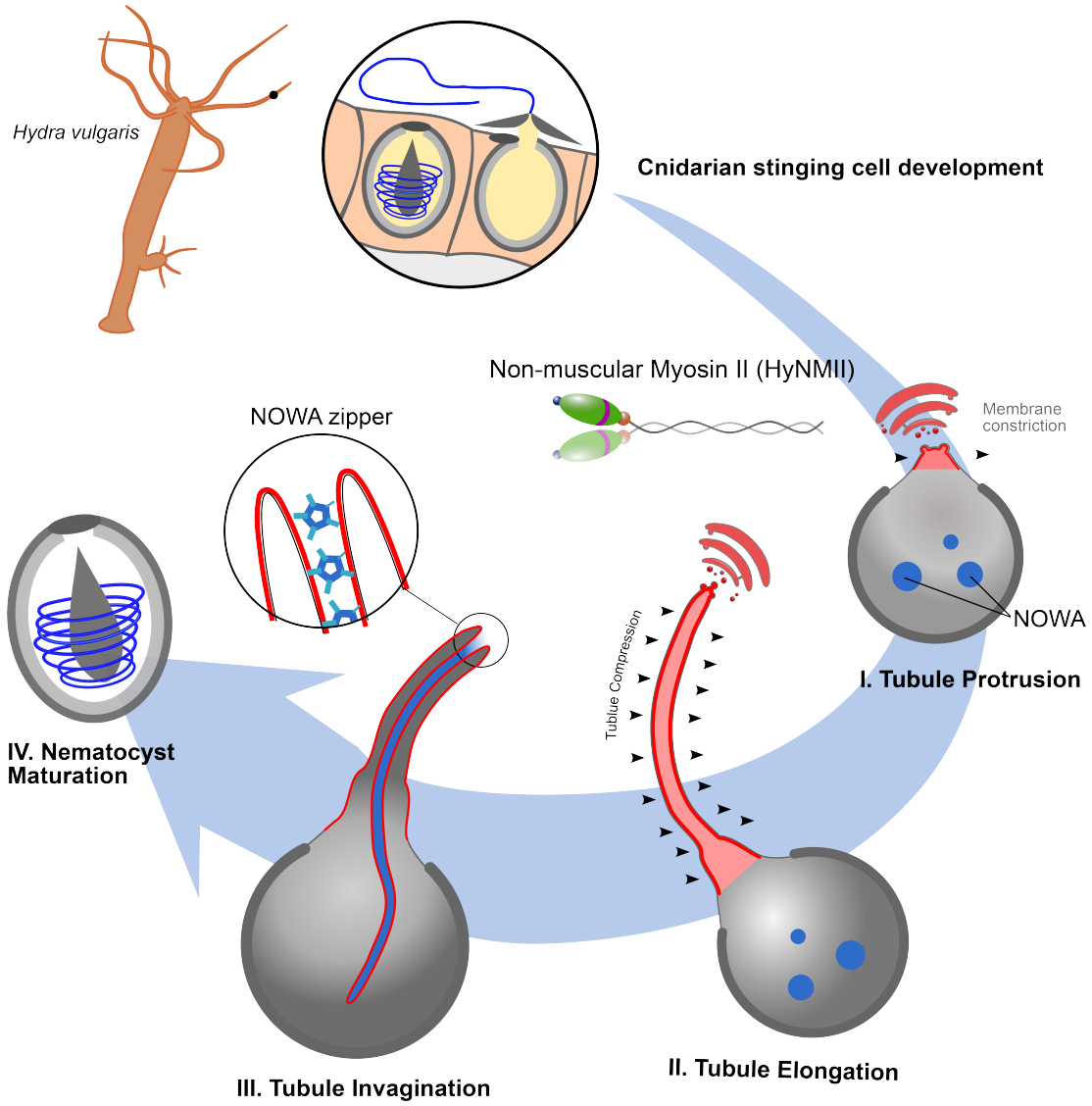

Figure 3.3 Summary of roles of HyNMII and NOWA. A schematic representing the role of HyNMII in shaft formation during tubule morphogenesis by assembling at the collar at the onset of membrane tubulation (I) and keeping the tubule structure stabilised during the entire tubule elongation (II). This is followed by the role of NOWA which undergoes a phase transition and acts as the driving force for tubule invagination (III) and hence leading to Nematocyst maturation(IV). Schematic designed by Gideon Bergheim.

Chapter 4

Materials and Methods

4.1 Materials

4.1.1 Antibodies

The protocol used for specific primary antibodies is described in the methods section, the secondary antibodies were always diluted 1:400. Following is the list of primary and secondary antibodies used for immunofluorescence experiments and western blots.

Antibodies	Source	Identifier
Alexa Fluor® 568 goat anti-rabbit IgG (H+L)	Thermo Fisher Scientific	Cat# A-11011, RRID:AB_143157
Alexa Fluor® 488 goat anti-rat IgG (H+L)j	Thermo Fisher Scientific	Cat# A-11006, RRID:AB_2534074
Peroxidase AffiniPure Goat Anti-Rabbit IgG (H+L)	Jackson ImmunoResearch Labs	Cat# 111-035-003, RRID:AB_2313567
Goat Anti-Guinea Pig IgG (H+L) Highly Cross-adsorbed Antibody, Alexa Fluor 488 Conjugated	Molecular Probes	Cat# A-11073, RRID:AB_2534117
Anti-HyNMII	Eurogentec	N/A
Anti-Cpp1	Eurogentec	N/A

Anti-Ncol-1 pp	Eurogentec	N/A
Anti-Beta Tubulin	Sigma-Aldrich	N/A
Anti-Cnidoin	Eurogentec	N/A
Anti-NOWA-CTLD	Eurogentec	N/A

Table 4.1 List of primary and secondary antibodies used for immunohistochemistry experiments.

4.1.2 Software tools

The raw images obtained after microscopy were analyzed, quantified and documented using the following software tools.

Software tools	**Source**	**Identifier**
Image J version 2.1.0/1.53c	Open-source image processing software	https://imagej.nih.gov/ij/ RRID:SCR_003070
Bio-formats plugin (FIJI)	Opensource	RRID:SCR_000450
Nikon A1R Confocal Laser Scanning Microscope	Nikon A1R Confocal Laser Scanning Microscope	RRID:SCR_020317
Nikon Eclipse 80i microscope	Nikon Eclipse 80i Advanced Research Microscope	RRID:SCR_015572
NIS elements Imagine software	Nikon Instruments Inc	https://www.microscope. healthcare.nikon.com /products/software /nis-elements
Microsoft Word version 16.64	Microsoft	https://www.microsoft .com/
Microsoft Excel version 16.63.1	Microsoft	RRID:SCR_016137 https://www.microsoft .com/
Inkscape version 1.0.2	Opensource	https://www. inkscape.org

Geneious Prime version 2020.2	Dotmatics	https://www. geneious.com/
Python version 3.9.7	Python Software Foundation	https://www. python.org/
Pandas version 1.4.3	Opensource	https://pandas. pydata.org/
ptitprince 0.2.5	Opensource	https://pypi.org/project/ptitprince/
Jupyter lab version 3.2.1	Opensource	https://jupyter.org
Adobe Illustrator 2022 version 26.0	Adobe Inc.	https://www.adobe.com/products/illustrator
Adobe Photoshop CC 2022 version 23.4.2	Adobe Inc.	https://www.adobe.com/products/photoshop
GraphPad Prism 9.3.1 (350)	Dotmatics	www.graphpad.com

Table 4.2 List of software tools and packages used for data analysis.

4.1.3 siRNAs

For the genetic knockdown experiments, the following siRNAs were designed using the protocol described in the methods section in detail.

siRNAs	Source	Sequences
siHyNMII	Sigma-Aldrich, Merck KGaA, Darmstadt,Germany	siNMY-1: AAGUUCAAUUGCAGCUUGAUA; siNMY-2: AAAGACAAAAGUUGCAACUCG
siNOWA	Sigma-Aldrich, Merck KGaA, Darmstadt,Germany	siNOWA-1:AACGAAGUCAUGUGCAUCAUA; siNOWA-2: AACGAAGUCAUGUGCAUCAUA

siGFP	Sigma-Aldrich, Merck KGaA, Darmstadt,Germany	AAGGUGAUGCAACAUACGGAA

Table 4.3 Amino acid sequence of siRNAs used for genetic knockdown experiments.

4.1.4 Inhibtors

The following inhibitors were used to perturb the desired functionality (Myosin II, Actin and attachment of coat proteins to membrane).

Inhibitors	**Source**
(-)-Blebbistatin	Sigma-Aldrich
Cytochalasin D	EMD Millipore Corp (Affiliate of Merck KGaA)
(+)-Brefeldin A	EMD Millipore Corp (Affiliate of Merck KGaA)

Table 4.4 List of chemical inhibitors.

4.1.5 Chemicals

Essential chemicals which were used to prepare buffer solutions and fixatives are listed below.

Chemicals	**Source**
2-Propanol ≥99.8%	Riedel-de Haën™, Honeywell
2-Propanol 99.9% (for cleaning)	Zentralbereich Neuenheimer Feld Abteilung 2.4 Zentrallager
4´,6-Diamidine-2´-phenylindole dihydrochloride (DAPI)	Roche Diagnostics GmbH
Acetic acid	Fluka™, Honeywell

Albumin Fraktion V, NZ-Origin (BSA)	Carl Roth GmbH
D(+)-Saccharose	Carl Roth GmbH
Formaldehyde solution min. 37%	Merck KGaA
Glycerol 99.5% bidistilled	VWR International
Glycine	neoFroxx GmbH
Methanol ≥99.8%	Riedel-de Haën™, Honeywell
Mowiol	Sigma-Aldrich
NaCl	neoFroxx GmbH
Na2HPO4 * 2 H2O	Fluka™
KCl	AppliChem GmbH
KH2PO4	Chemsolute, Th. Geyer GmbH & Co. KG
Paraformaldehyde	Carl Roth GmbH + Co. KG
Percoll™	GE Healthcare Bio-Sciences AB

Table 4.5 List of chemical solutions used for buffers and Fixatives.

4.1.6 Other lab apparatus

Some other lab apparatus for performing general lab tasks such as apparatus used while sample preparation for microscopy is listed below.

Other lab apparatus	**Source**
Cover slips 24x32 mm	Paul Marienfeld GmbH & Co. KG
Disposal bags	Sarstedt, Nürnbrecht
Double-sided adhesive tape	Tesa SE
Light source KL1500 LCD	Schott AG

Microscope slide 76x26 mm	neoLab Migge GmbH
Pasteur capillary pipettes	neoLab Migge GmbH
Roller mixer	Ingenieurbüro CAT, M. Zipperer GmbH
Stereo microscope	Nikon Minato, Tokyo, Japan
Test tube shaker	REAX 1 R, Heidolph
Whatman™ 3 MM CHR	GE Healthcare UK Limited
Whatman® lens cleaning tissue, Grade 105	Whatman, Cytiva

Table 4.6 List of other miscellaneous lab apparatus.

4.1.7 Model Organisms

The *Hydra* strains used for the experiments which included wild type and transgenic strain and the organism (Artemia salina nauplii) which served as the food to feed *Hydra* along with their source of availability is listed below.

***Hydra* strains**	**Source**
Hydra vulgaris AEP	Dr. Toshitaka Fujisawa
Artemia salina nauplii	Tropic Marine
Hydra vulgaris AEP NOWAp::NOWA:GFP	Dr. Anna Linn, Dr. Patrizia Adamczyk
Hydra vulgaris AEP Act::GFPectoderm/Act::RFPendoderm	Dr. Robert Steele
Hydra vulgaris AEP Cnnos1::GFP	Dr. Chiemi Fujisawa

Table 4.7 List of model organisms

4.2 Methods

4.2.1 *Hydra* culture and transgenic animals

Hydra magnipapillata strain 105 was kept at 18 °C in Hydra medium (HM, 1 mM $CaCl_2$, 1 mM NaH_2CO_3, 0.1 mM $MgCl_2$, 0.1 mM KCl, pH 6.8) and fed two to three times per week with freshly hatched Artemia salina nauplii. The medium was renewed 3–4 h after feeding and again the following day. Prior to each experiment animals were starved for at least 24 hours. A glass pipetted with flame polished tip (softening the edge) is used to handle the animals.

The transgenic NOWA::NOWA-GFP vector was designed on the basis of the previously described hOT G construct expressing EGFP under the control of the hydra actin promotor [134]. For this, the actin promotor sequence was replaced by 1127bp of the NOWA 5' region preceding the open reading frame using KpnI and BamHI restriction sites, respectively. In the expression construct the EGFP sequence is flanked by the NOWA signal peptide at the 5' end and the full-length NOWA sequence lacking the signal peptide at the 3' end. The coding sequence of the eGFP-NOWA fusion is followed by the actin 3' UTR. Generation of the transgenic NOWA::NOWA-GFP line was performed by microinjection as described before [134].

4.2.2 Inhibitor treatments

Blebbistatin Treatment (BBS)

(-)-Blebbistatin (Sigma – B0560) was solubilized in DMSO at 17 mM and stored at -20°C. For the treatment, a stock solution was prepared, by diluting BBS in HM to 0.25 µM. For controls, DMSO was dissolved in HM to the corresponding concentrations. At least 10 animals per day were collected for the BBS treatment and a time series of 7 days was done. Animals were kept at 18°C in 25 ml Petri dishes in incubators in BBS/HM. BBS/HM Medium was exchanged daily with a freshly prepared medium. Animals were fed twice during the treatment. At the end of 7 days, all the animals were fixed respectively depending upon the type of immunostaining to be performed with them.

2. Brefeldin A Treatment (BFA)

(+)-Brefeldin A (BFA), Eupenicilli (Merck-203729), was first solubilized in HM to prepare a stock solution of 0.5 mg/ml and stored at -20°C. For the treatment, the stock solution was diluted in HM to 30 µg/ml. Animals were incubated with BFA in 2ml Eppendorf tubes at RT on a shaker for a time series of 30 minutes, 1, 2 and 4 hours

and fixed for staining with respective fixatives. At least 10 animals were treated and analyzed per treatment time.

Cytochalasin D treatment

Cytochalasin D was solubilized in HM to prepare a stock solution of 1 mg/ml and stored at -80°C. For treatment, the stock solution was diluted to 5 µg/ml and 10 animals were incubated with the inhibitor in 2 ml Eppendorf tubes at RT on a shaker for 3 hours and fixed for staining with respective fixatives.

4.2.3 Immunohistochemistry

Fixatives were used depending on their compatibility with the primary antibody staining, mainly following two fixatives were used- • Freshly prepared 4% paraformaldehyde (Ncol-1pp,Cnidoin) and • Lavdovsky's fixative (50 % ethanol, 10 % formaldehyde, 4 % acetic acid) (HyNMII, CPP1,NOWA-CTLD and Beta tubulin) Prior to the addition of fixatives, animals were starved for 24 hours. On the following day, animals were then relaxed in 2% urethane for 1-2 minutes. After that, they were incubated with respective fixatives for 30 minutes at room temperature. After incubation with the fixative, animals were washed starting with PBS/0.1% Tween-20, followed by PBS/ 0.1 % Triton X-100 and again with PBS/0.1% Tween-20. All washing steps were done three times with an incubation time of 10 minutes for each step. Animals were then incubated overnight at 4 °C with the primary antibodies in PBS / 0.5 % BSA. Following is the list of primary antibodies with their dilutions and fixatives which were used:

Antibody	Dilution	Fixative	Host animal
Anti-HyNMII	02:40	Lavdovsky	Rabbit
Anti-CPP-1	04:20	Lavdovsky	Rat
Anti-Cnidoin	09:20	4% paraformaldehyde	Guineapig
Anti-Ncol1-pp	05:10	4% paraformaldehyde	Rabbit
Anti-Beta-tubulin	17:40	Lavdovsky	Mouse
Anti-NOWA-CTLD	07:40	Lavdovsky	Rabbit

Table 4.8 List of primary antibodies and corresponding fixatives

On the following day, the primary antibodies were washed using PBS/0.1 % Tween-20, three times with 10 minutes of incubation. Respective secondary antibodies were diluted 1:400 in PBS/1% BSA. Animals were incubated for 2-3 hours with secondary antibody/ PBS/1% BSA, followed by the addition of DAPI (1:1000) for nuclei staining and incubated for 10 minutes. After this, animals were washed in PBS two times with 10 minutes of incubation and mounted on clean glass slides using Mowiol as a mounting agent and sealed with a cover slip and spacers. For peptide competition, the antigenic peptide used for immunization was added at 1 mg/mL during primary antibody incubation. For the transgenic NOWA::NOWA-GFP strain, the animals were imaged life without prior fixation and either mounted in 2% agarose or 90% glycerol. For this, approximately 5 adult animals were collected and relaxed by incubating in 2% Urethane in HM for 5 minutes or in Linalool (1/1000, prepared in HM) for 15 minutes. Next, the samples were washed once with PBS, mounted on slides with spacers in 90% Glycerol, covered with a cover slip and sealed with nail polish. The prepared slides were imaged directly after mounting. For mounting in 2% agarose, the collected animals were relaxed with 1:1000 Linalool in HM for approximately 10 minutes. The foot and tentacles were cut off and the remaining body columns were transferred on the slides with double-sided tape spacers. After removing the remaining medium, 2% low gelling temperature agarose (Sigma) with 1:1000 Linalool was added and the slides were sealed with a coverslip. The samples were imaged on the same day. The images were acquired with the following microscopes: Nikon A1R confocal laser scanning microscope using the NIS Elements software, Versions 4.51.01 (Build 1146) or 5.11.01 (Build 1367) and objectives Apo LWD 40x WI λS DIC N2, Apo 60x Oil λS DIC N2, and Plan Apo λ 20x. Nikon AX microscope using the NIS Elements software, Version 5.40.02 (Build 1659) and the objectives Plan Apo λ 10x, Plan Apo VC 20x DIC N2 and Plan Apo λ 60x Oil. Further image processing was performed with Adobe Photoshop CS6 and Fiji.

4.2.4 siRNA knockdown by electroporation

siRNAs were designed using the following rules [126, 135, 136] • Find 19-21 bp sequence in the coding region starting with AA dinucleotide.

• GC contents between 30-50% seem to be more effective than those with higher GC contents, Keeping GC content 30-50%

• Avoiding poly(T) sequences (more than 3 nucleotides) since this serves as a termination signal for RNA pol III

• Design siRNAs targeting different loci within the gene of interest□ combination of

several siRNAs may result in a better knockdown efficiencies
• Check for off targets using the *Hydra* 2.0 database

Designed siRNAs were used for knockdown of expression of the protein of interest which was performed by electroporation using a transgenic *Hydra* vulgaris strain expressing endodermal GFP and ectodermal RFP as described before [137]. In the control condition 3 µM of siGFP (1 µM siGFP (AAGGUGAUGCAACAUACGGAA) and 2 µM scrambled siGFP (AAACCGGUGUGAAUCGAUGAGUUUU)) was used, in the experiment condition a combination of siGFP and two different HyNMII target siRNAs (siNMY-1: AAGUUCAAUUGCAGCUUGAUA; siNMY-2: AAAGACAAAAGUUGCAACUCG). The following steps were followed for the electroporation process and for taking care of the animals' post-electroporation.

• Collect medium-sized *Hydra* in a petri dish (20 animals /cuvette) that have been fed one day before electroporation.
• Wash 2x shortly in ddH2O (long incubation (>20min) with ddH2O will result in additional tissue destabilization).
• Transfer 20 animals into a 0.4 cm gap cuvette (BioRad), remove residual water and add 200µL siRNA mix (final concentration of siRNA: 1-4 µM in ddH2O; we usually use a final concentration of 3µM).
• Wait until animals are relaxed, put them into a pulse chamber and apply a single square pulse (range: 220-250V; 20-30msec/ Gene Pulser XCell with CE module; Bio-Rad).
• Add ice-cold restoration medium to cuvette and store on ice until all electroporations are done.
• Carefully transfer *Hydra* into petri dish filled with restoration medium (20% dissociation medium (v/v) in HM.
NOTE: Avoid excessive movement of the petri dish after the transfer • Let animals recover overnight; replace restoration medium with HM (animals are unaffected when pulsed at 220V; however, when animals are pulsed at 240V or higher in order to hit the endoderm/i-cells, they will lose their tentacles. They should regenerate within the first two days post-electroporation).
• Feed animals daily (knock-down should be detectable 3-4 days post-electroporation; recommended time window for experiments: 6-14 days post-electroporation).

Dissociation medium (3.6 mM KCl, 6 mM CaCl2, 1.2 mM MgSO4, 6 mM NaCitrate, 6 mM pyruvate, 4 mM glucose, 12.5 mM TES and Adjust pH to 6.9 before adding following antibiotics) prior to the electroporation process.

4.2.5 Recombinant protein expression and Western Blot analysis

Recombinant protein expression:

Amplification of the cDNA coding for the HyNMII motor domain (residues 84-760) was done PCR and cloned via a NdeI site into the pet19b vector (Novagen), which introduces an N-terminal polyhistidine tag. This was followed by the expression of recombinant protein in E. coli BL21 (DE3) cells by IPTG induction. Using ultrasound treatment several freeze/thaw cycles, the bacteria were lysed. This was followed by washing steps in which the obtained pellets containing the motor domain protein in inclusion bodies were washed 3 times using PBS/Tween-20 and then solubilized in protein sample buffer for SDS-PAGE using precast 4-15% gradient gels (Carl Roth).

Western blot detection:

The proteins (HyNMII or NOWA) were transferred to methanol activated PVDF membranes by wet blotting. This was followed by blocking the membranes for 1 hr at RT in PBS containing 5% BSA and 0.2% Tween-20 (PBST). Membranes were then incubated with polyclonal rabbit HyNMII antibody at 1:500 concentration in 1% BSA at 4 °C overnight. The next day, they were washed 3 × 5 min with PBST, and for detection, they were incubated with anti-rabbit horseradish peroxidase-conjugated antibody (Jackson ImmunoResearch, #115-035-044) at 1:10,000 concentration in PBST/ 5% BSA for 1 hr at RT. The membrane was then washed 2 × 5 min with PBST and 2 × 5 min with PBS. For enhanced chemiluminescence, blots were developed using a peroxidase substrate. For peptide competition, the antigenic peptide used for immunization was added at 1 mg/mL along with primary antibody incubation.

Nematocyst isolation and detection:

Isolation of intact nematocysts from wild-type and NOWA::NOWA-GFP transgenic animals was adapted from [34]. *Hydra*s were first frozen at 80°C (CryoCube F740h, Eppendorf, Hamburg, Germany) for at least 24 hours. Next step was to add homogenization buffer (50% Percoll, 10% sucrose, 0.3% Triton-X 100 in ddH2O) to the thawed tissue. The tissue was homogenized with a syringe in three steps using a 0.9, 0.7 and 0.55 diameter needle. The homogenized tissue was centrifuged for 15 minutes at 7500 rpm and 4 °C (5430 R + FA-45-30-11, Eppendorf, Hamburg, Germany). The supernatant was removed, and the pellet was resuspended in a homogenization buffer with a 0.55-diameter needle. After a second centrifugation, (15 minutes, 7500 rpm, 4°C) the pellet was resuspended in washing buffer (10% sucrose, 0.3 % Triton-X 100 in PBS) and centrifuged again. The resulting pellet

was resuspended in a small volume resuspension buffer (10% sucrose in PBS). For quantification in a Neubauer improved counting chamber (40442, Assistant®, Glaswarenfabrik Karl Hecht GmbH & Co KG, Sondheim vor der Rhön) an aliquot of the isolated nematocysts was diluted 1:100. At least one square of the chamber was counted (Axiovert 100, Zeiss, Oberkochen, Germany) and the mean of a square was multiplied by 1000 to get the number of nematocysts per microliter.

For detection of NOWA-CTLD, 200,000 isolated nematocysts were diluted with ddH2O and heated for 30 minutes at 96°C (Thermomixer comfort 5355, Eppendorf, Hamburg, Germany) with 1M DTT. After adding 3 µl sample buffer (300 mM TRIS pH 6.8, 10% SDS, 50% glycerol, 25% β-mercaptoethanol, 0.05% bromophenol blue), the nematocysts were heated again for 20 minutes at 96°C and centrifuged at 13,300 rpm for 5 minutes (Heraeus Pico 17, Thermo Fisher Scientific, Waltham, MA, USA). The samples were separated by SDS-PAGE using a precast 4-15% gradient gel (Q-PAGE TGN precast gel, SMOBIO Technology Inc., Hsinchu, Taiwan) which was pre-run for 70 minutes at 200 V. PageRuler™ Prestained protein ladder (26616, Thermo Fisher Scientific, Waltham, MA, USA) was used. The electrophoresis was done for 110 minutes at 160 V. The membrane was incubated overnight with the primary NOWA-CTLD antibody at 1:2000 and the secondary anti-rabbit-HRP antibody at 1:10000. The western blot analysis was performed as described above.

4.2.6 Image Analysis and Acquisition

Image acquisition was done at COS and partially at NIKON Imaging center using the following Microscopes:

1. Nikon A1R confocal laser scanning microscope (Nikon, Minato, Tokyo, Japan)
Objective: Plan Apo 10x
Imaging software: NIS Elements AR (version 4.51.01 (Build 1146)).
2. Nikon A1R confocal laser scanning microscope (Nikon, Minato, Tokyo, Japan) (NIKON imaging center)
Objective: Nikon Apo 60x Oil λS DIC N2
Imaging software: NIS Elements AR (version 5.11.01 (Build 1367))
3. Nikon AX confocal laser scanning microscope (Nikon, Minato, Tokyo, Japan)
Objective: Plan Apo VC 20x DIC N2 and a Plan Apo λ 60x oil immersion objective
Imaging software: NIS Elements AR (version 5.40.02 (Build 1659)).
4. Nikon SMZ 25(Made in Tokyo, Japan)

Image processing and analysis was done using FIJI The raw images were multiple stacks and multiple channels in nd2 format. Images were first converted to a

Maximal projection image and then into composite to have an overlap of the multiple channel image. Followed by this, they were converted to image format. Different FIJI MACROS were used to process multiple images. Python programming language was used to create some graphical plots such as the Raincloud plot in accordance with the inbuilt algorithm of 'Raincloud plots' [138] and also to convert the images into 300 DPI. 'GraphPad-Prism' was used to plot the graphs and as well as to test the statistical significance of the data from quantification results.

4.2.7 Quantification

To quantify the observations in BBS treated animals, a time series of 7 days was done as described above in the 'Inhibitors treatment' section. For each day, 3 animals were quantified, where the stenoteles nests in the body column of the animal was counted manually. The results were plotted in form of a standard bar graph, portraying the standard deviation and the difference in data significance was tested using one-way ANOVA test [139]. This particular quantification method was followed for 2 sets of results, BBS treated animals co-stained by 1.CPP1-HyNNMII and 2.Ncol1-pp.

4.2.8 Protein analysis and Single-cell expression

The analysis of proteins of interest (HyNMII and NOWA-CTLD) was done using Geneious Prime software. Tasks performed using this software included: Visualizing the binding region of siRNAs to their respective protein, Domain characterization of protein and Protein alignments 'NCBI database' and '*Hydra* genome 2' portals were used to perform the BLAST search for the proteins. Single-cell expression plot was derived from published cell clusters which are available online on *Hydra* Transcriptome database [110]. Firstly, the gene ID of the protein of interest is derived from an available online source for Hydra genome (https://research.nhgri.nih.gov/hydra/sequenceserver/). This was done by entering the annotated sequence of the protein (HyNMII) and BLASTing it in *Hydra* Genome 2 and selecting the Juliano aepLRv2" checkbox. The first two hits were *Hydra* striated muscle (t10222aep) and non-muscle (t8308aep) myosins. These were used to search their respective single-cell expression in different cell lineages in *Hydra* using the above-mentioned *Hydra* transcriptome database.

4.2.9 *Hydra* live imaging

NOWA::NOWA-GFP animals were used for live imaging. The transgenic strain was first starved for one week before live imaging. For immobilization during imaging, they were relaxed in 1µM linalool [140] in HM The tentacles and foot were

removed to further minimize any movements. 2% ultra-low gelling temperature agarose was used for mounting the remainder of the animals that is the body column in coverslip bottom dishes. A coverslip with spacers was mounted on top of the animals/agarose as a seal to limit the evaporation of the linalool during continuous live imaging. Nikon Ti2 microscope equipped with an LWD 40x NA 1.1 water immersion objective and water dispenser was used to carry out the time lapse imaging. Andor Zyla CMOS camera in wide field mode was used to capture the eGFP signal. Image specifications are as follows: A z-stack of 20 µm with a step size of 2 µm, imaged at 8 minutes intervals continuously over 10 hours at low illumination. The resulting images were processed by denoising using Nis-Elements 5.2. The movie shows a 3 slices projection.

4.2.10 Electron microscopy (EM)

Electron Microscopy was done in collaboration with Dr. Michael W. Hess, PhD, Associate, Professor of Cell Biology, Department of Anatomy, Histology and Embryology, Müllerstrasse 59, A-6020 Innsbruck. The methods are described in detail as follows.

EM method employed was adapted with slight modifications from the protocols described in [141, 142]. For sample preparation to do morphology studies, whole polyps were first subjected to rapid cryofixation (high-pressure freezing, freeze-substitution). This was followed by epoxy resin embedding and an optional section post-staining with heavy metals (uranyl acetate and lead; hot ethanolic phosphotungstic acid to highlight the cytoskeleton and membranes). Depending upon the antigen pre- and post-embedding labelling techniques both were employed to carry out the final immuno-EM. The pre-embedding NANOGOLD™ immunolabelling of HyNMII and actin in developing nematocytes with strong permeabilization was performed simultaneously with chemical fixation. This resulted in indispensable results (note that those protocols are not standard for immuno-EM because of the limited ultrastructure preservation). HyNMII was detected after fixation of the specimen using 80% (v/v) methanol plus 20 % (v/v) DMSO for 30 minutes at −20 °C, whereas actin in the cytoplasm of nematocytes was detected after the fixation with 4 % (w/v) formaldehyde in 0.1M phosphate buffer, mixed with 0.5 % (v/v) TritonTM X-100 (peroxide- and carbonyl-free: #9036-19-5 X100PC-5ML from Sigma) for 30 minutes at room temperature (modified after). This was followed by overnight storage of fixed samples at +4 °C in 4% buffered formaldehyde. Subsequent pre-embedding NANOGOLD™ immunolabelling was carried out as per protocols described in [141]. Bound rabbit anti-HyNMII (1:100) or mouse anti-actin

(Chemicon, clone C4 MAB1501R, 1:250) were visualized with NANOGOLD-Fab′ goat anti-rabbit/-mouse IgG (H + L) (#2004/2002; diluted at 1:150). This was followed by silver enhancement of the 1.4 nm small NANOGOLD™ conjugates using HQ-Silver (#2012, all from Nanoprobes Yaphank, NY, USA), and resin embedding. Next, post-embedding indirect immunogold labelling using rabbit anti-NOWA-CTLD (diluted 1:100) or with mouse anti-actin (from Chemicon) was performed on ultrathin cryosections from samples after thawing and fixing for 30 minutes at room temperature with 8 % (w/v) formaldehyde in 0.1 M phosphate buffer based on the standard protocols [141]. CM120 TEM (Philips, Eindhoven, The Netherlands) equipped with a MORADA G1 digital camera (EMSIS, Münster, Germany) was used for sample analysis. Image processing such as adjusting brightness, greyscale, and sharpness of the digital images, and pseudocolouring was carried out using Photoshop CS6 (Adobe). Size measurements were done with iTEM software (EMSIS).

4.2.11 *In situ* hybridization

WISH was performed as adapted from the methods as described before [143]. DIG-RNA Labeling Kit (Roche) was used to prepare the Digoxygenin (DIG)-labelled RNA probes. The RNA fragment which was used corresponds to the tail domain of HyNMII (bp 3720-4747). The final working concentration of each probe was set to 0,025 ng/mL for 60 hours at 55 °C to carry out the hybridization. This was followed by washing, and then the samples were left for overnight incubation in alkaline phosphatase (AP)-conjugated anti-DIG antibody (Roche). Colour reaction substrate used was an Undiluted BM purple. After incubation at RT for 13 minutes, the reaction was terminated. This was followed by the rehydration of whole animals and the samples were finally mounted on object slides using PBS and 90 % glycerol as the mounting agents. A Nikon Eclipse 80i microscope was used for imaging the sample.

4.2.12 Mathematical modelling

The mathematical model was done in collaboration with Dr. Moritz Mercker(Heidelberg University, AG Anna Marciniak-Czochra, Institute of Applied Mathematics, Mathematikon; Office: 02.225, Im Neuenheimer Feld 205, D-69120 Heidelberg, Germany). The mathematical model was adapted from a previously described membrane simulation framework based on interactions between ESCRT proteins shape and membrane curvature. This approach was adopted to verify if bud-neck scaffolding due to myosin II is sufficient to explain the early steps of nematocyst morphogenesis. The technical details of the model can be found in [133].

Chapter 5

Supplementary figures

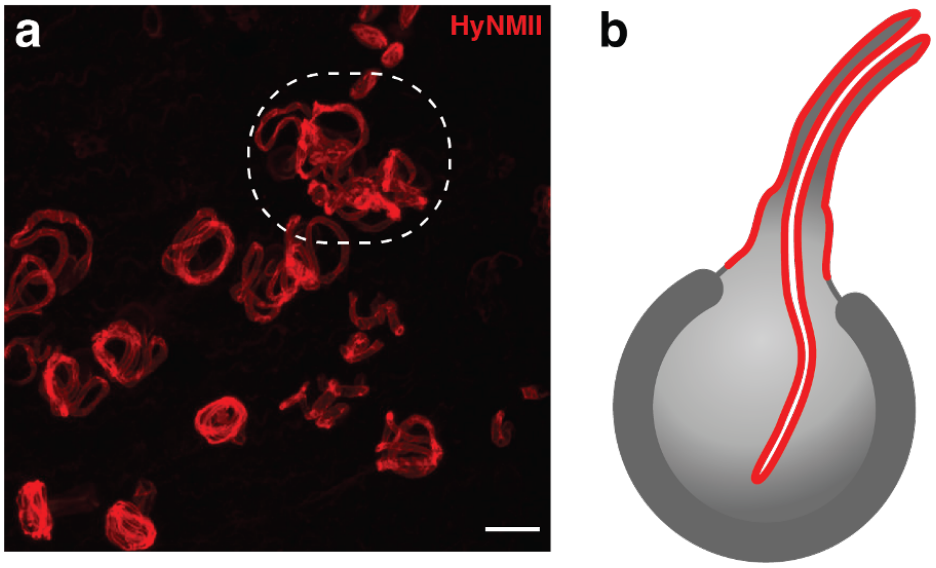

Figure 5.1 Localization of HyNMII during an Intermediate stage of nematocyst morphogenesis.

a) Intermediate stage of tubule invagination with partially invaginated tubule (related to figure 2.4), stained by HyNMII (red) (Scale bar- 10µm). **b)** Schematic of the transition stage corresponding to 'a', It can be noticed that tubule is thicker in the part external of the capsule matrix whereas the everted tubule invaginated is comparatively much thinner.

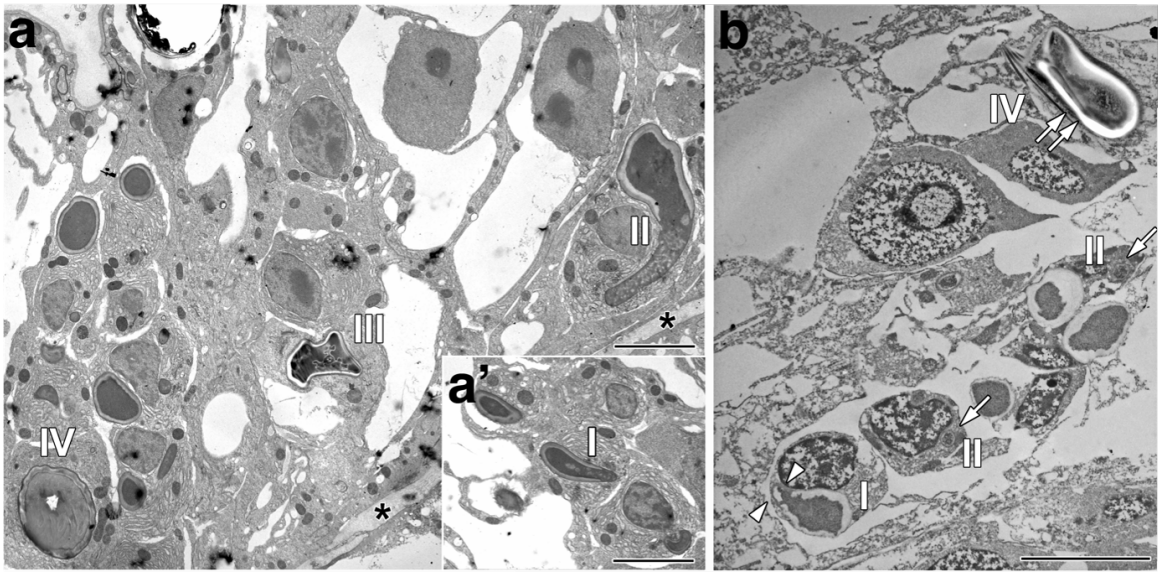

Figure 5.2 NANOGOLD™-silver-immunoelectron microscopy of nematocyst development stages, related to figure 2.5.

a, a') Overviews of cryofixed Hydra with all the developmental stages as follows: I, initiation of external tubule formation; II, tubule elongation; III, capsules with invaginated tubule, IV matured capsule with fully coiled and invaginated tubule. Asterisks (*) represents the mesoglea. Scale bars = 0.5 µm. **b)** Overview of MeOH + DMSO fixed nematocyte nests illustrating moderate, but acceptable structural preservation. Arrowheads mark the stage I nematocyst with protruding tube shown in figure 2.5a. Arrows points to cross-sectional, stage II external tubules corresponding to figure 2.5b , double arrows pointing towards stages III or IV nematocyte with inverted tubule (corresponding to figure 2.5c). Scale bar = 0.5 µm. Immuno-EM analysis was done in collaboration with Dr. Michael Hess.

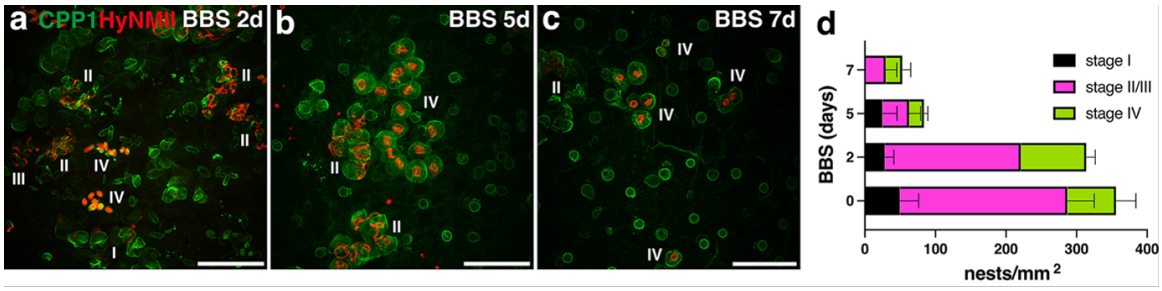

Figure 5.3 Quantification of stages of nematocysts development post-BBS treatment, related to figure 2.6

a-c) Representative images of the gastric region after BBS treatment, stained with CPP1 and HyNMII antibodies. **a)** Day 2 post-BBS treatment with all stages detectable, **b)** Day 5 post-BBS treatment with dramatic depletion of stages I-III nematocyst nests, Stage II nematocysts (elongating external tube) at day 5 of BBS treatment were associated with large HyNMII-positive particles indicating dissociation from the external tube (figure 2.6 b'-d') **c)** Day 7 of BBS treatment shows again dramatic depletion of stages I-III. It was also seen that at day 7, stage IV nests constituted nearly 43 % (19% in controls) of the population while stage I nematocysts were almost absent. **d)** Quantification of nematocyst stages in the gastric region of BBS-treated polyps at different days of treatment as in a-c. Data represents mean +/− S.D. from at least 3 animals compared to control polyps. Scale bars = 50 µm. Quantifictaion in 'd' was done with the help of Urška Knez Štibler

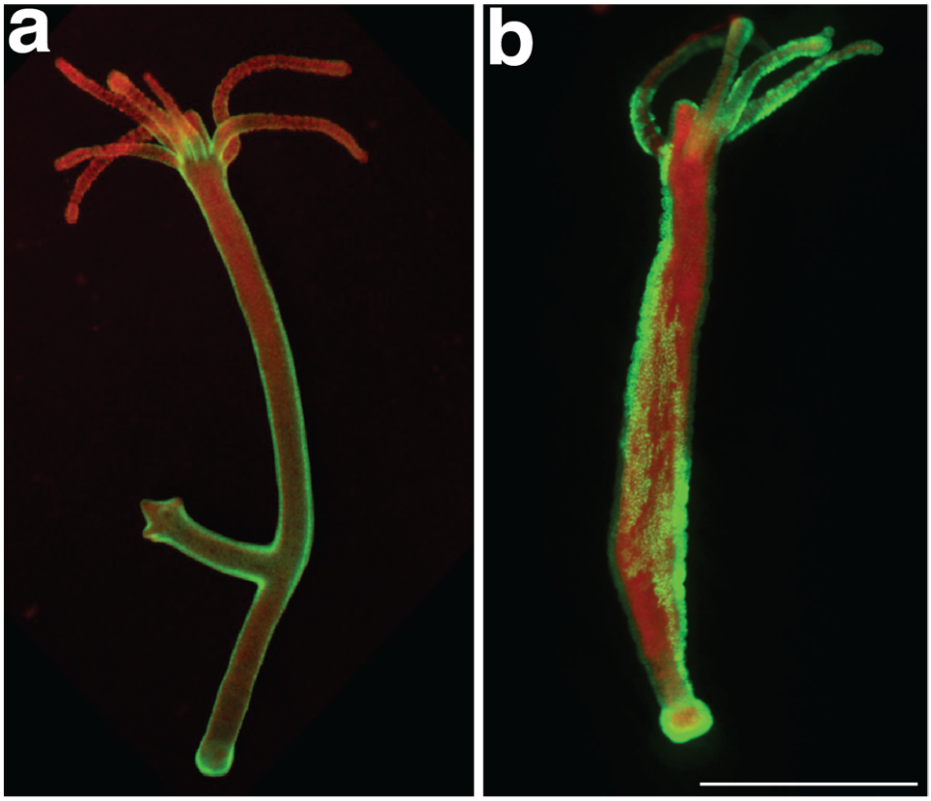

Figure 5.4 Transgenic animals expressing GFP in the ectoderm and RFP in the endoderm (Act::Endo-RFP/Ecto-GFP).

a) Cross-sectional image of a non-electroporated animal with intact GFP in the ectoderm and RFP in the endoderm. **b)** Electroporated animal treated with siGFP with visible compromised GFP layer in the ectoderm (related to figure 2.9 and figure 2.14). Scale bars-1mm

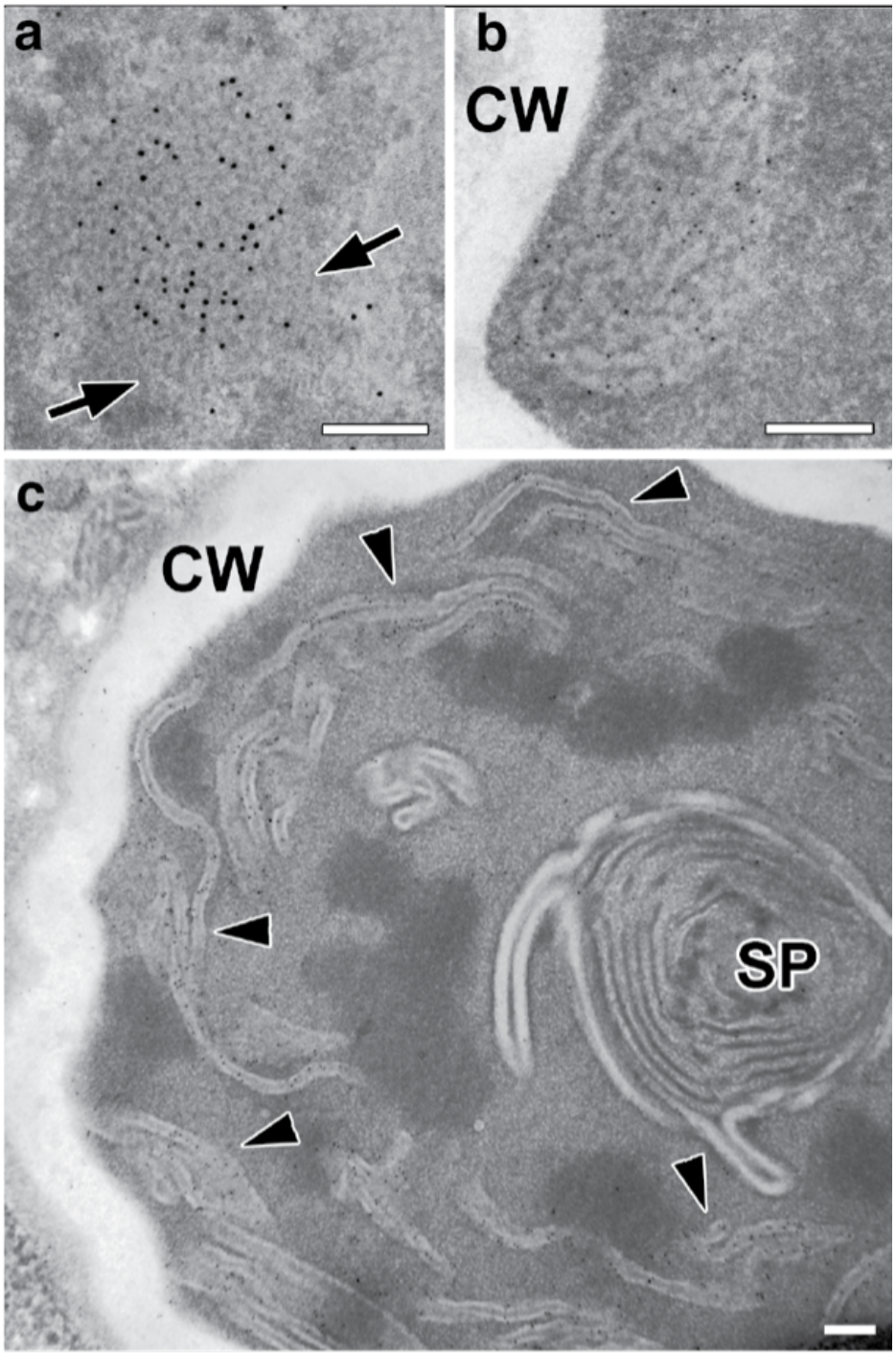

Figure 5.5 NOWA-CTLD detection by cryosection immunogold-EM (formaldehyde fixation).

a) In stage I nematocysts (see Figure 2.4a, d and 2.12a) with protruding external tubule, NOWA-CTLD was confined to 0.5-1 µm wide spots within the capsule which first comprised honeycomb-like patterns (arrows). **b)** more loosely arranged strand-like elements in stage II nematocysts. **c)** Stage III nematocysts showed NOWA-CTLD along the profiles of the inverted tube (marked by arrowheads). The multi-layered structure in the centre represents the spines (SP) that differentiate within the lumen of the tubule shaft region. CW = capsule wall. Scale bars = 200 nm. Immuno-EM analysis was done in collaboration with Dr. Michael Hess.

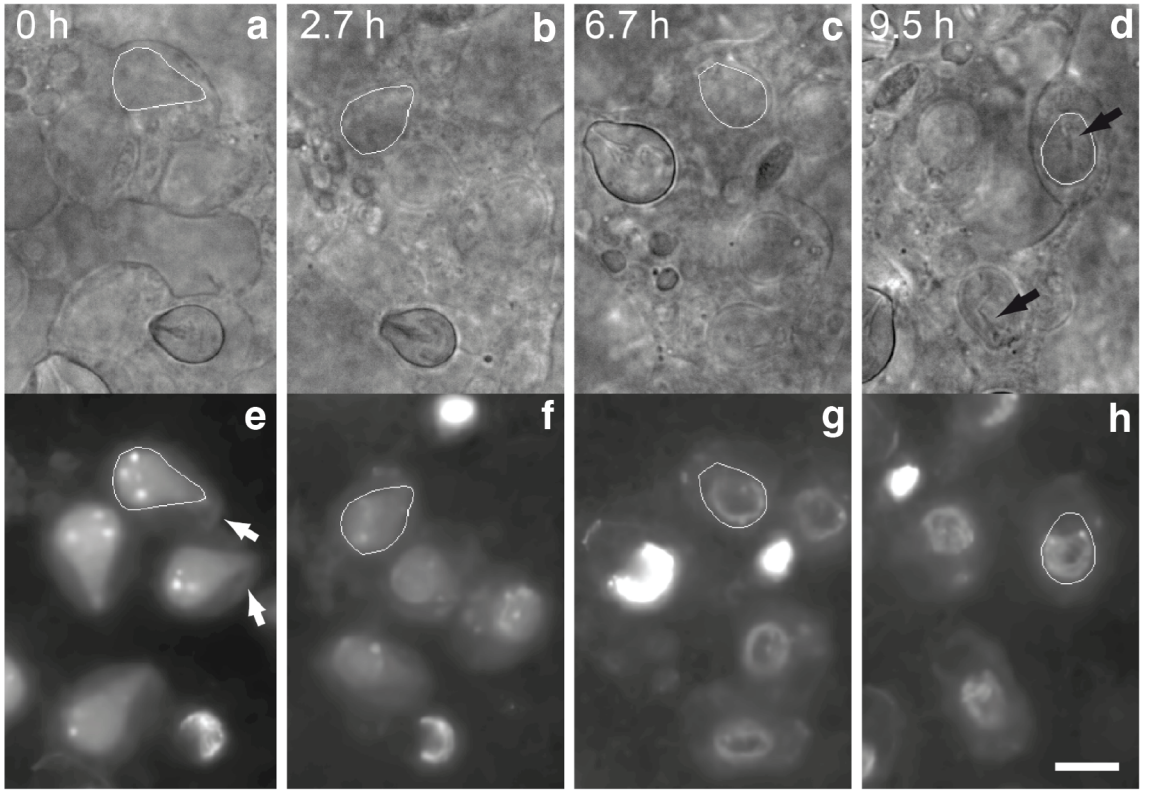

Figure 5.6 Live imaging of nematocysts morphogenesis using NOWA-GFP transgenics, related to figure 2.12

Time lapse video from **(a-d)** representing the fluorescent channel of different time points and corresponding bright field images **(e-h)**. During the invagination process of the tubule, NOWA aggregates(marked by arrows in 'e') continuously dissolve and NOWA protein associates with the tubule **(e-f)**. In image 'f' the pointed end of the capsule indicates that the invagination is still ongoing, whereas after 6.7 hours invagination seems to be completed **(c and g)** and the capsule is matured. Black arrows highlight the developing stylet apparatus at the end after invaginations are completed. Time-lapse imaging was done by Dr. Ulrike Engel and Annika Ohl.

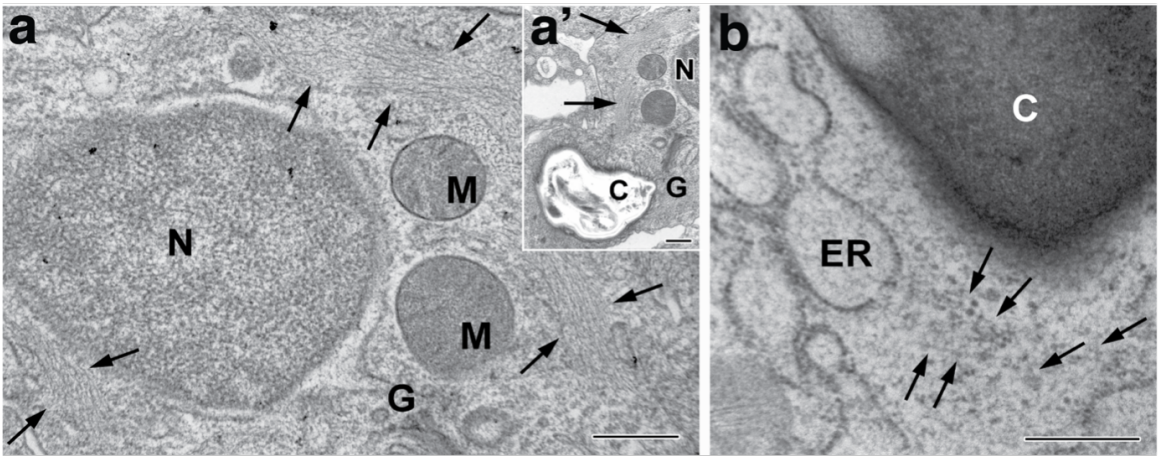

Figure 5.7 Immuno-EM data of actin localization at the ultrastructural level (related to figure 2.17

a) Cryofixed Hydra sample showing bundles of approximately 7nm wide microfilaments (arrows) possibly representing actin, in stage III nematocyte with inverted tubule; N = nucleus, M = mitochondria, G = Golgi/TGN. Scale bar= 500 nm. **(a')** Low magnification mirrored insert of the respective nematocyte shows possible signs of capsule (C) disintegration. Scale bar = 500 nm. **(b)** Single 6-7 nm microfilaments (arrows) in close vicinity of the ER and protruding tubule (T) of cryofixed state I nematocyte (figure 2.4a). Scale bar = 500 nm. Immuno-EM analysis was done in collaboration with Dr. Michael Hess.

References

[1] J. M. Allen. The molecular control of cellular activity. *The molecular control of cellular activity.*, 1962.

[2] Matthew D. Shoulders and Ronald T. Raines. COLLAGEN STRUCTURE AND STABILITY. *Annual review of biochemistry*, 78:929, 2009.

[3] Glareh Askarieh, My Hedhammar, Kerstin Nordling, Alejandra Saenz, Cristina Casals, Anna Rising, Jan Johansson, and Stefan D. Knight. Self-assembly of spider silk proteins is controlled by a pH-sensitive relay. *Nature*, 465(7295):236–238, 5 2010.

[4] J. T. Yen, J. A. Nienaber, D. A. Hill, and W. G. Pond. Potential contribution of absorbed volatile fatty acids to whole-animal energy requirement in conscious swine. *Journal of animal science*, 69(5):2001–2012, 1991.

[5] Rani Gupta, Paresh Gigras, Harapriya Mohapatra, Vineet Kumar Goswami, and Bhavna Chauhan. Microbial α-amylases: a biotechnological perspective. *Process Biochemistry*, 38(11):1599–1616, 6 2003.

[6] Anthony J. Roberts, Takahide Kon, Peter J. Knight, Kazuo Sutoh, and Stan A. Burgess. Functions and mechanics of dynein motor proteins. *Nature Reviews Molecular Cell Biology 2013 14:11*, 14(11):713–726, 9 2013.

[7] C. Rabouille, N. Hui, F. Hunte, R. Kieckbusch, E. G. Berger, G. Warren, and T. Nilsson. Mapping the distribution of Golgi enzymes involved in the construction of complex oligosaccharides. *Journal of cell science*, 108 (Pt 4)(4):1617–1627, 1995.

[8] Lidia Bonfanti, Alexander A. Mironov, José A. Martínez-Menárguez, Oliviano Martella, Aurora Fusella, Massimiliano Baldassarre, Roberto Buccione, Hans J. Geuze, Alexander A. Mironov, and Alberto Luini. Procollagen traverses the Golgi stack without leaving the lumen of cisternae: Evidence for cisternal maturation. *Cell*, 95(7):993–1003, 12 1998.

[9] Benjamin S. Glick and Akihiko Nakano. Membrane traffic within the Golgi apparatus. *Annual Review of Cell and Developmental Biology*, 25:113–132, 11 2009.

[10] Jennifer Lippincott-Schwartz, Nelson B. Cole, Alex Marotta, Patricia A. Conrad, and George S. Bloom. Kinesin is the motor for microtubule-mediated Golgi-to-ER membrane traffic. *Journal of Cell Biology*, 128(3):293–306, 2 1995.

[11] George M. Langford. Actin- and microtubule-dependent organelle motors: interrelationships between the two motility systems. *Current Opinion in Cell Biology*, 7(1):82–88, 1995.

[12] Sebastian Hoepfner, Fedor Severin, Alicia Cabezas, Bianca Habermann, Anja Runge, David Gillooly, Harald Stenmark, and Marino Zerial. Modulation of receptor recycling and degradation by the endosomal kinesin KIF16B. *Cell*, 121(3):437–450, 5 2005.

[13] Laurent Guillaud, Mitsutoshi Setou, and Nobutaka Hirokawa. KIF17 dynamics and regulation of NR2B trafficking in hippocampal neurons. *The Journal of neuroscience : the official journal of the Society for Neuroscience*, 23(1):131–140, 1 2003.

[14] Stéphanie Miserey-Lenkei, Hugo Bousquet, Olena Pylypenko, Sabine Bardin, Ariane Dimitrov, Gaëlle Bressanelli, Raja Bonifay, Vincent Fraisier, Catherine Guillou, Cécile Bougeret, Anne Houdusse, Arnaud Echard, and Bruno Goud. Coupling fission and exit of RAB6 vesicles at Golgi hotspots through kinesin-myosin interactions. *Nature Communications*, 2017.

[15] Steven P. Gross, Michael Vershinin, and George T T. Shubeita. Cargo Transport: Two Motors Are Sometimes Better Than One. *Current Biology*, 17(12):R478–R486, 6 2007.

[16] Richard E. Cheney, Maura K. O'Shea, John E. Heuser, Milton V. Coelho, Joseph S. Wolenski, Enilza M. Espreafico, Paul Forscher, Roy E. Larson, and Mark S. Mooseker. Brain myosin-V is a two-headed unconventional myosin with motor activity. *Cell*, 75(1):13–23, 10 1993.

[17] Bernardo J. Foth, Marc C. Goedecke, and Dominique Soldati. New insights into myosin evolution and classification. *Proceedings of the National Academy of Sciences of the United States of America*, 103(10):3681–3686, 3 2006.

[18] Richard E. Cheney and Mark S. Mooseker. Unconventional myosins. *Current Opinion in Cell Biology*, 4(1):27–35, 1992.

[19] Christopher Batters and Claudia Veigel. Mechanics and Activation of Unconventional Myosins. *Traffic*, 17(8):860–871, 8 2016.

[20] James W. Grant, Rui Q. Zhong, Pat M. Mcewen, and Susan L. Church. Human nonsarcomeric 20,000 Da myosin regulatory light chain cDNA. *Nucleic Acids Research*, 18(19):5892, 10 1990.

[21] J. S. Berg, B. C. Powell, and R. E. Cheney. A millennial myosin census. *Molecular Biology of the Cell*, 12(4):780–794, 2001.

[22] James R. Sellers. Myosins: a diverse superfamily. *Biochimica et Biophysica Acta (BBA) - Molecular Cell Research*, 1496(1):3–22, 3 2000.

[23] Inju Park, Cecil Han, Sora Jin, Boyeon Lee, Heejin Choi, Jun Tae Kwon, Dongwook Kim, Jihye Kim, Ekaterina Lifirsu, Woo Jin Park, Zee Yong Park, Do Han Kim, and Chunghee Cho. Myosin regulatory light chains are required to maintain the stability of myosin II and cellular integrity. *Biochemical Journal*, 434(1):171–180, 2 2011.

[24] Jie Sun, Yan Ning Qiao, Tao Tao, Wei Zhao, Li Sha Wei, Ye Qiong Li, Wei Wang, Ye Wang, Yu Wei Zhou, Yan Yan Zheng, Xin Chen, Hong Chun Pan, Xue Na Zhang, and Min Sheng Zhu. Distinct Roles of Smooth Muscle and Non-muscle Myosin Light Chain-Mediated Smooth Muscle Contraction. *Frontiers in Physiology*, 11:1610, 12 2020.

[25] Yong Liang, Aihui Wang, Inna A. Belyantseva, David W. Anderson, Frank J. Probst, Thomas D. Barber, Webb Miller, Jeffrey W. Touchman, Long Jin, Susan L. Sullivan, James R. Sellers, Sally A. Camper, Ricardo V. Lloyd, Bechara Kachar, Thomas B. Friedman, and Robert A. Fridell. Characterization of the human and mouse unconventional myosin XV genes responsible for hereditary deafness DFNB3 and shaker 2. *Genomics*, 61(3):243–258, 11 1999.

[26] Valerie Mermall, Penny L. Post, and Mark S. Mooseker. Unconventional myosins in cell movement, membrane traffic, and signal transduction. *Science*, 279(5350):527–533, 1 1998.

[27] Li Wang, Janelle Geist, Alyssa Grogan, Li Yen R. Hu, and Aikaterini Kontrogianni-Konstantopoulos. Thick filament protein network, functions, and disease association. *Comprehensive Physiology*, 8(2):631–709, 4 2018.

[28] Susan S. Brown. Myosins in yeast. *Current Opinion in Cell Biology*, 9(1):44–48, 1997.

[29] P Marz, J Stetefeld, K Bendfeldt, C Nitsch, J Reinstein, R L Shoeman, B Dimitriades-Schmutz, M Schwager, D Leiser, S Ozcan, U Otten, and S Ozbek. Ataxin-10 interacts with O-linked beta -N-acetylglucosamine transferase in the brain. *J Biol Chem*, 2006.

[30] Jeffrey P. Baker and Margaret A. Titus. A family of unconventional myosins from the nematode Caenorhabditis elegans. *Journal of Molecular Biology*, 272(4):523–535, 10 1997.

[31] Anthony J. Kee, Lingyan Yang, Christine A. Lucas, Michael J. Greenberg, Nick Martel, Gary M. Leong, William E. Hughes, Gregory J. Cooney, David E. James, E. Michael Ostap, Weiping Han, Peter W. Gunning, and Edna C. Hardeman. An actin filament population defined by the tropomyosin Tpm3.1 regulates glucose uptake. *Traffic (Copenhagen, Denmark)*, 16(7):691–711, 7 2015.

[32] Dennis Zimmermann, Alicja Santos, David R. Kovar, and Ronald S. Rock. Actin age orchestrates myosin-5 and myosin-6 run lengths. *Current biology : CB*, 25(15):2057–2062, 8 2015.

[33] Anne Müsch, David Cohen, and Enrique Rodriguez-Boulan. Myosin II is involved in the production of constitutive transport vesicles from the TGN. *Journal of Cell Biology*, 1997.

[34] Prakash G. Balasubramanian, Anna Beckmann, Uwe Warnken, Martina Schnölzer, Andreas Schüler, Erich Bornberg-Bauer, Thomas W. Holstein, and Suat Özbek. Proteome of Hydra Nematocyst. *Journal of Biological Chemistry*, 287(13):9672–9681, 3 2012.

[35] D. Bridge, C. W. Cunningham, R. DeSalle, and L. W. Buss. Class-level relationships in the phylum Cnidaria: molecular and morphological evidence. *Molecular biology and evolution*, 12(4):679–689, 1995.

[36] Simon Conway Morris. The Cambrian ”explosion”: slow-fuse or megatonnage? *Proceedings of the National Academy of Sciences of the United States of America*, 97(9):4426–4429, 4 2000.

[37] U. Technau and R. E. Steele. Evolutionary crossroads in developmental biology: Cnidaria. *Development*, 2012.

[38] Casey W. Dunn, Andreas Hejnol, David Q. Matus, Kevin Pang, William E. Browne, Stephen A. Smith, Elaine Seaver, Greg W. Rouse, Matthias Obst, Gregory D. Edgecombe, Martin V. Sørensen, Steven H.D. Haddock, Andreas Schmidt-Rhaesa, Akiko Okusu, Reinhardt Møbjerg Kristensen, Ward C. Wheeler, Mark Q. Martindale, and Gonzalo Giribet. Broad phylogenomic sampling improves resolution of the animal tree of life. *Nature*, 452(7188):745–749, 4 2008.

[39] Allen G. Collins. Phylogeny of medusozoa and the evolution of cnidarian life cycles. *Journal of Evolutionary Biology*, 15(3):418–432, 2002.

[40] Abraham Trembley. Mémoires pour servir à l'histoire d'un genre de polypes d'eau douce à bras en forme de cornes, 1744.

[41] Richard N Mariscal. *Experimental marine biology*. Academic Press, New York„ 1974.

[42] T W Holstein and C N David. Cell cycle length, cell size, and proliferation rate in hydra stem cells. *Dev Biol*, 142(2):392–400, 1990.

[43] Bruno Gideon Bergheim and Suat Özbek. Extracellular matrix and morphogenesis in cnidarians: A tightly knit relationship, 2019.

[44] U Technau, C Cramer von Laue, F Rentzsch, S Luft, B Hobmayer, H R Bode, and T W Holstein. Parameters of self-organization in Hydra aggregates. *Proc Natl Acad Sci U S A*, 97(22):12127–12131, 2000.

[45] A. Gierer, S. Berking, H. Bode, C. N. David, K. Flick, G. Hansmann, H. Schaller, and E. Trenkner. Regeneration of hydra from reaggregated cells. *Nature: New biology*, 239(91):98–101, 9 1972.

[46] Robert E. Steele. Developmental Signaling in Hydra: What Does It Take to Build a "Simple" Animal? *Developmental Biology*, 248(2):199–219, 8 2002.

[47] H R Bode and C N David. Regulation of a multipotent stem cell, the interstitial cell of hydra. *Prog Biophys Mol Biol*, 33(2):189–206, 1978.

[48] T C Bosch and C N David. Decision making in interstitial stem cells of Hydra. *In Vivo*, 5(5):515–520, 1991.

[49] C K Teragawa and H R Bode. Migrating interstitial cells differentiate into neurons in hydra. *Dev Biol*, 171(2):286–293, 1995.

[50] Hydra budding Art Print by Science Photo Library - Fine Art America.

[51] Hans R. Bode. The Role of Hox Genes in Axial Patterning in Hydra1. *American Zoologist*, 41(3):621–628, 2001.

[52] Robert E. Steele, Charles N. David, and Ulrich Technau. A genomic view of 500 million years of cnidarian evolution. *Trends in Genetics*, 27(1):7–13, 1 2011.

[53] Yu Chang and Hua Chun Zeng. Controlled synthesis and self-assembly of single-crystalline CuO nanorods and nanoribbons. *Crystal Growth and Design*, 4(2):397–402, 3 2004.

[54] J Weber, T Schurholz, and E Neumann. The nematocyst extract of Hydra attenuata causes single channel events in lipid bilayers. *Toxicon*, 28(4):403–409, 1990.

[55] Anna Beckmann and Suat Özbek. The nematocyst: A molecular map of the cnidarian stinging organelle. *International Journal of Developmental Biology*, 2012.

[56] R Weill. Contribution a l'etude des cnidaires et de leurs nematocystes. II. Valeur taxonomique du cnidome. *Trav*, (11):351–701, 1934.

[57] R Weill. Contribution a l'etude des cnidaires et de leurs nematocystes, I. Recherehes sur les nema-tocystes (Morphologie, Physiologie Developpement). *Trav*, (10):1–347, 1934.

[58] T Holstein. The morphogenesis of nematocytes in Hydra and Forskalia: an ultrastructural study. *J Ultrastruct Res*, 75(3):276–90, 1981.

[59] T W Holstein, R D Campbell, and P Tardent. Identity crisis. *Nature*, 346:21–22, 1990.

[60] G B Chapman and L G Tilney. Cytological studies of the nematocysts of Hydra. II. The stenoteles. *J Biophys Biochem Cytol*, 5(1):79–84, 1959.

[61] Thomas L Lentz. INTRAMITOCHONDRIAL GLYCOGEN GRANULES IN DIGESTIVE CELLS OF HYDRA.

[62] C N David and D Challoner. Distribution of interstitial cells and differentiating nematocysts in nests in Hydra attenuata. *American Zool*, 14(2):537–542, 1974.

[63] R D Campbell and B A Marcum. Nematocyte migration in hydra: evidence for contact guidance in vivo. *J Cell Sci*, 41:33–51, 1980.

[64] D B Slautterback and D W Fawcett. The development of the cnidoblasts of Hydra; an electron microscope study of cell differentiation. *J Biophys Biochem Cytol*, 5(3):441–452, 1959.

[65] R J Skaer. The secretion and development of nematocysts in a siphonophore. *J Cell Sci*, 13(2):371–93, 1973.

[66] Patrizia Adamczyk, Claudia Zenkert, Prakash G. Balasubramanian, Shuhei Yamada, Saori Murakoshi, Kazuyuki Sugahara, Jung Shan Hwang, Takashi Gojobori, Thomas W. Holstein, and Suat Özbek. A non-sulfated chondroitin stabilizes membrane tubulation in cnidarian organelles. *Journal of Biological Chemistry*, 2010.

[67] Ulrike Engel, Olivier Pertz, Charlotte Fauser, Jürgen Engel, Charles N. David, and Thomas W. Holstein. A switch in disulfide linkage during minicollagen assembly in hydra nematocysts. *EMBO Journal*, 2001.

[68] J Weber. Poly(gamma-glutamic acid)s are the major constituents of nematocysts in Hydra (Hydrozoa, Cnidaria). *J Biol Chem*, 265(17):9664–9, 1990.

[69] M Klug, J Weber, and P Tardent. Hemolytic and toxic properties of Hydra attenuata nematocysts. *Toxicon*, 27(3):325–339, 1989.

[70] K Hausmann and T Holstein. Bilateral symmetry in the cnidocil-nematocyst complex of the freshwater medusa Craspedacusta sowerbii Lankester (Hydrozoa, Limnomedusae). *JOURNAL OF ULTRASTRUCTURE RESEARCH*, 90(1):89–104, 1985.

[71] T Holstein and P Tardent. An ultrahigh-speed analysis of exocytosis: nematocyst discharge. *Science*, 223(4638):830–3, 1984.

[72] P Tardent and T Holstein. Morphology and morphodynamics of the stenotele nematocyst of Hydra attenuata Pall. (Hydrozoa, Cnidaria). *Cell Tissue Res*, 224(2):269–290, 1982.

[73] Qian Ba, Yuanyuan Hei, Anasuya Dighe, Wenxue Li, Jamie Maziarz, Irene Pak, Shisheng Wang, Günter P. Wagner, and Yansheng Liu. Proteotype coevolution and quantitative diversity across 11 mammalian species. *Science Advances*, 8(36):756, 9 2022.

[74] Leslie S. Babonis, Camille Enjolras, Joseph F. Ryan, and Mark Q. Martindale. A novel regulatory gene promotes novel cell fate by suppressing ancestral fate in the sea anemone Nematostella vectensis. *Proceedings of the National Academy of Sciences of the United States of America*, 119(19):e2113701119, 5 2022.

[75] E M Kurz, T W Holstein, B M Petri, J Engel, and C N David. Mini-collagens in hydra nematocytes. *J Cell Biol*, 115(4):1159–1169, 1991.

[76] U. Engel. Nowa, a novel protein with minicollagen Cys-rich domains, is involved in nematocyst formation in Hydra. *Journal of Cell Science*, 2002.

[77] Anna Beckmann, Senbo Xiao, Jochen P. Müller, Davide Mercadante, Timm Nüchter, Niels Kröger, Florian Langhojer, Wolfgang Petrich, Thomas W. Holstein, Martin Benoit, Frauke Gräter, and Suat Özbek. A fast recoiling silk-like elastomer facilitates nanosecond nematocyst discharge. *BMC Biology*, 2015.

[78] Jung Shan Hwang, Yasuharu Takaku, Tsuyoshi Momose, Patrizia Adamczyk, Suat Özbek, Kazuho Ikeo, Konstantin Khalturin, Georg Hemmrich, Thomas C.G. Bosch, Thomas W. Holstein, Charles N. David, and Takashi Gojobori. Nematogalectin, a nematocyst protein with GlyXY and galectin domains, demonstrates nematocyte-specific alternative splicing in Hydra. *Proceedings of the National Academy of Sciences of the United States of America*, 2010.

[79] A W Koch, T W Holstein, C Mala, E Kurz, J Engel, and C N David. Spinalin, a new glycine- and histidine-rich protein in spines of Hydra nematocysts. *J Cell Sci*, 111(Pt 11):1545–54, 1998.

[80] S Hellstern, J Stetefeld, C Fauser, A Lustig, J Engel, T W Holstein, and S Ozbek. Structure/function analysis of spinalin, a spine protein of Hydra nematocysts. *Febs J*, 2006.

[81] S F Altschul, T L Madden, A A Schaffer, J Zhang, Z Zhang, W Miller, and D J Lipman. Gapped BLAST and PSI-BLAST: a new generation of protein database search programs. *Nucleic Acids Res*, 25(17):3389–3402, 1997.

[82] Sarah Hunter, Rolf Apweiler, Teresa K. Attwood, Amos Bairoch, Alex Bateman, David Binns, Peer Bork, Ujjwal Das, Louise Daugherty, Lauranne Duquenne, Robert D. Finn, Julian Gough, Daniel Haft, Nicolas Hulo, Daniel

Kahn, Elizabeth Kelly, Aurélie Laugraud, Ivica Letunic, David Lonsdale, Rodrigo Lopez, Martin Madera, John Maslen, Craig Mcanulla, Jennifer McDowall, Jaina Mistry, Alex Mitchell, Nicola Mulder, Darren Natale, Christine Orengo, Antony F. Quinn, Jeremy D. Selengut, Christian J.A. Sigrist, Manjula Thimma, Paul D. Thomas, Franck Valentin, Derek Wilson, Cathy H. Wu, and Corin Yeats. InterPro: the integrative protein signature database. *Nucleic acids research*, 37(Database issue), 2009.

[83] Hiroyuki Tanaka, Shiori Ishimaru, Yasuhiro Nagatsuka, and Keisuke Ohashi. Smooth muscle-like Ca2+-regulation of actin-myosin interaction in adult jellyfish striated muscle. *Scientific Reports*, 8(1), 12 2018.

[84] Setsuko Fujita-Becker, Georgios Tsiavaliaris, Reiko Ohkura, Takashi Shimada, Dietmar J. Manstein, and Kazuo Sutoh. Functional Characterization of the N-terminal Region of Myosin-2. *Journal of Biological Chemistry*, 281(47):36102–36109, 11 2006.

[85] Masaki Hayashida, Tetsuo Maita, and Genji Matsuda. The Primary Structure of Skeletal Muscle Myosin Heavy Chain: I. Sequence of the Amino-Tenninal 23 kDa Fragment. *J. Biochem*, 110:54–59, 1991.

[86] R. W. Lymn and E. W. Taylor. Mechanism of Adenosine Triphosphate Hydrolysis by Actomyosin. *Biochemistry*, 10(25):4617–4624, 12 1971.

[87] Aibing Wang, Xuefei Ma, Mary Anne Conti, and Robert S. Adelstein. Distinct and redundant roles of the non-muscle myosin II isoforms and functional domains. *Biochemical Society transactions*, 39(5):1131, 10 2011.

[88] S Siebert, J A Farrell, J F Cazet, Y Abeykoon, A S Primack, C E Schnitzler, and C E Juliano. Stem cell differentiation trajectories in Hydra resolved at single-cell resolution. *Science*, 365(6451):341–+, 2019.

[89] Albert H. Coons. Histochemistry with Labeled Antibody. *Intern. Rev. Cytol.*, 5(C):1, 1956.

[90] Theresa Bentele, Federico Amadei, Esther Kimmle, Mariam Veschgini, Philipp Linke, Mariana Sontag-González, Jutta Tennigkeit, Anthony D. Ho, Suat Özbek, and Motomu Tanaka. New Class of Crosslinker-Free Nanofiber Biomaterials from Hydra Nematocyst Proteins. *Scientific Reports 2019 9:1*, 9(1):1–9, 12 2019.

[91] S. J. Singer. Preparation of an Electron-dense Antibody Conjugate. *Nature 1959 183:4674*, 183(4674):1523–1524, 1959.

[92] John Limouze, Aaron F. Straight, Timothy Mitchison, and James R. Sellers. Specificity of blebbistatin, an inhibitor of myosin II. *Journal of Muscle Research & Cell Motility 2004 25:4*, 25(4):337–341, 2004.

[93] M Srivastava, O Simakov, J Chapman, B Fahey, M E Gauthier, T Mitros, G S Richards, C Conaco, M Dacre, U Hellsten, C Larroux, N H Putnam, M Stanke, M Adamska, A Darling, S M Degnan, T H Oakley, D C Plachetzki, Y Zhai, M Adamski, A Calcino, S F Cummins, D M Goodstein, C Harris, D J Jackson, S P Leys, S Shu, B J Woodcroft, M Vervoort, K S Kosik, G Manning, B M Degnan, and D S Rokhsar. The Amphimedon queenslandica genome and the evolution of animal complexity. *Nature*, 466(7307):720–726, 2010.

[94] Chiemi Nishimiya-Fujisawa and Satoru Kobayashi. Germline stem cells and sex determination in Hydra. *International Journal of Developmental Biology*, 56(6-8):499–508, 2012.

[95] S Ozbek, U Engel, and J Engel. A switch in disulfide linkage during minicollagen assembly in hydra nematocysts or how to assemble a 150-bar-resistant structure. *J Struct Biol*, 137(1-2):11–14, 2002.

[96] Ulrike Engel, Saut Oezbek, Ruth Engel, Barbara Petri, Friedrich Lottspeich, and Thomas W. Holstein. Nowa, a novel protein with minicollagen cys-rich domains, is involved in nematocyst formation in Hydra. *Journal of Cell Science*, 2002.

[97] Patrizia Adamczyk, Sebastian Meier, Thomas Gross, Bert Hobmayer, Stephan Grzesiek, Hans Peter Bächinger, Thomas W. Holstein, and Suat Özbek. Minicollagen-15, a Novel Minicollagen Isolated from Hydra, Forms Tubule Structures in Nematocysts. *Journal of Molecular Biology*, 2008.

[98] Elina Ikonen, J. Bruno De Almeid, Karl R. Fath, David R. Burgess, Keith Ashman, Kai Simons, and Jennifer L. Stow. Myosin II is associated with Golgi membranes: Identification of p200 as nonmuscle myosin II on Golgi-derived vesicles. *Journal of Cell Science*, 110(18):2155–2164, 1997.

[99] Robert P. Stidwill and Thomas G. Honegger. A single layer of microtubules is part of a complex cytoskeleton in mature nematocytes of hydra. *Tissue and Cell*, 21(2):179–188, 1 1989.

[100] M. Fritzsche, D. Li, H. Colin-York, V. T. Chang, E. Moeendarbary, J. H. Felce, E. Sezgin, G. Charras, E. Betzig, and C. Eggeling. Self-organizing actin patterns shape membrane architecture but not cell mechanics. *Nature Communications 2017 8:1*, 8(1):1–14, 2 2017.

[101] J. A. May, H. Ratan, J. R. Glenn, W. Lösche, P. Spangenberg, and S. Heptinstall. GPIIb-IIIa antagonists cause rapid disaggregation of platelets pretreated with cytochalasin D. Evidence that the stability of platelet aggregates depends on normal cytoskeletal assembly. *Platelets*, 9(3):227–32, 1998.

[102] C N David, S Ozbek, P Adamczyk, S Meier, B Pauly, J Chapman, J S Hwang, T Gojobori, and T W Holstein. Evolution of complex structures: minicollagens shape the cnidarian nematocyst. *Trends Genet*, 24(9):431–438, 2008.

[103] T W Holstein, G M Benoit, G v. Herder, G Wanner, C N David, and H E Gaub. Fibrous Mini-Collagens in Hydra Nematocysts. *Science*, 265:402–404, 1994.

[104] Anna Beckmann, Senbo Xiao, Jochen P. Müller, Davide Mercadante, Timm Nüchter, Niels Kröger, Florian Langhojer, Wolfgang Petrich, Thomas W. Holstein, Martin Benoit, Frauke Gräter, and Suat Özbek. A fast recoiling silk-like elastomer facilitates nanosecond nematocyst discharge. *BMC Biology*, 2015.

[105] C N David and A Gierer. Cell cycle kinetics and development of Hydra attenuata. III. Nerve and nematocyte differentiation. *J Cell Sci*, 16(2):359–375, 1974.

[106] Ilse Foissner, Diedrik Menzel, and Geoffrey O. Wasteneys. Microtubule-dependent motility and orientation of the cortical endoplasmic reticulum in elongating characean internodal cells. *Cell Motility and the Cytoskeleton*, 66(3):142–155, 3 2009.

[107] Susanne Liebe and Diedrik Menzel. Actomyosin-based motility of endoplasmic reticulum and chloroplasts in Vallisneria mesophyll cells. *Biology of the cell*, 85(2-3):207–222, 1995.

[108] G. R. Pasternack and R. H. Racusen. Erythrocyte protein 4.1 binds and regulates myosin. *Proceedings of the National Academy of Sciences of the United States of America*, 86(24):9712–9716, 1989.

[109] Oliver Holz, David Apel, Patrick Steinmetz, Ellen Lange, Simon Hopfenmüller, Kerstin Ohler, Stefanie Sudhop, and Monika Hassel. Bud detachment in hydra requires activation of fibroblast growth factor receptor and a Rho–ROCK–

myosin II signaling pathway to ensure formation of a basal constriction. *Developmental Dynamics*, 246(7):502–516, 7 2017.

[110] J A Chapman, E F Kirkness, O Simakov, S E Hampson, T Mitros, T Weinmaier, T Rattei, P G Balasubramanian, J Borman, D Busam, K Disbennett, C Pfannkoch, N Sumin, G G Sutton, L D Viswanathan, B Walenz, D M Goodstein, U Hellsten, T Kawashima, S E Prochnik, N H Putnam, S Shu, B Blumberg, C E Dana, L Gee, D F Kibler, L Law, D Lindgens, D E Martinez, J Peng, P A Wigge, B Bertulat, C Guder, Y Nakamura, S Ozbek, H Watanabe, K Khalturin, G Hemmrich, A Franke, R Augustin, S Fraune, E Hayakawa, S Hayakawa, M Hirose, J S Hwang, K Ikeo, C Nishimiya-Fujisawa, A Ogura, T Takahashi, P R Steinmetz, X Zhang, R Aufschnaiter, M K Eder, A K Gorny, W Salvenmoser, A M Heimberg, B M Wheeler, K J Peterson, A Bottger, P Tischler, A Wolf, T Gojobori, K A Remington, R L Strausberg, J C Venter, U Technau, B Hobmayer, T C Bosch, T W Holstein, T Fujisawa, H R Bode, C N David, D S Rokhsar, and R E Steele. The dynamic genome of Hydra. *Nature*, 464(592):7288, 2010.

[111] Isabelle Philipp, Roland Aufschnaiter, Suat Özbek, Stefanie Pontasch, Marcell Jenewein, Hiroshi Watanabe, Fabian Rentzsch, Thomas W. Holstein, and Bert Hobmayer. Wnt/β-Catenin and noncanonical Wnt signaling interact in tissue evagination in the simple eumetazoan Hydra. *Proceedings of the National Academy of Sciences of the United States of America*, 106(11):4290–4295, 3 2009.

[112] Nilay Taneja, Matthew R. Bersi, Sophie M. Baillargeon, Aidan M. Fenix, James A. Cooper, Ryoma Ohi, Vivian Gama, W. David Merryman, and Dylan T. Burnette. Precise Tuning of Cortical Contractility Regulates Cell Shape during Cytokinesis. *Cell reports*, 31(1), 4 2020.

[113] Matthias Krause and Alexis Gautreau. Steering cell migration: lamellipodium dynamics and the regulation of directional persistence. *Nature reviews. Molecular cell biology*, 15(9):577–590, 2014.

[114] Aidan M. Fenix, Nilay Taneja, Carmen A. Buttler, John Lewis, Schuyler B. Van Engelenburg, Ryoma Ohi, and Dylan T. Burnette. Expansion and concatenation of nonmuscle myosin IIA filaments drive cellular contractile system formation during interphase and mitosis. *Molecular Biology of the Cell*, 27(9):1465–1478, 5 2016.

[115] Akiyoshi Kawamura and Yūzō. Aoyama. Immunofluorescence in medical science. page 262, 1983.

[116] Robert E. Mandrell, J. Mcleod Griffiss, and Bruce A. Macher. Lipooligosaccharides (LOS) of Neisseria gonorrhoeae and Neisseria meningitidis have components that are immunochemically similar to precursors of human blood group antigens. Carbohydrate sequence specificity of the mouse monoclonal antibodies that recognize crossreacting antigens on LOS and human erythrocytes. *The Journal of Experimental Medicine*, 168(1):107–126, 7 1988.

[117] Shi Shu, Randall J. Lee, Janine M. LeBlanc-Straceski, and Taro Q.P. Uyeda. Role of myosin II tail sequences in its function and localization at the cleavage furrow in Dictyostelium. *Journal of Cell Science*, 112(13):2195–2201, 1999.

[118] Sara O. Dean, Stephen L. Rogers, Nico Stuurman, Ronald D. Vale, and James A. Spudich. Distinct pathways control recruitment and maintenance of myosin II at the cleavage furrow during cytokinesis. *Proceedings of the National Academy of Sciences of the United States of America*, 102(38):13473–13478, 9 2005.

[119] Anne Müsch, David Cohen, and Enrique Rodriguez-Boulan. Myosin II is involved in the production of constitutive transport vesicles from the TGN. *Journal of Cell Biology*, 1997.

[120] Masahito Tanaka, Takeomi Kikuchi, Hiroyuki Uno, Keisuke Okita, Toshiko Kitanishi-Yumura, and Shigehiko Yumura. Turnover and flow of the cell membrane for cell migration. *Scientific Reports 2017 7:1*, 7(1):1–13, 10 2017.

[121] Elina Ikonen, J. Bruno De Almeid, Karl R. Fath, David R. Burgess, Keith Ashman, Kai Simons, and Jennifer L. Stow. Myosin II is associated with Golgi membranes: Identification of p200 as nonmuscle myosin II on Golgi-derived vesicles. *Journal of Cell Science*, 1997.

[122] J. Bernd Helms and James E. Rothman. Inhibition by brefeldin A of a Golgi membrane enzyme that catalyses exchange of guanine nucleotide bound to ARF. *Nature 1992 360:6402*, 360(6402):352–354, 1992.

[123] Aaron F. Straight, Amy Cheung, John Limouze, Irene Chen, Nick J. Westwood, James R. Sellers, and Timothy J. Mitchison. Dissecting temporal and spatial control of cytokinesis with a myosin II inhibitor. *Science*, 299(5613):1743–1747, 3 2003.

[124] H Shimizu and H R Bode. Nematocyte differentiation in hydra: commitment to nematocyte type occurs at the beginning of the pathway. *Dev Biol*, 169(1):136–150, 1995.

[125] Jan U. Lohmann, Ingrid Endl, and Thomas C.G. Bosch. Silencing of developmental genes in Hydra. *Developmental Biology*, 214(1):211–214, 10 1999.

[126] Mark Lommel, Anja Tursch, Laura Rustarazo-Calvo, Benjamin Trageser, and Thomas W Holstein. Genetic knockdown and knockout approaches in Hydra. *bioRxiv*, 2017.

[127] Lou Fourriere, Ana Joaquina Jimenez, Franck Perez, and Gaelle Boncompain. The role of microtubules in secretory protein transport. *Journal of Cell Science*, 133(2), 1 2020.

[128] David B. Slautterback. CYTOPLASMIC MICROTUBULES. I. HYDRA. *The Journal of cell biology*, 18(2):367–388, 8 1963.

[129] H. E. Huxley. ELECTRON MICROSCOPE STUDIES ON THE STRUCTURE OF NATURAL AND SYNTHETIC PROTEIN FILAMENTS FROM STRIATED MUSCLE. *Journal of molecular biology*, 7(3):281–308, 1963.

[130] Geoffrey M Cooper. Structure and Organization of Actin Filaments. 2000.

[131] B Rogez, L Wurthner, A B Petrova, F B Zierhut, D Saczko-Brack, M A Huergo, C Batters, E Frey, and C Veigel. Reconstitution reveals how myosin-VI self-organises to generate a dynamic mechanism of membrane sculpting. *Nature Communications*, 10, 2019.

[132] S Ebrahim, D Chen, M Weiss, L Malec, Y Ng, I Rebustini, E Krystofiak, L H Hu, J Liu, A Masedunskas, E Hardeman, P Gunning, B Kachar, and R Weigert. Dynamic polyhedral actomyosin lattices remodel micron-scale curved membranes during exocytosis in live mice. *Nature Cell Biology*, 21(8):933–+, 2019.

[133] Moritz Mercker and Anna Marciniak-Czochra. Bud-Neck Scaffolding as a Possible Driving Force in ESCRT-Induced Membrane Budding. *Biophysical Journal*, 108(4):833–843, 2 2015.

[134] J Wittlieb, K Khalturin, J U Lohmann, F Anton-Erxleben, and T C Bosch. Transgenic Hydra allow in vivo tracking of individual stem cells during morphogenesis. *Proc Natl Acad Sci U S A*, 103(16):6208–6211, 2006.

[135] Amanda Birmingham, Emily Anderson, Kevin Sullivan, Angela Reynolds, Queta Boese, Devin Leake, Jon Karpilow, and Anastasia Khvorova. A protocol for designing siRNAs with high functionality and specificity. *Nature Protocols*, 2(9):2068–2078, 9 2007.

[136] Svetlana A. Shabalina, Alexey N. Spiridonov, and Aleksey Y. Ogurtsov. Computational models with thermodynamic and composition features improve siRNA design. *BMC bioinformatics*, 7, 2 2006.

[137] Berenice Ziegler, Irene Yiallouros, Benjamin Trageser, Sumit Kumar, Moritz Mercker, Svenja Kling, Maike Fath, Uwe Warnken, Martina Schnölzer, Thomas W. Holstein, Markus Hartl, Anna Marciniak-Czochra, Jörg Stetefeld, Walter Stöcker, and Suat Özbek. The Wnt-specific astacin proteinase HAS-7 restricts head organizer formation in Hydra. *BMC biology*, 19(1), 12 2021.

[138] Micah Allen, Davide Poggiali, Kirstie Whitaker, Tom Rhys Marshall, Jordy Van Langen, Rogier A Kievit, Lisa M Debruine, and Elena Allen. Raincloud plots: a multi-platform tool for robust data visualization. *Wellcome Open Research 2021 4:63*, 4:63, 1 2021.

[139] R. A. Fisher. XV.—The Correlation between Relatives on the Supposition of Mendelian Inheritance. *Earth and Environmental Science Transactions of The Royal Society of Edinburgh*, 52(2):399–433, 1919.

[140] Tapan Goel, Rui Wang, Sara Martin, Elizabeth Lanphear, and Eva Maria S. Collins. Linalool acts as a fast and reversible anesthetic in Hydra. *PLOS ONE*, 14(10):e0224221, 10 2019.

[141] Michael W. Hess, Georg F. Vogel, Teodor E. Yordanov, Barbara Witting, Karin Gutleben, Hannes L. Ebner, Mariana E.G. de Araujo, Przemyslaw A. Filipek, and Lukas A. Huber. Combining high-pressure freezing with pre-embedding immunogold electron microscopy and tomography. *Traffic*, 19(8):639–649, 8 2018.

[142] Thomas W. Holstein, Michael W. Hess, and Willi Salvenmoser. Preparation Techniques for Transmission Electron Microscopy of Hydra. *Methods in Cell Biology*, 96(C):285–306, 1 2010.

[143] M Lommel, J Strompen, A L Hellewell, G P Balasubramanian, E D Christofidou, A R Thomson, A L Boyle, D N Woolfson, K Puglisi, M Hartl, T W Holstein, J C Adams, and S Ozbek. Hydra Mesoglea Proteome Identifies Throm-

bospondin as a Conserved Component Active in Head Organizer Restriction. *Sci Rep*, 8(1):11753, 2018.